2011

One-Dimensional Radial Diffusion of Small Molecules (376 Da) in Bone Tissue

Kurt W. Farrell
Cleveland State University

ONE-DIMENSIONAL RADIAL DIFFUSION OF SMALL MOLECULES (376 Da) IN BONE TISSUE

KURT W FARRELL

Bachelors of Science Chemistry

Bachelors of Science Evolution, Ecology, and Organismal Biology

The Ohio State University

June, 2009

Submitted in partial fulfillment of requirements for the degree
MASTER OF SCIENCE IN BIOMEDICAL ENGINEERING
at
CLEVELAND STATE UNIVERSITY
December, 2011

This thesis has been approved

for the Department of Chemical and Biomedical Engineering

and the College of Graduate Studies by

_____

Thesis Chairperson, Dr. Joanne M. Belovich

Chemical and Biomedical Engineering Dept.

_____

Date

_____

Dr. Surendra N. Tewari

Chemical and Biomedical Engineering Dept.

_____

Date

_____

Dr. Ronald J. Midura

Chemical and Biomedical Engineering Dept.

_____

Date

This thesis is dedicated to my mother Colleen Farrell, and my father, William Farrell. I would like to thank my close friends and brother for their support. I would like to recognize my Mary Jo Gartland for her constant support and encouragement in my scientific and academic endeavors.

ACKNOWLEDGMENTS

I would first like to acknowledge all my committee members for their support. I would like to thank my advisor and mentor Dr. Belovich for her support and vision. Her guidance made me understand what it means to be an engineer. I would like to thank Dr. Tewari, whose broad knowledge and attention to details helped me understand what it means to be a scientific researcher. Dr. Midura played a crucial role in understand the biological aspects of the experiment and his resources and staff at the Cleveland Clinic made this experiment possible. Outside of the thesis committee, Dr. Charlie Androjna spent numerous hours teaching and aiding in the preparation of bone samples, as well as providing key insights during lab group meetings.

Outside resources played a strong role in making this research possible. Rick Rozic and the Image IQ at the Cleveland Clinic provided training and the usage of high quality florescent images. The biochemical engineering lab, including the algae research group and bone research group at Cleveland state. Becky Laird for her aid and support. Jeffrey Dilorenzo for his aid in editing and revision.

Lastly, I would like to acknowledge the resources of the staff at both Cleveland State University and the Lerner Research Institute at the Cleveland Clinic. Support for this research comes from an FRD grant as well as the Choose Ohio first Scholarship.

ONE-DIMENSIONAL RADIAL DIFFUSION OF SMALL MOLECULES (376 Da) IN BONE TISSUE

KURT W FARRELL

ABSTRACT

The flow of nutrients through any biological tissue is important to maintain homeostasis. If the transport process is understood, medical research teams can better design medications, prosthetic implants, and tissue scaffolds. Additionally, transport rates help physicians to better understand disease states and wound healing, including minor injuries such as breaks and sprains, which will aid in better diagnoses. We developed a novel method that measures the rate of diffusion in *vitro*, of fluorescein sodium salt. Samples were incubated at 37°C in a 5% CO_2 atmosphere for various periods of time. Samples were sliced and analyzed using Image-Pro Plus and MATLAB to obtain concentration profiles. The diffusivity was estimated from the data using the model equation for one-dimensional transport in a finite medium. We found that radial diffusivity in canine bone in 1-dimension was $1.27 \times 10^{-7} \pm 1.96 \times 10^{-8}$ cm^2/s. As a point of reference, the diffusivity of fluorescein sodium salt in PBS is 2.7×10^{-6} cm^2/s. Given the average distance between a Haversian canal and an osteon radius is 250 μm, our data shows it would take approximately 20 minutes for a nutrient of a weight of 376 Da to travel between the two locations. This indicates that the diffusion time of key nutrients, such as vitamin D, with molecular weight of 384 Da, would be about 20 minutes.

TABLE OF CONTENTS

Page

LIST OF TABLES

Page

LIST OF FIGURES

CHAPTER I

INTRODUCTION

Bone is a type of dense connective tissue that provides a protective support frame for all the other organs in vertebrates, as well as locomotion. Because their function is to support and protect, their structure is complex both internally and externally. Bone is the general term for a dynamic tissue that has a hierarchical structure, interacting with several other surrounding tissues, including osseous tissue, cartilage, dense connective tissue, nervous tissue, epithelium, and adipose tissue[1]. Given that bone is a dynamic tissue, it is constantly remolding and rebuilding itself. It is for this reason that a constant supply of nutrients and removal of wastes must be maintained in order to promote healthy bone tissue. Given that fact, it is important to quantify the rate of this exchange of materials within the tissue. One of the best ways to quantify transport is to look at one specific type of transport, isolate the variables that allow that form of transport to occur, and quantify the rate at which it is occurring. Diffusion is a common means of transport in bone tissue that,

although previously studied, has some ambiguity in the rate it is occurring given the complexities of biological system it is occurring within. The purpose of this paper is to accurately quantify, in the radial direction, the rate that small molecules (376 Da) diffuse through bone tissue. We are concerned with radial direction for two reasons, the first being has been little research done in this area in the past, and the second is that radial direction is much more dense, as opposed to the axial direction in which vascular transport dominates.

The mechanical stability of bone tissue is a major concern in engineering a compatible substitute to native tissue as it directly pertains to the tissue's load-bearing capacity and porosity. The mechanical performance of bone is related to its architecture and composition; additionally, the biological environment directly influences the process of bone formation and subsequently affects the architecture and composition of the tissue[2]. Fluid flow inside cortical bone is important for nutrient and waste transport, which maintains osteocyte viability and regulates the physiological processes of bone remodeling and homoestasis[6].

If we understand the rate of transport in bone, we can better design drugs and medications targeting specific areas of bone tissue, and be able to predict the rate of transport to the target tissue. Additionally, metallic prosthetic implants are common in the femur, and patella, and knowing the rate at which molecules diffuse into native bone tissue, we could better design artificial implants to better function as normal tissue. Even common injuries, breaks and sprains, could be better understood if we could quantify the rate of the removal

of the damaged necrotic tissue and the replacement of new tissue. All of these processes are limited by the rate at which the body can send nutrients, signaling factors, and remove wastes, thus knowing the absolute rate that diffusion is occurring in bone could help medical research teams develop more innovative solutions to bone disease states.

The purpose of this research is to find the rate at which a small molecule diffuses into bone that has no mechanical force applied to it. We used fluorescein sodium salt as a tracer molecule, and fluorescent microscopy which tracked how far this molecule traveled into canine bone tissue. We then applied a transport model to quantify the rate, in cm^2/s, the molecule moved into the tissue, radially, in one dimension. The process was repeated for different periods of time. The goal of the study is to have developed a method that can reproducibly quantify diffusion rates in bone. Most importantly, this method has the flexibility to accommodate other variables, such as mechanical loading, convection, and different sized molecules/markers. This being the first round of experiments we aim to have a benchmark rate of diffusion given simple conditions, with conditions mimicking native physiological environments, including temperature, molarity of solute, and atmospheric composition, but in the absence of mechanical loading.

CHAPTER II

BACKROUND

2.1 Bone Composition and structure

Bone Architecture

In general, human bone tissue is classified as a biocomposite material. Its composition in adults is roughly 67% mineral salts and 33% organic matrix by dry weight. The organic matrix consists of 62% type I collagen, 26% minor collagens and non-collagenous proteins, 6% lipids and 6% complex carbohydrates[8, 9]. Bone can be broken down into two broad categories on the macro scale, cortical bone and trabecular (cancellous) bone. It is worth noting that each has a different composition, affecting the porosity and canalicular structure, in turn directly affecting the rate of diffusion. This study will focus on cortical bone, as it is denser and thus should be more diffusion limited. Figure 2.1 displays the key structural differences between cortical and trabecular bone.

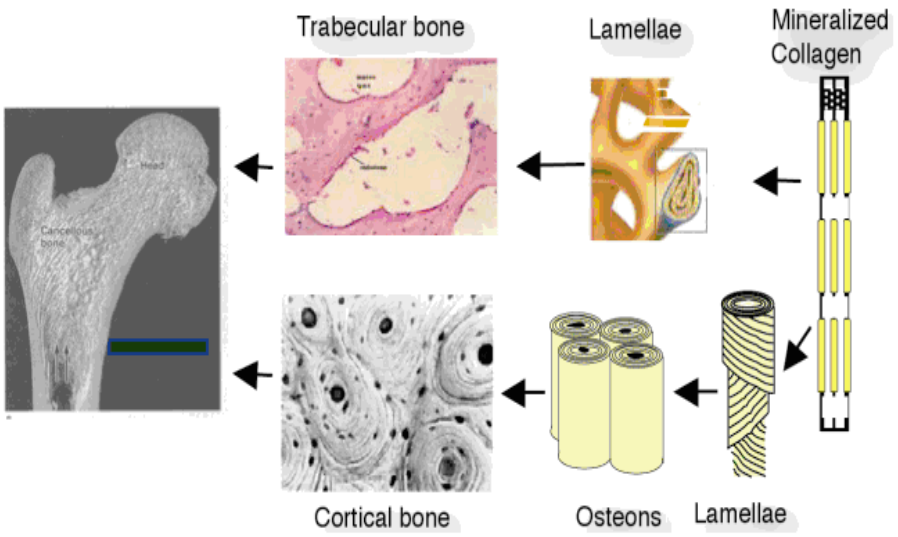

Figure 2.1 Differentiation of the location and hierarchical structure of bone Image source: Fundamental Biomechanics in Bone Tissue Engineering[2]

Trabecular bone, found within the metaphysis, epiphyses, and medullary cavities of long bone, has three main components, trabecular, lacunae, and bone marrow. The porosity of this type of tissue is generally 75%-95% of the total volume[2]. Because of the high-percent porosity of trabecular bone, diffusion is generally not limited, which is why this study will not focus on this type of bone.

Cortical bone composes 80% of the total mass of the skeleton and is thus a crucial component in most types of tissue-engineered bone substitutes. Additionally, cortical bone is dense, with its porosity being only 5%-10%[3] of its total volume. Before we go into a discussion on the porosity, I will briefly highlight the basic structural features of cortical bone.

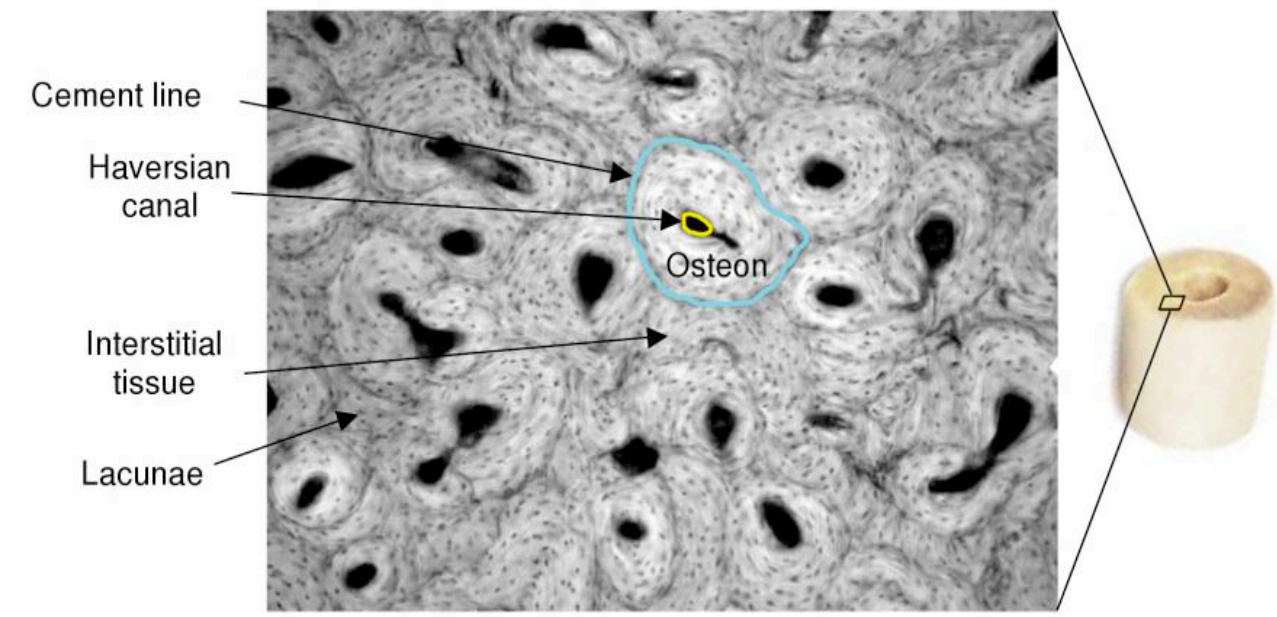

Figure 2.2 Cortical Bone Structure. Image source: Fundamental Biomechanics in Bone Tissue Engineering[2]

In a radial slice of bone tissue, as highlighted in figure 2.2, under 10X magnification, one can easily distinguish most of the important features involved in nutrient transport. The most obvious feature is the cylindrical lamellar osteons, or Haversian system[5]. Most of these features average a size of 200 μm, containing nervous tissue and feed and return blood vessels located in the center[10]. Osteons are separated by a boundary layer called the cement line. Surrounding the cement line is the interstitial tissue, which is constantly being remodeled and may contain either primary bone or remnants of primary and secondary osteons.[5] The lacunae are cavities where osteocytes are located, and they communicate to one another via tiny canals called canaliculi.

Now that we have discussed the major structural features that are observable under a microscope, I will discuss the less obvious system of canals that aid in the radial transport of nutrients to bone tissue. As highlighted above, the Haversian canals run axially down the length of a long bone, and are not of interest to the type of diffusion discussed in this study. Rather, Volkmann's canals and reabsorption cavities play a strong role in transverse (radial) diffusion[5] across the transverse plane of symmetry. Volkmann's canals connect Haversian canals to one another across a given long bone. Thus, they are an important canal system of our study. Additionally, reabsorption cavities are temporary spaces created by bone-removing cells in the initial stage of bone remodeling. As mentioned earlier, canaliculi are another multi-directional pore system that molecules could diffuse through, however the total volume of lacunae and canaliculi contributes to only about 10% of the total porosity[6, 11], bearing in mind that overall cortical bone is dense, with its porosity being only 5%-10%[3] of its total volume. One major misconception about the porous network within bone tissues is that Haversian canals, Volkmann's canals and their inclusive vasculature run at precise right angles to one another and are parallel and perpendicular to the long axis of bone[15]. This is an oversimplification. The actual vascular architecture consists of a mixture of canal orientations, many of which form an oblique angle with the surface of bone[15]. In general, the porosity and tortuosity of a bone tissue is heterogeneous. To summarize, the porous compartments of bone are channels that include Haversian canals, Volkman's canals, reabsorption cavities, and a filipodial-like

canalicular system. All of these components aim to maintain homeostatic conditions by allowing for the exchange of biological fluids, nutrients and metabolic waste products[5,10,11].

The exchange of wastes is crucial for bone remodeling, and as stated previously bone remodeling is crucial for the maintenance of homeostatic conditions. To be brief, as this is not the primary focus of our study, the cells responsible for bone metabolism are known as osteoblasts, which secrete new bone, and osteoclasts which break bone down[4,5]. Complex signaling pathways achieve proper rates of growth and differentiation. These signaling pathways include the action of several hormones, including parathyroid hormone, vitamin D, growth hormones, steroids, and calcitonin, glucose, and several cytokines[4,5]. The body maintains proper levels of all these molecules, (some of which we will discuss their structure in more detail in section 2.6) via simple mass transport mechanisms, such as diffusion, which is the focus of this study.

Layer of bone tissue studied

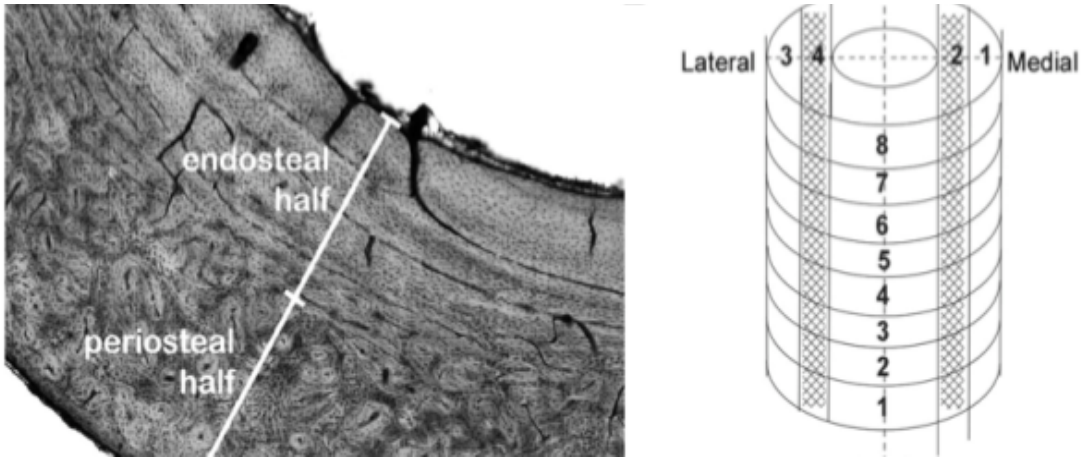

Figure 2.3 Histological bone sample. Ref. Cortical Bone Tissue Engineering: Scaffold Design and Cell Selection[22].

Figure 2.3 shows the exact location of the harvested bone samples. On the right is an idealized sketch of a clinical cortical bone, with the shaded regions is representing the portion of the bone used in our diffusion experiments. The image on the left is of a magnified histological slice of bone. It is clear that there is a different organizational scheme to the Volkmans' canals in the periosteal half than in the endosteal half. In the endosteal half, some of these channels traversed radially throughout its entire width. This point was investigated in a paper by Meinel *et al.*. in 2003, and a doctoral thesis by Wen in 2009. Both had more success measuring radial permeability in the endosteal halves than in the corresponding periosteal halves[23,24,40]. To be specific, most research publications commonly cited that the fluid movement through bone samples in the endosteal to periosteal direction was so small so as to be below the limits of detection (although the numerical limit was not reported). When approximately 3.6% of the bone thickness was removed from the periosteal surface, fluid passed through the cortical sample[40]. In our particular design, this was approximately .5-1 mm of bone, located approximately 4-5 mm from the cortex. Again, this was commonly reported in several papers dating back to 1987, using a variety of different analytical methods and solutes, including florescent markers, india ink, and others.[40] Thus, for our studies, all diffusion measurements were taken in the endosteal region of the bone.

Porosity and connectivity of bone

Past studies have analyzed the structural properties of cortical bone, most implementing the use of a micro-CT scan to better quantify the internal structure of the tissues[11]. The samples analyzed were harvested from the same canine, (Lot number O7D-256) as the bone used in the work presented here, with the difference being ours were taken from the right tibia, theirs the left. Using environmental scanning electron microscopy, they noticed that each bone wafer displayed numerous large pores (50 – 100 μm width) and intermediate-sized pores (10 - 50 μm width) on the endosteal surface[22,41], see figure 2.4. Similar imaging of the opposing cut surface of these bone wafers revealed fewer intermediate-sized pores and numerous small pores (1–5 μm width), but no large pores[22,41]. Noticing that there are pores on both ends of the sample, they used 3-D micro-CT imaging (at 3 μm resolution) to see if the pores connected across the bone. The imaging showed that the pores on both sides of the cortical bone samples were in fact interconnected both radially and axially, which is a crucial observation for our experimentation measuring diffusion radially across the bone. They then calculated total porosity of their samples as being 2.95 ± 0.91%. The radial porosity was 0.60 ± 0.17%, and axial porosity was 2.36 ± 0.71% [22,41]. Connectivity density calculations revealed a value for radial connectivity of 175 ± 87mm^3 and axial connectivity of 438 ± 204 mm^3 [22,41].

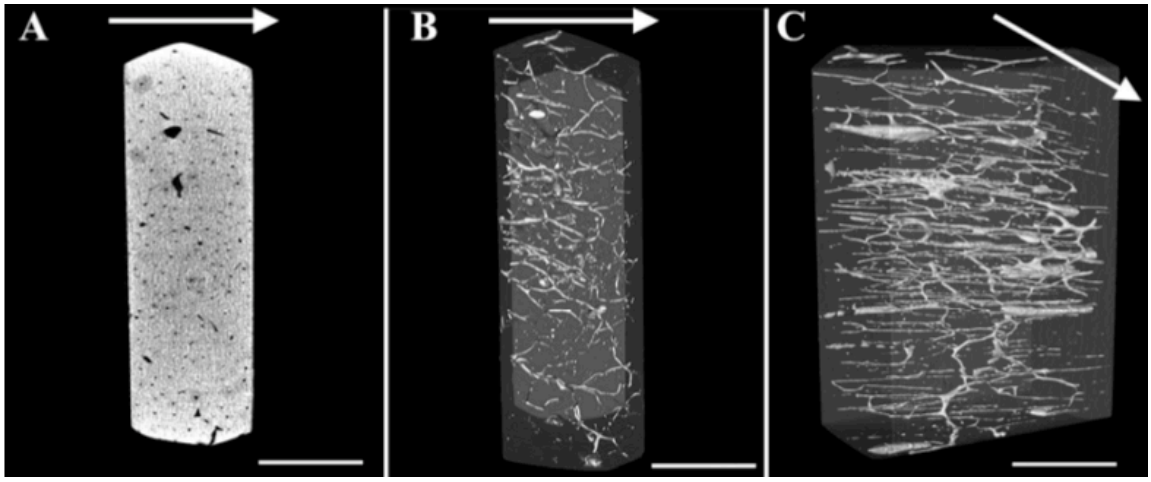

Figure 2.4 Porosity and connectivity measurement of endosteal region cortical bone.

(A)Representative 3D micro-CT scanning image. (B) Inverted 3-D micro-CT image in the radial direction. (C) Inverted 3-D micro-CT image in the axial direction. Scale bars in panel A-C are 200 μm. Ref. Cortical Bone Tissue Engineering: Scaffold Design and Cell Selection[22,41].

2.2 Selection of Animal Model

In humans, bone structure is dependent on multiple factors, including age, gender, and anatomic locations[2]. In general, for most tissue engineering applications, many animal models have been developed and proposed, however it should be understood that each model has its own utility and limitations for the study of human bone tissue engineering[25]. Because our study is based on fluid movement through the tissue, the biochemistry and growth of the tissue was not as important as the actual composition of bone, when compared to humans. Based on a review of the literature, we concluded that canine bone would be the best-suited model for our experimentation. Much research has been done on the differences in bone composition, density, and quality between various species, including humans, dogs, sheep, pigs, cows, and chickens[24]. The conclusion was that bone composition and structure, including density and porosity, were most similar between dogs and humans[24]. Based on previous

research in similar bone studies and the plentiful amount of data already gathered relating basic bone physiology in canines and humans, we believe that our test model using canine tissue will be translatable to how native human tissue behaves[25].

2.3 Diffusion

One can broadly describe the transport of molecules two ways, namely diffusion and convection. By definition, diffusion is a random motion of molecules that arises from thermal energy transferred by molecular collisions[15]. One may also refer to this movement as Brownian motion, named after the scientist who originally developed the concept. Convection is a mechanism of transport resulting from the bulk motion of fluids[16]. Either of these mechanisms influences the movement of energy and momentum in biological systems individually and concurrently. In the context of our study, we assume convection to be negligible, and from this point on we will focus primarily on diffusion.

When a molecule is in the gas or liquid phase, it has random interactions with the surrounding environment. Diffusion is based on several factors, most importantly the size and shape of the molecule, temperature, fluid viscosity, and a property that reflects the resistance to flow. Although one may classify the nature of the phenomenon as random, a net motion or direction occurs, which is based primarily on the movement from higher concentration to a region of lower concentration. The net movement of a molecule through a unit area in a given direction per unit time is known as flux, and the diffusion flux is proportional to

the gradient of the concentration[16]. The relationship between diffusion flux and concentration gradient was first quantified in 1855 by Adolph Fick and is hence referred to as Fick's law[16].

$$J = -D\frac{\partial \phi}{\partial x} \tag{1}$$

Where J is diffusion flux, or amount substance per unit area per time, and D binary diffusion coefficient, or D_{ij}, is the variable used to represent diffusion, where the *i* represents the solute and *j* the solvent. The coefficient is a function of temperature and pressure. The magnitude is dependent on the medium traveled through and the solute traveling. There is a difference between diffusivity and effective diffusivity, that being the effective diffusivity assumes the rate of diffusion of species i depends on the composition gradient of the species, which for our purposes is invalid as we also have to be considerate of the bone sample our molecule is diffusing through. For our study, we will apply the conditions of unsteady diffusion in one dimension, meaning the concentration of the diffusing molecule changes with time and distance. Thus the study of our molecule of interest will have a time dependent behavior and have to be modeled via a partial differential equation[16]. Details of the model and its solution are outlined in the methods section.

Role of diffusion in biological tissue

Diffusion of small molecules and macromolecules plays an important role in maintaining homeostasis in most living organisms[21]. The rate of diffusion is a strong function of both the tissue it is occurring in, and the direction (laterally or radially) of transport. If one were to design a replacement biological tissue, he or she must understand the rate of diffusion, as diffusion is often the primary mass transport mechanism in engineered tissue constructs[19]. Bone tissue is a heterogeneous structure, formed by the assembly of cells and the accumulation of matrix material in the extracellular space[20]. The heterogeneous composition of tissue can have a dramatic influence on local rates of molecular movement through the tissue, which will affect the overall rate of diffusion.[20] For our experiment, we focused on the diffusion within bone tissue, bearing in mind that our ultimate goal is to create a synthetic construct that has identical diffusive properties as native bone, since bone grafts and bone replacements depend on diffusion for growth and maturation[16].

Bone tissue health depends largely on efficient fluid and solute transport between the blood supply and cells that are the living component of the tissue[13]. Currently, a significant body of research has shown that there is a pronounced and rapid flow of fluids and associated solutes through the extravascular spaces in bone[14]. Many *in vivo* experiments focus on injecting large molecules directly into the bones of various animals and monitoring their movement throughout the osteocytic lacunae and canaliculi of the cortical bone[14]. However these types

of experiments do not differentiate between radial and lateral diffusion; in fact, they primarily measure axial diffusion. Nonetheless, it is clear that within bone tissue diffusion is one of the primary mechanisms for transport. Our experiment focuses on radial diffusion across the bone tissue, as the literature shows there is a lack of data in this particular area.

To conclude, the transport of nutrients across bone tissue is important for cell viability as well as tissue health. The ease with which solutes can move through pore spaces or fractures is an inherent property of bone tissue, referring to the tissue's architecture and porosity, matrix biochemistry, and pericellular fluid properties[14]. By first gathering a baseline of how diffusion occurs in vitro (the purpose of this experiment), we can later interpret how external factors such as mechanical, chemical and/or electrical effects change these rates[14]. A basic understanding of diffusion within bone can help us better design various pharmaceuticals, prosthetic implants, and bone tissue scaffolds.

2.4 Relevant studies on diffusion

There is plenty of current research available on the structure of bone tissue and the physiology behind how it maintains homoeostatic conditions and how its function is impaired by a disease state. Given the previous background on the structure of bone, it is clear that there are many pathways through various canals for nutrients to diffuse in and out of the tissue. As stated previously, there is little research focused on the radial direction through the

smaller Volkmann's canals and cannuliculi. In this section, we will briefly outline the prior research techniques used to analyze bone tissue diffusion.

Early studies on bone diffusion focused more on pore size than on diffusion; however, bone is not a uniformly porous material. The idea was to match the porosity found within bones to a porosity of a well known biocompatible substance. These early studies found the minimum pore size for significant ingrowth of natural bone was indicated to be between 75 and 100 μm[17]. Knowing bone porosity and pore sizes, researchers then began to model computationally the fluid flow dynamics across bone. One study in particular conducted in 1991 by Dillamen *et al.* used this approach in conjunction with hydrostatic pressures to determine the time needed for nutrients to diffuse within rat and chicken bones[13]. They noticed that minutes after injection, large molecules (ferritin and horseradish peroxidase) had been localized throughout the osteocytic lacunae and canaliculi of cortical bone in both the chick and rat[13]. They noticed that there was bulk flow even within the dense portion of bone but failed to report any diffusion coefficients, since they were seeking qualitative data instead[13]. In summary this work qualitatively provided evidence that even in the densest portion of bone some transport had occurred, and thus it provided the foundation for future studies.

Moving away from bone structure and computational modeling, research shifted to qualitative non-loaded bone studies. One study, conducted by Knothe Tate *et al.*., used procion red dye and a paralyzed group of rats, with the goal of

studying the transport into their bones[32]. They hypothesized that it is unlikely that diffusion alone can account for molecular transport in the porous, yet relatively impermeable matrix of bone. To test this they conducted short-term and long-term studies *in vivo* on the rat bones, taking cross-sectional cuts of the bones and viewing them under a fluorescent microscope[32 33]. They concluded that diffusion alone cannot account for efficient transport of larger molecules into the bones and argued that connective tissue transport by a load-induced fluid flow could be the answer to transporting large nutrients[32 33]. They used this for the basis of their quantitative studies, which will be discussed in more detail in the subsequent paragraphs.

Although non-loading studies provide a good control for how molecules transport within bone, the ultimate goal of most research is to focus on the effect of mechanical loading on transport rate within bone. This is also a long-term goal of our diffusion study. Before quantifying diffusion rates, bone transport research focused on combining mechanical loading, noticing how it affected diffusion qualitatively[31]. A study conducted again Knothe-Tate *et al.,* proved diffusion was occurring under loaded conditions, and possibly at a higher rate than unloaded samples. In their experiment, which parallels the long-term goal of our experiment, they hypothesized that load-induced fluid flow enhances the transport of key substances, thus helping to regulate cellular activity associated with processes of functional adaptation and remodeling[31]. Their setup was performed *in vivo* on a rat, in particular within the contralateral tibia. However, we must use caution when considering this data and its applications to humans,

as the rat model lacks an abundance of osteons, and consequently it has low Haverision remodeling, which is different from the native function of human bones[42]. Their experimental design had a 4-point bending device applying specific mechanical loads. Using a red tracer, they showed that mechanical loading promotes molecular transport significantly within the relatively impermeable matrix of cortical bone[31]. However, they did not provide any quantitative diffusion coefficients and thus advised for further studies to be conducted[31].

Transitioning to more quantitative studies, the same research group (Knothe-Tate) focused on the effects of loading again, but this time using a large sheep bone sample. The bone was compressed in short cycles—2, 4, 8, 16 min.—and then the fluid flow was compared to an unloaded bone control[25]. The results showed that transport in the mid-diaphysis of the cortex was significantly higher in the loaded bone[25]. Procion Red was the dye used in the experiment in conjunction with the "FRAP" technique (Fluorescence recovery after photo-bleaching). However the experimental design had some drawbacks, the most important being that the bone was screwed to an apparatus, and tension and compression was applied to the long bone in a lateral fashion[25]. They did not differentiate between axial and radial flow, and again they did not find a numerical diffusion coefficient[25].

The FRAP technique, developed by Wang *et al* [28], has been used to quantitatively measure diffusivity in various biological tissue. The methodology

behind the FRAP technique is presented here. One first obtains images of the sample using the laser scanning confocal microscope saturated in fluorescent dye[28]. Then, one measures diffusion at the level of the matrix micro-porosity using the illuminated fluorescent spots that appear on a small area of the sample between canaliculi. Overall, tissue level diffusion is measured by bleaching a tissue region consisting of a matrix, canaliculi, and lacunae and measuring the recovery of the fluorescent probes. One measures this by calculating the mean intensity of the bleached region within an image collected after bleaching. Thus, the technique focuses on transport between individual canaliculis within the dense tissue portion, and not across an entire tissue sample. In one of their most recent studies the Knothe-Tate research group used this technique again and concluded that the diffusivity measured at the matrix-porosity level was 7.0×10^{-10} cm^2/s using a 300 Da dye [26]. Not surprisingly, this value is extremely low, considering the dense, inorganic nature of this portion of the tissue. They also attempted to diffuse 3000 Da molecule in the longitudinal direction of the bone sample, they recorded a diffusivity value of 3.0×10^{-10} cm^2/s. They questioned the validity of the 3000 Da radial diffusion value, however they did not discuss it further in the paper. In conclusion, this experiment proves most similar to ours because it does adequately distinguish between radial and axial diffusion.

Wang *et. al* utilized fluorescein sodium salt, the same molecule of interest as used in our study. They also used the same equation that we followed and arrived at a numerical solution to the diffusion coefficient. They used the FRAP technique described above, with some slight alterations, which of most

importance included injecting a fluorescent dye (fluorescein sodium salt) into individual osteocytic lacunae and then visualized them *in situ* beneath the periosteal surface of mouse cortical bone at depths up to 50 μm with laser scanning confocal microscopy[28]. Again, this study used a mouse/rat model, which as stated previously has few osteons and little Haversion remodeling[42]. This study assigned a numerical value to diffusion and is commonly referenced in the subsequent literature. The diffusion coefficient of fluorescein sodium salt (376 Da) was determined to be $3.3 \pm 0.6 \times 10^{-6}$ cm^2/s [28]. They note that this is 62% of its diffusion coefficient in water and is similar to diffusion coefficients measured for comparably sized molecules in cartilage[28]. However, note that this represents diffusion through and within one canaliculi, not across the entire heterogeneous tissue, which contains low porosity. This is not to say transport would be unhindered in a single canaliculi, as this pathway would contain many twists, and obstacles within, including charged ions, and lipids. Of the most important factors listed, lipid interactions could have an significant effect on the transport rate given the structure of the fluorescein sodium salt molecule because it has the ability to capture and hold charged particles, given the biochemistry of a lipid. Temperature would also play a large role in effecting the rate, which was not discussed at length in their study. However, as discussed previously a canaliculi is just one pathway a nutrient can follow in bone, and for our study we will be looking at e radial route possible in a given slice of bone, given a 2-D slice thickness as described in the next section.

To further establish the ambiguity of the Wang *et. al* diffusion coefficient for fluorescein sodium salt, a study released in December of 2010 by Banks-Sills *et al.*. attempted to computationally model the flow of small molecules under loaded conditions using the Wang coefficient[29]. Using a variety of mathematical models to model transport, they found difficulty in accurately assessing the effect of mechanical loading on bone remodeling given the Wang diffusion coefficient[29]. Their model did predict a difference in concentration of nutrients at the bone's edge as they increased strain levels and number of cycles imposed, but not at such a rate as they originally hypothesized[29]. They recommended that "it is desirable to obtain more accurate values of the diffusion coefficient, the molar volume and the ambient concentration of the bone nutrients[29]." This is the purpose of our experiment.

Two other bone diffusivity studies have been published that utilize two approaches that are different from the aforementioned FRAP techniques. The first, conducted by Lang *et al.*, used radioactively labeled glucose to measure diffusion rates. The test tissue of canine femur was placed in a pseudo-diffusion cell, which allowed for a mechanical force to be exerted on the bone sample. They then used a radiotracer, [^{3}H] glucose, and standard liquid scintillation counting techniques[34]. Concentration was measured by determining the number of radioactively labeled glucose molecules that infiltrated the bone tissue sample. They concluded diffusion coefficient in bone tissue would have a magnitude of approximately 3×10^{-9} cm^2/s. The test was also repeated under non-loaded conditions in an identical setup, and they reported no significant difference in

the diffusion coefficient, when compared to the loaded test [34]. Some of the designs flaws of this experiment are as follows. They opted to use a grinder to remove all the peritoneal surface of the bone, which they later mentioned might have blocked some of the pores, and skewed their mathematical model, which is dependent on uniform surface porosity. The maximum length of their study was only 24 hours. Using the scintillation counting technique it would not be possible to measure across large distances. Lastly, their discussion of concentration is only done in cpm/ml, which is a radioactive counting technique of a molecule per ml, never are we given an absolute initial molarity, and it is difficult to correlate their data with a physiological benchmark or specific activity.

Another study conducted by Fernández-Seara *et al.* used a combination or radio-nucleotides and NMR to study diffusion rates. They sought to understand the transport of D_2O, which is a radioactively labeled water, across the mineralized matrix of bone using proton nuclear magnetic resonance spectroscopy and imaging by measuring the diffusion fluxes of tissue water in cortical bone[35]. They used the midshaft of rabbit tibiae as their test tissue, and found the diffusion coefficient to be 7.8×10^{-7} cm^2/s measured at 40°C [35]. Another important observation they made was that they found diffusion rates to be higher close to the endosteal and periosteal surfaces, decreasing toward the center of the cortex, in contrast to most other reports[35]. The rabbit bone structure is again not as suitable as the canine model as it has a dissimilar structure to humans; primarily it has vascular canals running parallel to the long

axis of the bone[42]. The micro and macro structure of rabbit bone is not similar to human bone[42].

In conclusion, there are currently only a few techniques being used to study the rate of diffusion within bone, and the selected technique and animal models vary widely. Most publications discussing the transport phenomena within bone provide vastly different values, and thus it is not uncommon for a paper to state, "The literature reports on quantitative diffusion measurements in bone are sparse[35]." Table 2.5 summarizes the previously discussed diffusion coefficients and the associated experimental techniques, and compares them to the values of the fluorescein sodium salt molecule diffusing in water alone*.

Table 2.1 Summary of all found diffusion coefficients in bone tissue and a comparison of known fluorescein sodium salt and glucose diffusion coefficients in water.

	Diffusion coefficient cm^2/s	Description of area measured	Solute used	Ref
smallest	3×10^{-10}	FRAP methodology entire cortical bone	3000 Da Dye	Patel and Knothe-Tate *et al.*[26]
	7×10^{-10}	FRAP methodology entire cortical bone	300 Da Dye	Patel and Knothe-Tate *et al.*[26]
	3×10^{-9}	Entire femur	glucose	Lang *et al.* [34]
	6.4×10^{-7}	*diffusion of BSA-FITC in a 3% agrose gel	FITC-BSA 66,000 Da	Pluen *et al* .[43]
	8×10^{-7}	cortical bone using radioactive markers	water	Fernández-Seara *et al.*[35]
	3×10^{-6}	FRAP methodology in a single canaliculi	Fluorescein sodium salt 376 Da	Wang *et al.*[28]
	7×10^{-6}	*diffusion in only water (no bone)	glucose	Landolt-Börnstein *et al.*[37]
largest	2.7×10^{-6}	*diffusion in only PBS (no bone)	Fluorescein sodium salt	Periasamy *et. al*[36]

Diffusion coefficients in water

As highlighted in the Table 2.5, there are well-known diffusion coefficients associated with fluorescein sodium salt and glucose diffusing through water. In the case of fluorescein sodium salt in water, a study conducted by Periasamy *et al.*. focused on relating photo-bleaching recovery data to transport phenomena[36]. They mathematically modeled their data and used a fluorescent microscope to aid in defining the unknowns in their complex mathematical model and found that the diffusion of fluorescein sodium salt in PBS (phosphate buffer solution) was $2.7x10^{-6}$ cm^2/s [36]. They felt this number should be considered a benchmark, meaning if one was calculating a diffusion value within a biological tissue or any material that would create a barrier to hinder the rate of diffusion should be lower than the value they calculated[35]. Similarly, another well-regarded study conducted in 1969 by Landolt-Börnstein set the standard for what we use as the diffusion coefficient for glucose in in water, 7.0×10^{-6} cm^2/s [37]. These rates will be used for comparative purposes in our experiment.

2.5 Fluorescence microscopy

One of the crucial components of this experiment is the use of chromophores and fluorescent microscopy. Fluorescent microscopes work by reflecting back a photo emission of light given a particular chromophore. The microscope utilizes a particular cube filter so that only that wavelength of light is seen. For our experiment, we will be using fluorescein sodium salt (376 Da). It is water soluble and in solution it is a salt. Fluorescein sodium salt can be seen in figure 2.5. Its maximum excitation peak is in the blue-green spectrum at 491 nm and its emission peak is in the green at 515 nm[38]. It is known to be one of the most brightly fluorescent low-molecular-weight chromophores known, with a quantum efficiency of 0.9 [38]. These qualities make fluorescein sodium salt a good choice for studying bone diffusion.

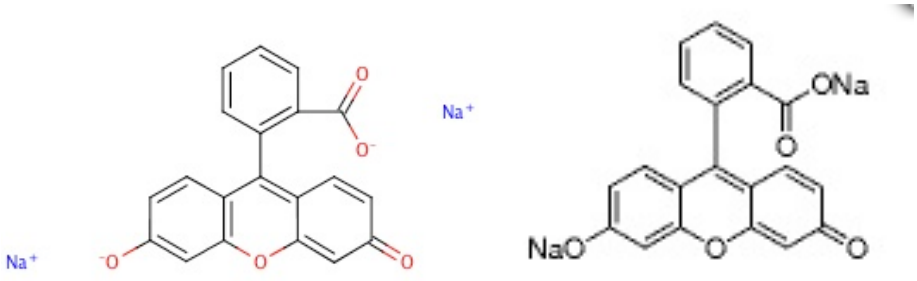

A **B**

Figure 2.5, (A)fluorescein sodium salt in its ionic form in solution and (B) its nonionic form

2.6 Structures of similar molecules that diffuse into bone tissue

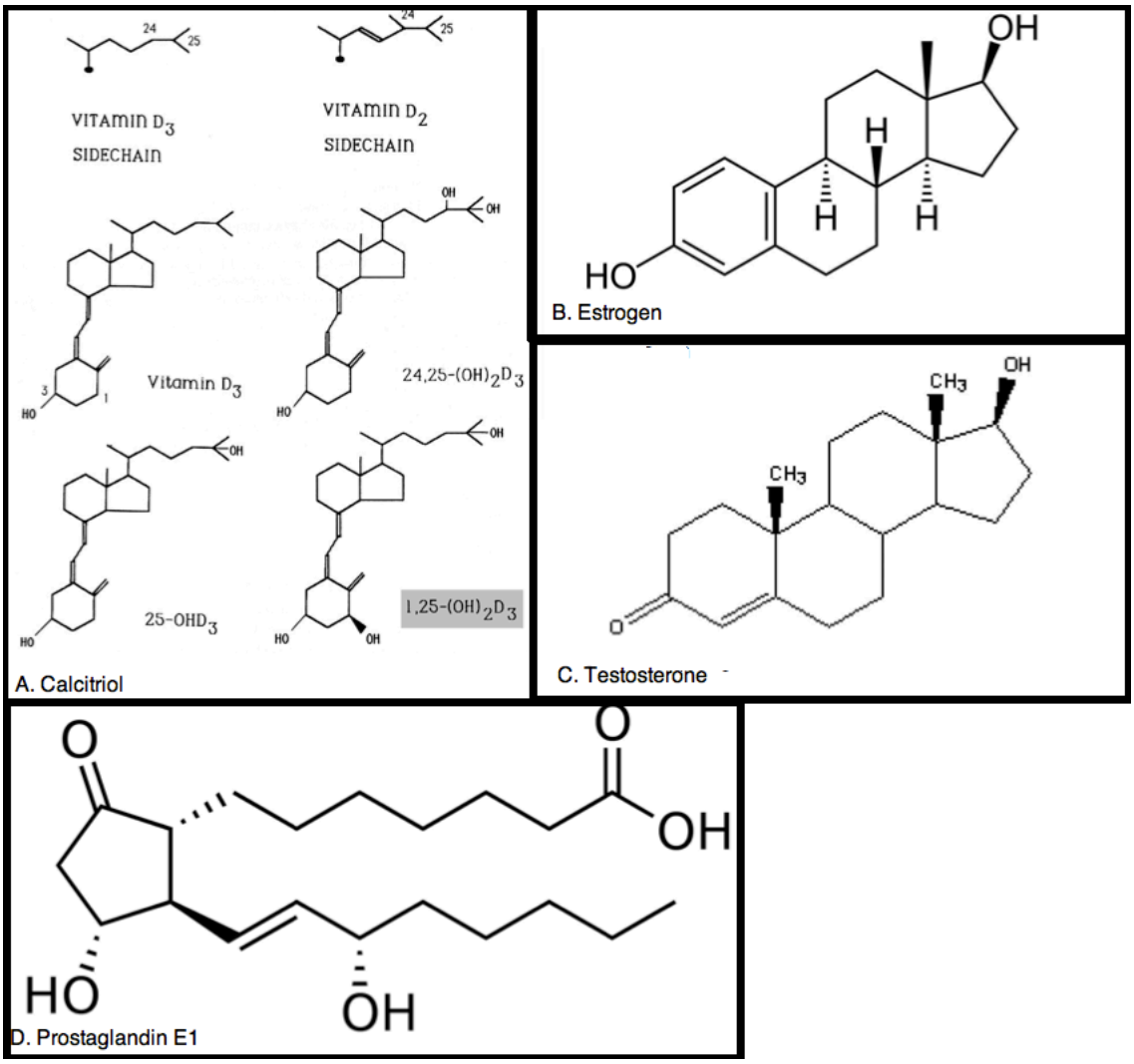

Figure 2.6 signaling molecules with similar properties to fluorescein sodium salt that commonly diffuse into bone. A. Calcitriol (vitamin D) B. Estrogen C. Testosteron D. Prostaglandin E1.

Figure 2.6 shows different molecules with similar chemical properties. While not identical structurally, these molecules all share amphipathic chemistries (miscible in water and organic solvents), including our test molecule, fluorescein sodium salt. Vitamin D (Calcitrol) is derived from a cholesterol derivative and shares chemistry with this family of bile salts. All of the molecules listed shown in figure 2.6 play an important role in maintaining homeostasis in bone. It for this reason, the similar amphipathic chemistries, that we choose

fluorescein sodium salt as an ideal test molecule. Given the environment these molecules will be diffusing through, which has an abundance of lipids and some carbohydrates, it is likely that an amphipathic molecule will become entrapped or slowed down within areas containing high amounts of lipids. We expect to observe this phenomena of dye pooling due to lipid capture in our results, just as the molecules in figure 2.6 commonly pool in bone tissue because of the high lipid content and their own amphipathic biochemistry. To conclude, the reason we choose fluorescein sodium salt as an ideal candidate to test diffusion rates is that it should mimic the biochemical interactions within the bone similar to native growth factors that commonly diffuse in and out of bone routinely in human.

CHAPTER III

METHODS

3.1 Acquisition and preparation of bone samples

Animal Specifications. Bone samples were harvested from sacrificed canine (approximately 25-30 kg body weight) according to the procedures and guidelines outlined by the IACUC conducted by another department at the Cleveland Clinic Foundation in 2007. Upon sacrifice the entire canine tibia, including layers of both periosteal and basal cambium, was dissected from the rest of the animal. Bone marrow was flushed out of the bone with a phosphate buffer saline (PBS). The tibia was then stored in a PBS with 0.05% sodium azide (Sigma) at 4° C. The samples were labeled by year, type of animal, lot number of animal and location of tissue in animal, which for the present work is 07D-151 RIGHT TIBIA.

In-House Production of Bone Beams. After being removed from refrigerated storage, the sample was cleaned a second time. All remaining layers of periosteal and basal cambium were completely removed using only forced

manual rubbing of a sterile towel on the bone surface in conjunction with excessive PBS solution poured onto the bone. This resulted in a sample of bone consisting only of osseous tissue. For a detailed diagram of the bone beam and the slices that were acquired, see figure 4.1 and 4.2. This section will describe the techniques used to produce the visualization seen in those figures. After cleaning, the entire piece of bone was then cut radially into five equal sections, although the section most proximal to the tibial plateau and the section most distal were not used or machined into beams as we sought only to run experiments on the medial sections. This was done using a Labcut 1010 Low Speed Diamond Saw (EXTEC Corp). The blade of the saw was kept wet during the cut with a solution of PBS to avoid dehydration of the samples.

These five sections were then machined into 3 x 3 x 30 mm bone beams using a custom jig built in-house designed specifically for the Labcut 1010 Low Speed Diamond Saw. The jig was a plastic guide-rail that allowed the user to make square cuts on each surface of bone surface. This jig/guide-rail was 3 cm tall and 10 cm long and ran parallel to the blade. The "customizable" part of the jig/guide-rail was that the operator could move it a distance of 1-10 mm from the blade, depending on the length of the sample one wanted to cut. As cuts were being made the blade of the saw was kept wet using a PBS solution. Each large cylindrical section of bone was first cut in an axial fashion so that it had four straight sides, essentially turning the circular section of tibia into a four-sided polygon. This polygon-shaped bone section was then cut again, axially, approximately 3 mm into the bone tissue, producing four long sections

measuring 3 x 12 x 30 mm. It should be noted that these sections contain only the endosteal region of bone, as the jig allowed for the removal of all of the periosteal tissue. Each of these pieces of endosteal bone were then cut into either 3 or 4 bone "beams" depending on the width of the rectangular piece of bone, which ultimately created beams with dimensions of 3 x 3 x 30 mm. Thus the total number of beams produced from each section of bone can be as small as 12 and as great as 20 beams.

Lastly, the upper 2 mm of the 30 mm interior endosteal face of the bone was marked with a biocompatible paint to distinguish it from the posterior 30 mm face (this is the face where endosteal meets periosteal). This is because we will be measuring radial diffusion flowing in the direction from the interior of the bone out radially to the surface of the bone. As stated previously, we discarded two of the five sections, thus approximately 45 total sample beams were machined. Samples were placed into three Falcon tubes containing PBS, grouped according to the original section of bone from which they were machined. They were stored in a 4°C refrigerator until their use in experimentation in PBS and azide.

3.2 Bone Sealing Methodology

Full Encapsulation of a Bone Beam. As the created beams are 3-dimensional polygons, it is necessary to seal off all of the sides except for one axial section, the endosteal face, for the experiment to follow the prescribed mathematical model. We chose to use orthodontic resin (Dentsply) as our sealant, an epoxide

that has been proven in previous experiments to effectively bond to the surface of bone and not leech into porous material. Dentsply is a 2-part epoxide, consisting of a resin powder and liquid hardener. It is commonly used to create orthodontic retainers. A rubber mold was constructed in-house with an open top and closed bottom, with interior dimensions of 4 x 4 x 30 mm. To fully seal the bone, a 1 mm basement layer of resin was first mixed and poured by adding 0.3 g of resin powder and pouring 1 mL of liquid hardener into the mold. This basement layer, which occupied one quarter of the mold, was then allowed five minutes to set, giving it enough viscosity to support a bone beam. Next, a bone beam was placed into the mold and pushed down 0.5 mm into the resin. The bone was then fully encapsulated, all six sides, in the mold by adding 0.2 g of the powder resin and 3 mL of the liquid directly into the mold surrounding the bone. The sample, now fully encapsulated was then allowed to set for a period of 24 hours.

Exposure of the Interior Endosteal Surface. Using a low speed diamond saw (Buehler Isomet), again with PBS as the liquid solvent on the blade, the 30 mm interior endosteal surface to the tibia was exposed. To ensure that all of the dental resin was fully removed and to dismiss the possibility of leeching into the interior of the bone beam, the cut exposing the periiosteal surface was made approximately 0.2 mm into the bone. This created a discarded bone beam with dimensions of .2 x 3 x 30 mm and a target beam with dimensions of 2.8 x 3 x 30 mm, with 5 of 6 six sides fully sealed and one side--the interior endosteal

surface--open. The sample was then re-soaked in sterile PBS and left at 4°C for 24 hours to ensure proper hydration.

3.3 Preparation of Diffusion Solution

PBS solution was prepared by dissolving 16 g of NaCl (Fisher), 0.4 g of KCl (Sigma-Aldrich), 2.88 g of Na_2HPO_4 (Sigma-Aldrich), and 0.48 g of KH_2PO_4 (Sigma-Adlrich) in 1600 ml of deionized H_2O. The pH was then adjusted with HCl to 7.4, and 400 mL more of H_2O was added, bringing the total volume to 2 L. This was then aliquoted into two 500ml amounts, then four 225 mL amounts. Next, 0.564 g of fluorescein sodium salt (Sigma-Aldrich Lot# 0001440598) was dissolved into the 500 ml PBS, creating a 0.003 M solution of fluorescein sodium salt/PBS. Several dilutions into PBS were then done, staring with the 0.0003 M solution, and ending at a solution of 3×10^{-7} M. This final fluorescein sodium salt/PBS solution was then autoclaved (Steris Amsco Lab 250) for 90 minutes to ensure sterility. The bottle was then wrapped in aluminum foil to prevent light damage to the fluorescein sodium salt, and stored at 4°C until it was needed for use.

3.4 Incubation with dye

Diffusion experiments were conducted in sterile covered polystyrene six-well plates (Falcon) incubated (Forma Scientific No. 3159 single-chamber) at 37°C and 5% CO_2 in 95% air humidified atmosphere.

Controls consisted of incubating the bone samples in PBS without fluorescein sodium salt. One control from each of the 3 tibial sections was incubated for 18 hours. The sample was completely immersed in the solution and placed in the incubator. The main purpose of this set of data was to gather a baseline number for bone auto-fluorescence per section. These tissues were then immediately prepared for imaging.

Experimental trials took place concurrently with the control trial with the same set of standards described above. All sealed bone beams were placed with the exposed surface parallel to the base of the well and fully submerged in the fluorescein sodium salt/PBS solution. Note that in these trials samples were placed in a solution of fluorescein sodium salt/PBS, not just PBS. This data was allowed to diffuse for a period of 18 hours. These tissues were then immediately prepared for imaging.

Previously described technique for the 18 hour sample was repeated for a 30 hour trial. The one exception was the start time of incubation was delayed roughly 1 hour after the 18 hour samples were incubated; this was done to minimize the time between removal from the incubator and imaging.

3.5 Slide Preparation for Imaging

***Cutting technique*.** Upon removal from the incubator, bone beams were immediately sectioned off into slices that could be mounted onto microscope slides, using the low speed diamond saw (Buehler Isomet), perpendicular to the 30 mm exposed surface that diffusion had occurred through. Again, the saw was

operated with the blade constantly moistened by PBS. To successfully image these pieces, they needed to be as thin as possible (less than 500 microns). Samples were prepared at Cleveland State University, and transported 4 miles to the Cleveland Clinic for imaging. The dimensions of these slices were 3 mm x 2.5 mm x 250 μm. The cutting technique is visually represented in figure 4.1

For each of the beams that were diffused, five random cross-sectional slices were taken as described above. No slices were obtained from the two outermost 5 mm portions of the 30 mm bone beams (slices were only taken randomly from the inner 20 mm portion of the beams). To create these slices, two cuts were made by the low speed diamond saw. The first cut was made to isolate the target portion of the bone and remove the excessive material. The second was made 200 μm directly behind the first cut, producing a slice of 200-250 μm thickness. This process was then repeated at any given estimate of 1 to 5 mm away from the first cut. Ultimately this was done five times, producing five cross section slices to be imaged.

Only 3 slices were taken from each of the control beams. This was done to expedite the mounting process and begin the imaging process one hour after removal from the incubator.

Mounting technique. After the thin slices were created from the bone beam a lead pencil was used to lightly mark the edge that diffusion had occurred from, as this would provide a reference point during imaging. Using forceps the slice of bone was placed on a superfrost microscope slide (Cole Palmer 75 x 25 x 1.0

mm). To adhere the bone to the surface of the slide, a small amount (< .01 ml) of biocompatible, non-fluorescent adhesive, cyanacrolate, was used (loctite™). All five slices were mounted to the slide and let sit for two minutes. Vectashield Hardset ™ (H-1400, Vectalabs) was then added in excess (3-6 mL) around and on the five slices, and a cover slip (Cole Palmer 22 x 22 mm #1) was placed on top. Note that one coverslip was used to cover all five slices of bone. The slide was then marked based on the time allowed for diffusion and section of bone from which the slices were derived. The slices were positioned on the slide such that the diffused edge was positioned facing the left edge of the slide. There were a total of seven slides: five diffused samples on each of six slides, and the six control samples on the seventh slide. As stated previously the times of incubation were staggered by one hour to minimize time between being taken from the incubator and imaged. Sample mounting was completed within 1 hour of removal of the bone from the incubator. Imaging took 3 hours including travel to the Cleveland Clinic, setup of parameters on the scope, calibration of exposure time and image intensity, and actual time to image a sample. Because of the staggering of removal times of the 18 and 30-hour samples, all images were taken within 4 hours (from the time of removal from the incubator), and control samples imaged within 4.5 hours.

3.6 Image Acquisition using the Robotic-Stage Microscope

All images were acquired using a robotic stage fluorescent microscope at the imaging core facilities at the Cleveland Clinic. The hardware specifications

are as follows; a Leica DM4000B microscope was used fitted with a QImaging Retiga 2000R CCD Camera, res of 0.74um/px at 10x bin 1, with Image-Pro Plus 7.0 as the software/montaging package. The microscope, camera and mercury bulb were powered on and allowed 15 minutes to warm up. During this warm up time all of the slides were loaded onto the robotic stage and the camera mode was switched to MONO from the standard color acquisition. Large field of view acquisition macro tab was selected, and the program was told to capture 36 images. The acquisition mode was set to fluorescence and the filter was changed to the FITC cube. A 10X objective lens was used. The camera binning was set at 2 x 2, the gain at 8 and the exposure time at 25 ms. The scan dimensions, both X and Y, were then defined for all 36 samples. This was accomplished by moving to all four of the outer edges of each bone sample and saving the coordinates into an Excel file. Included in saving all of the coordinates were five predictive focus points, meaning changes in the Z axis (focus) based on the surface topography of the bone slice, with the aim to better enhance clarity of the photos. Photos were saved as large single uncompressed images using the TIFF format, each file size being roughly half a gigabyte. These images were montages, meaning that they were a single image that is made up of multiple non-overlapping images stitched together. The ranges of the number of photos in the montages were 4 x 4 (minimum) to 5 x 7 (maximum). A removable storage directory (portable hard drive, 8 Gigabytes) was used to store all of the images. Bright field color, exposure time and gain were kept the same for all images. The total time taken to scan all of the images was approximately 30 minutes. Additional scans were

taken at different exposure times and gain settings, including 20 ms with a gain of 3, 50 ms with a gain of 6, and 100 ms with a gain of 2. However, the lower exposure times resulted in images that were too dim, not producing a visible image. The higher exposure time produced images that were too bright, or "washed out," and the data pooled from these would be unreliable. After images were taken the mounted bone slides were placed in a slide case (Fisherbrand 12-587-10) and placed in a 5°C refrigerator.

3.7 Image analysis

ImagePRO Preliminary analysis. Before any images were analyzed, global threshold in all images was removed using JASC Paint Shop Pro (ver 9.0). The program has an inherent function that separates the various photo "layers." In this case we wanted the background to be solid black because solid black would register a 0 on a gray scale pixilation scale, which extends from 0-255 (8 bit). The raw photos taken on the robotic scope using Image Pro Plus contain some pixilation and noise surrounding the pieces of bone. Most of these were due to either a mounting error which created an air bubble in the Vectasheild™, or the Vectashield™ itself becoming slightly fluorescent and displaying a small signal (< 5 greyscale). These rendered photos had no image processing done on the actual 2 x 2 mm bone fragment; rather they created a central image that immediately transitions into a solid black background. All photos can be seen in the discussion section, in compressed format to fit the page. A select number of less compressed images can be seen in Appendix D.

Each rendered photo was then uploaded back into Image-Pro Plus. A preliminary line profile analysis was performed on each image (a built-in function of Image-Pro Plus). The line profile analysis outputs the fluorescent intensity (0-255) across the sample; it also gives the option to perform a thick profile plot across a horizontal band within the sample. The thick line plot averages all the values across the sample, which is useful in estimating how the sample performed as a whole. The output of this function is a graph of intensity versus distance in pixels as show in figure 3.1.

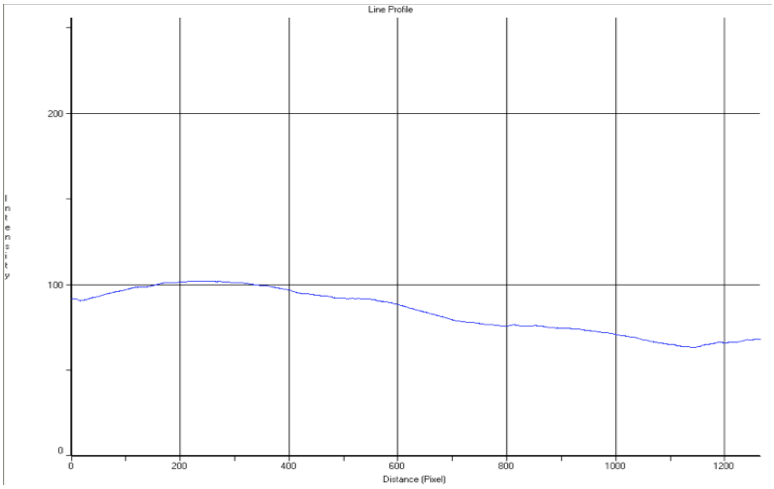

Figure 3.1. Preliminary thick-band line profile plot created by Image-Pro to validate transport of fluorescein sodium salt. The left side of the sample (pixel distance 0) represents the open edge of the tissue sample, and the right (pixel distance 1250) repents the sealed exterior edge.

This quick built-in Image-Pro function was used as a quick evaluation. This data was only used as a means to observe a general trend in each graph, which was then comprehensively examined by our MATLAB functions.

Matrix Conversion. To quantitatively analyze each image it was necessary to convert each image to a matrix. The number of elements in the matrix was the same as the number of pixels in the image. Each element carried a numerical

value in the range of 0 up to 255. As stated previously a value of zero would corresponds to absolute black, and a value of 255 corresponds to a maximum over-exposed image.

Matrix conversion was also performed in Image-Pro Plus. While in the "bitmap analysis" command within the "measure" menu one can select to save the image as a .BIT file. It is also possible to sample the pixels in the image to reduce the size of these large matrices. In our case we chose for the program to sample e 10 pixels, thus the 5000 x 5000 pixel image was sampled down to roughly 500 x 500 pixels. Remember the size of the matrix directly corresponds to the number of pixels in the image, and thus by sampling we reduced our data points down by a factor of 100 (2.5×10^7 elements to 2.5×10^5 elements). These files were stored as .bit data files and named identically to the corresponding image.

Conversion from .bit files to Excel files. The .bit files were then opened in MATLAB (R2010a ver 7.10) and viewed within the "command" window. As stated previously, these matrices were all roughly 500 x 500 elements, however we are only concerned with the central 300 x 300 matrix. The images converted into matrices had a lot of black space (0 values) surrounding the central bone, whereas our data analysis requires matrices containing values only from the bone sample. Since all 36 images had different locations within the large photo montage, one must manually locate the four corners of that bone fragment and enter the element values that correspond to those corners into an already

created MATLAB code. This code then cut out that central matrix and saved it as a Microsoft Excel file. Files were saved in Excel format because Excel has a better user interface to view and manually manipulate the files. We needed to set the first column as the "start" row. The bones were not perfect 90° angled squares, most of them actually had angled starting columns, meaning the "cut" matrix would still contain imperfections. For example row 1 may have 0 values for the first 12 columns and row 500 would start immediately with an integer value. If matrices were left and data was analyzed in this fashion, row 500 would have a head start over row 1, and that could have severe consequences in the diffusion coefficient when showing a diffusion gradient over 2.5 mm. Thus, the operator adjusted all rows manually by copying and pasting individual rows so they started at their first absolute value. All 0's cut out at the beginning of each row were pasted at the end of the row to ensure that one would still create a uniform matrix with integer values throughout. This process was repeated for all 36 samples. These fully rendered matrices were saved as .xls files and named identically to the .bit files.

3.8 Summary of MATLAB operations

MATLAB Acquisition of Auto-Fluorescent Values. To determine the average intensity of auto-fluorescence in each bone sample, the six control samples were uploaded into MATLAB using the "xlsread" function. After being uploaded, a FOR-loop was manually written to calculate the average of all non-zero values in the matrix. Zero values were excluded for the same reasons cited previously,

that they are non-representative of the tissue sample. Because there were two control samples per section of bone, this entire process was repeated for the second sample from the section, and the two values were then averaged. This was repeated for the other two sections of bone, and three total auto-fluorescent values were obtained, corresponding to the three experimental sections of bone. These values can be found in table 4.1. Auto-fluorescent values were subtracted from the entire matrix to give a signal that only represents the fluorescein sodium salt signal. Appendix C contains the custom MATLAB code that accomplished the task described above.

MATLAB Curve-fit and graphical output. Upon the conversion and rendering of the images into concise Excel spreadsheets and the subtraction of all auto florescent values, MATLAB was used to curve-fit the data to the model equation. Each bone sample matrix was broken into five quadrants, resulting in five separate diffusion coefficients per sample. Due to the length in the explanation behind the setup and math in the code, a lengthy discussion on this topic can be viewed in Appendix A, including the actual code used. To be brief, lets assume that the matrix produced by one sample had 250 rows and 250 columns where columns represent a distance into the tissue. Breaking it into 5 quadrants produces 5 matrices with height of 50 and a length of 250. Focusing now on one of these quadrants, we averaged all non-zero values in the height, producing a matrix of height 1 and length 250 (a vector). Five of these matrices were created per tissue sample (a schematic of the bone quadrants can be seen in figure 4.2). Then, using this experimental data, we were able to fit to the transport model

described in the next section using the method of the least sum of the squares. The transport model calculates the concentration as a function of distance, time, and diffusion coefficient. The value of the diffusion coefficient varied from 1 x 10^{-4} to 1 x 10^{-11}, and these numbers were compared to the experimental concentration using the following sum of the squares equation (SSE).

$$\sum_{i=1}^{250}(experimental\ concentration - theoretical\ concentration)^2 \quad (2)$$

The "best fit" for the diffusion coefficient will correspond to the smallest sum of the squares value. Lastly, the program produced a plot of experimental vs. "best fit" theoretical concentrations, with distance on the x-axis and light intensity on the y-axis. Again, a detailed explanation of the code, including the specifics of how it fit to the transport model is in appendix A.

3.9 Transport Model

Our transport model was derived with the aid of on the calculations found in Truskey et al.[15] . The experimental bone tissue is rectangular with thickness L. The fluorescent concentration within the sample is represented by C_i, and C_1 is a function of position and time. At time equal to zero, the surface y = 0 were raised to a concentration of C_1. Conservation of mass for one dimensional unsteady diffusion will apply, assuming reaction and convection do not occur:

$$\frac{\partial C_i}{\partial t} = D_{ij}\,\frac{\partial^2 C_i}{\partial y^2} \quad (3)$$

With the following initial boundary conditions:

(1) $0 \leq y \leq L$, $t \leq 0$, $C_i = C_0$

(2) $y = 0$ $t \geq 0$, $\frac{\partial C_i}{\partial y} = 0$

(3) $y = L$ $t \geq 0$ $C_i = C_1$

Whereas, C_i is the concentration found in tissue at a given position (intensity 0-255), C_1 is the concentration at the surface immersed in solution, (light intensity 0-255), C_0 is the initial concentration in tissue (intensity 0-255), y is the distance from the exposed face (cm), L is the total length of sample, (approximately .28 cm), t is time (s), and D_{ij} is diffusion coefficient ($\frac{cm^2}{s}$). Light intensity is easily substituted for concentration as the two measurements are linearly related, as if you increase the amount of the FITC dye, you will increase the number photo emission recorded in the microscope, which is discussed in section 2.5. For a more detailed explanation of where exactly C_0 and C_1 are read from in the image see Appendix A. We then generalize the solution to the problem by altering it into dimensionless form:

$$\theta = \frac{C_i - C_0}{C_1 - C_0}, \qquad \eta = \frac{y}{L}, \qquad \tau = \frac{t\, D_{ij}}{L^2}$$

Restating the equation 2 with the new dimensionless variables gives the following:

$$\frac{\partial \theta}{\partial \tau} = \frac{\partial^2 \theta}{\partial \eta^2}$$

(4)

With the new set of boundary conditions:

(1) $0 \leq \eta \leq 1$ $\tau \leq 0$ $\theta = 0$

(2) $\eta = 0$ $\tau \geq 0$ $\frac{\partial \theta}{\partial \eta} = 0$

(3) $\eta = 1$ $\tau \geq 0$ $\theta = 1$

Applying separation of variables, both boundary conditions need to be homogenous, which can be done with the aid of equation 4.

$$\theta'(\eta, \tau) = 1 - \theta(\eta, \tau)$$

(5)

Equation 3 now becomes

$$\frac{\partial \theta'}{\partial \tau} = \frac{\partial^2 \theta'}{\partial \eta^2}$$

(6)

And also its boundary conditions changes to the following:

(1) $0 \leq \eta \leq 1$ $\tau \leq 0$ $\theta' = 0$

(2) $\eta = 0$ $\tau \geq 0$ $\frac{\partial \theta'}{\partial \eta} = 0$

(3) $\eta = 1$ $\tau \geq 0$ $\theta' = 1$

Equation 5 can now be solved via the method of separation of variables, with the solution in the form of $\theta'(\eta, \tau) = X(\eta)T(\tau)$. Substituting this solution form and rearrangement of terms yields:

$$\frac{1}{T}\frac{dT}{d\tau} = \frac{1}{X}\frac{d^2X}{d\eta^2} \tag{7}$$

The left-side of equation 6 is a function only of τ and the right is a function only of η, thus they both must be equal to a constant called $-\lambda^2$. This value is negative to ensure concentration decreases with time and has a limit. The equation now becomes:

$$\frac{d^2X}{d\eta^2} = -\lambda^2 X \tag{8}$$

$$\frac{dT}{d\tau} = -\lambda^2 T \tag{9}$$

The solution of these two equations is

$$\theta' = XT = (A \sin(\lambda\eta) + B \cos(\lambda\eta)) \exp(-\lambda^2 \tau) \tag{10}$$

And applying the boundary conditions at 0

$$\left.\frac{\partial\theta'}{\partial\eta}\right|_{\eta=0} = 0 = \lambda(A \cos(\lambda\eta) - B \sin(\lambda\eta)) \exp((-\lambda^2)\ \tau) \mid_{\eta=0} \tag{11}$$

For η = 0, the sine term is 0, however the cosine term is unity, thus A must also equal 0 to satisfy this boundary condition, reducing the equation to

$$\theta' = B\ \cos(\lambda\,\eta)\exp(-\lambda^2\,\tau)$$

(12)

At, η = 1, θ' = 0. If B were equal to zero, then there would mathematically be no change in concentration. On the opposite end of the spectrum, the cosine term is zero when λ is integer value multiplied by $\frac{\pi}{2}$. Mathematically we represent this by the following equation:

$$\lambda = \left(n + \frac{1}{2}\right)\pi \quad where\ n = 1,2,3\ ....$$

(13)

This can be substituted into equation 11, yielding the following equation:

$$\theta' = \sum_{n=0}^{\infty} B_n\ \cos[\left(n + \frac{1}{2}\right)\pi\,\eta\,]\ \exp\,[-\left(n + \frac{1}{2}\right)^2\ \pi^2\tau]$$

(14)

The B_n is evaluated from the initial conditions stated previously, as well as the orthogonality relation of the cosine function over the domain [0,1]. At time $\tau = 0$,

$$1 = \sum_{n=0}^{\infty} B_n\ \cos[\left(n + \frac{1}{2}\right)\pi\eta]$$

(15)

And to keep the orthogonality condition, both sides of the equation are multiplied by $\cos\left[\left(m + \frac{1}{2}\right)\pi\,\eta\right]$ and integrated from $\eta = 0$ to $\eta = 1$, thus giving

$$\theta' = \sum_{n=0}^{\infty} B_n\ \cos\left[\left(n + \frac{1}{2}\right)\pi\,\eta\right]\exp\,(-\left(n + \frac{1}{2}\right)^2\ \pi^2\,\tau$$

(16)

Evaluation through integration from 1 to 0 of the B_n term yields the following

$$B_n = \frac{2\,(-1)^n}{\left(n+\frac{1}{2}\right)\pi} \tag{17}$$

And lastly substituting this into equation 14 and 15 yields the final equation for one-dimensional unsteady diffusion in a finite medium using rectangular coordinates.

$$\theta = 1-\theta' = 1-2\sum_{n=0}^{\infty}\frac{(-1)^n}{(n+{}^1\!/_2)\pi}\cos\left[\,(n+{}^1\!/_2)\pi\,\eta\,\right]\exp\left[-\,(n+{}^1\!/_2)^2\,\pi^2\,\tau\right] \tag{18}$$

3.10 Evaluation of transport model for diffusion in an infinitely long medium

If one assumes the medium of diffusion to be infinitely long, a simplified result of equation 17 is reached, given by[15]:

$$\theta = 1-\frac{2}{\sqrt{\pi}}\int_0^{\eta} e^{-z^2}\,dz \tag{19}$$

where all variables represent the same values previously stated in section 3.10. This concept of diffusion in an infinite medium is assumed to be valid only if[15] :

$$t < \frac{L^2}{36\, D_{ij}} \tag{20}$$

Where t is the total time allowed for diffusion.

Based on the experimental conditions of L ≈ 0.28 cm, t ≈ 18 hour or 30 hours, this assumption is only valid if D_{ij} < 2.01 x 10^{-8} cm^2/s. Given the large variability of the previously found D_{ij}, noted in table 2.5, it was decided that the more rigorous solution, equation 17, was needed.

CHAPTER IV

RESULTS AND DISCUSSION

4.1 Introduction

The following sections will present the data obtained for each sample of bone tissue. Before we begin discussing the data obtained, it is necessary to briefly summarize the terminology used. Each section of bone, as show in in figure 4.1a is marked as “section-#”. Three beams were taken from each section. Individual cross section histological bone piece as “sample-#”, the data averaged within each of 5 quadrants is denoted as “quadrant-#”. To review from chapter 3, from each section three samples of control were taken, five samples of experimental data for each period of diffusion, and two periods of diffusion used, 18 hours and 30 hours. It should be noted that the displayed images are highly compressed to fit in this paper, and thus some of the details of the photographs, including canal structure and visual intensity are greatly reduced.

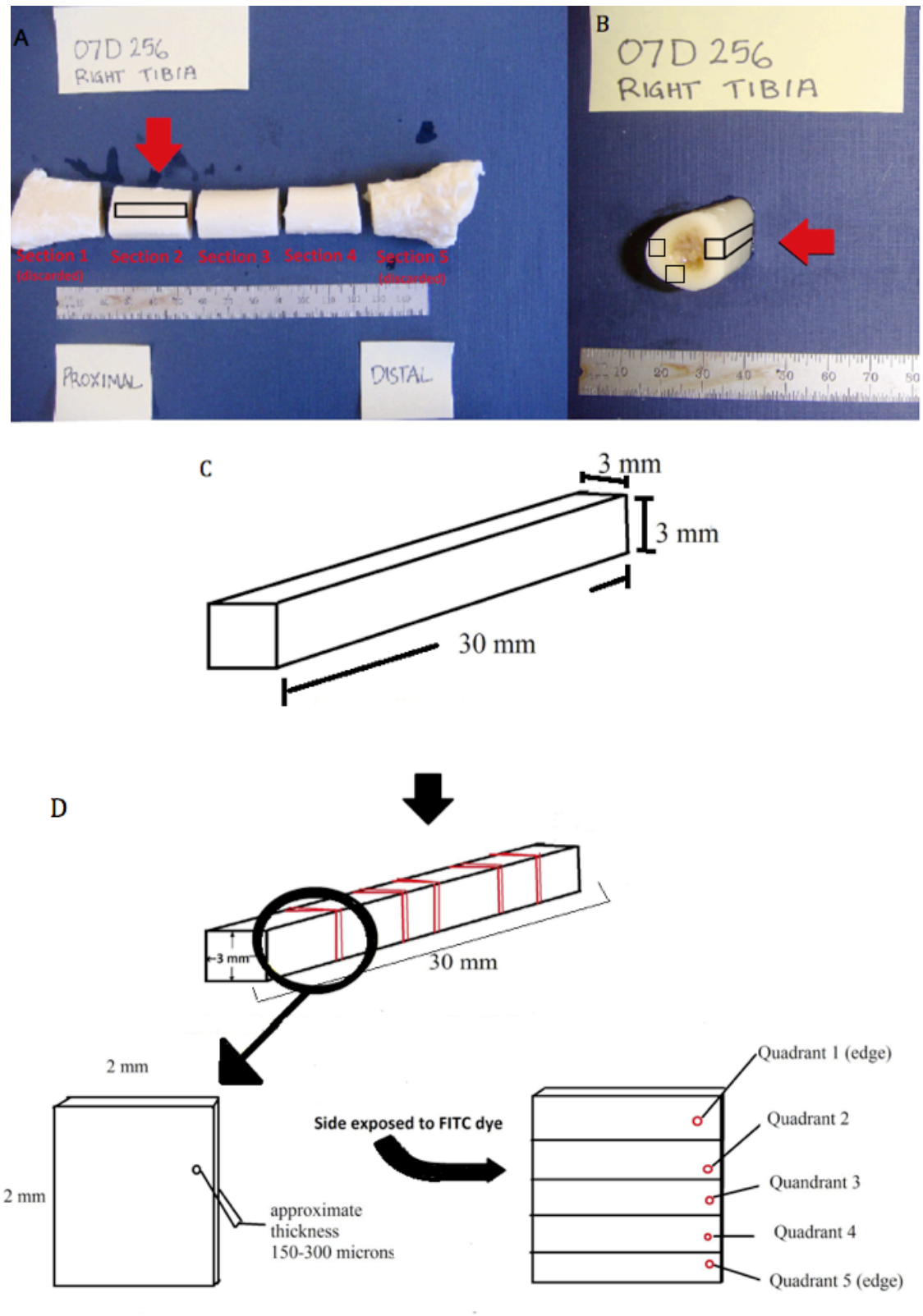

Figure 4.1 (A) (B) Labeling of bone "sections" and visual description for how bone samples were cut (C) Dimensions of the resulting bone beam. (D) Beam is cut into five "samples" and the result of those five trials is a slice of bone, that is then divided into 5 "quadrants"

4.2 MATLAB outputs

As stated in the methods section, each quadrant produced an average concentration profile that was analyzed via a curve-fitting program created in-house using MATLAB, and the predicted concentration profile given by equation 17. The diffusion coefficient values that minimized the sum of the square for each quadrant are shown for each sample. Figure 4.3 is a good example of a curve fit produced by MATLAB.

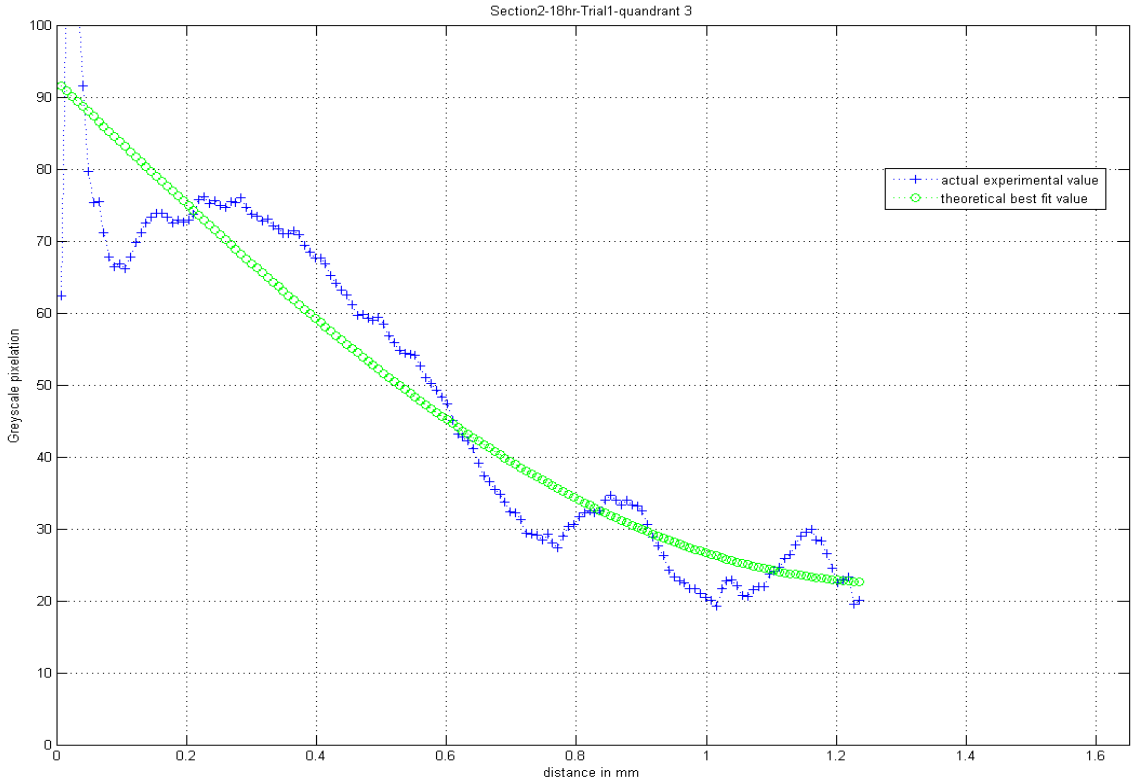

Figure 4.2 Comparison of best-fit curve from equation 17 (green) compared to the experimental data (blue). Note that auto fluorescence was subtracted off before calculations were made. The SSE value for this fit was 8,178

As stated in the literature review, cortical bone tissue has low porosity, and the canal system is not well connected, thus the dye tended to pool as it

became stuck diffusing through the material. In some samples, large pools of dye were evident, perhaps due to the lack of connectivity of the canal system further downstream from the diffusion front, or for the lipid content in the bone slowing down FITC diffusion, as discussed in section 2.6. Figure 4.4 is an example of this type of data, along with a best fit curve.

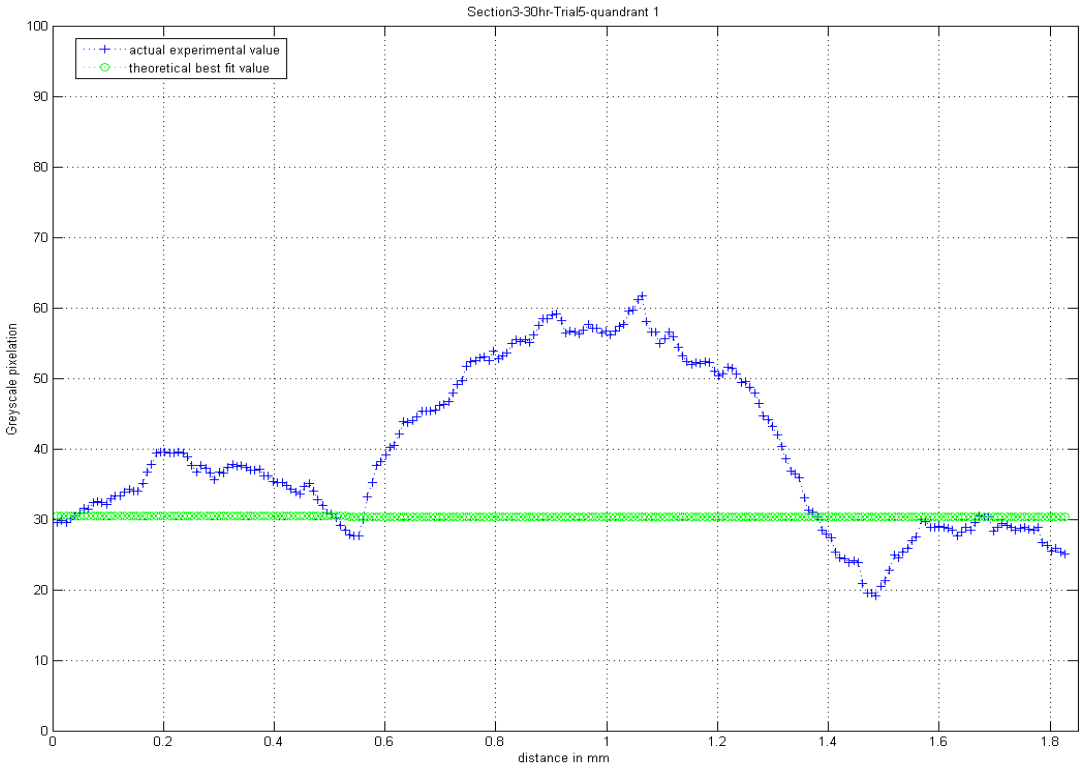

Figure 4.3 MATLAB poorly produced best fit curve for experimental values (blue) to theoretical (green). Note that auto fluorescence was subtracted off before calculations were made. The SSE value for this fit was 47,805

Two observations can be with this example; the first is the poor fit between the model and the data, which results in a high SSE, and the second is the program always converged to the same value 1.0 x 10^{-6} cm^2/s. These quadrants of data were considered not measurable and were not considered in the final data analysis and calculations. In the subsequent discussion per sample,

we will highlight this phenomena labeling this ouput as NM (non-measurable). We will include the SSE, and a reference bar on each graph exceeding the other measurable values.

4.3 Diffusion Data

Introduction

Given the large amount of data acquired, the organization of this section will be in the following format. We will discuss the given control value first, that being the value that is subtracted from all graphs as auto-fluorescence within the bone. We will then present the data acquired from section 2, running through each sample (1-5), first showing the 18-hour incubation data, and then the 30-hour incubation data. This same scheme will be repeated for section 3. We will then present the data as a whole, comparing sections and then comparing times. Lastly we will discuss section 4 qualitatively, as the data from this section failed to produce a signal above the auto fluorescence signal.

Control data

The control data was obtained as a way to gauge the auto-fluorescence of the bone. It was subtracted off of all experimental data that was acquired from the same section of bone. Table 4.1 summarizes the auto-fluorescence values acquired from each section. One can notice a broad pattern of auto-fluorescence, that being it ranged from roughly 30-50 (greyscale).

Table 4.1 Average auto fluorescent values of bone samples by section.

Section of bone	Auto fluorescence value (grey-scale value 0-255)
2	33.28 ± 11.16
3	36.86 ± 15.71
4	50.67 ± 1.72

Section 2, 18 hours diffused

Section 2, Sample 1, 18 hours diffused

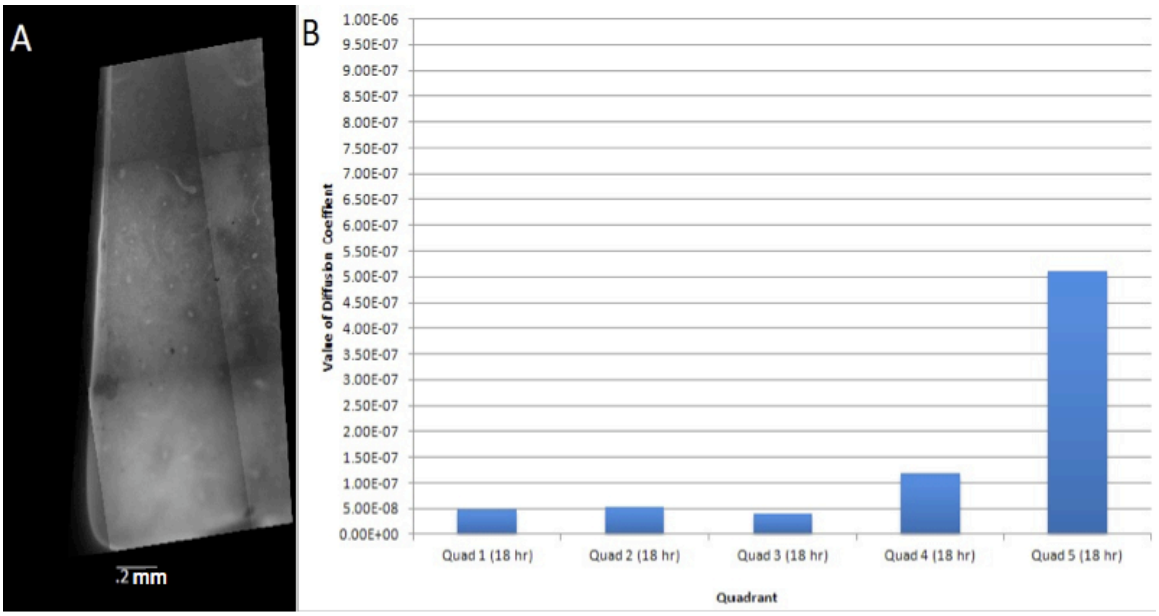

Sample 1	Diffusion coefficient cm^2/s	Sum of squares
Quad 1 (18 hr)	4.91E-08	12,435
Quad 2 (18 hr)	5.36E-08	10,667
Quad 3 (18 hr)	4.00E-08	8,178
Quad 4 (18 hr)	1.18E-07	21,554
Quad 5 (18 hr)	5.09E-07	75,794
Average	1.54E-07	
StDev	2.01E-07	
St error	8.98E-08	

Figure 4.4 (A) Image of the bone slice. (B) Comparison of the diffusion coefficient for each quadrant. Values of the diffusion coefficient reported in cm^2/s. Results in table correspond to this sample.

For this trial, the image was slightly overexposed, however it still produced viable data. The diffusion coefficients are fairly consistent with one another. The sum of the squares for quadrant 2 and 3 is low comparatively, however this sample had some of the highest SSE numbers when compared to the other 18 hour samples. Quadrant 5, with an SSE of roughly 75,000 is considerably higher then any other quadrant across the board, leading to possibility edge effects in the montaging. But, because the MATLAB code did not converge on a non-measurable value, this value is kept for the final evaluation. The other quadrants in this sample produced data within the range we suspected, that being lower then diffusion of PBS in water ($2.7x10^{-6}$ cm^2/s).

Section 2, Sample 2, 18 hours diffused

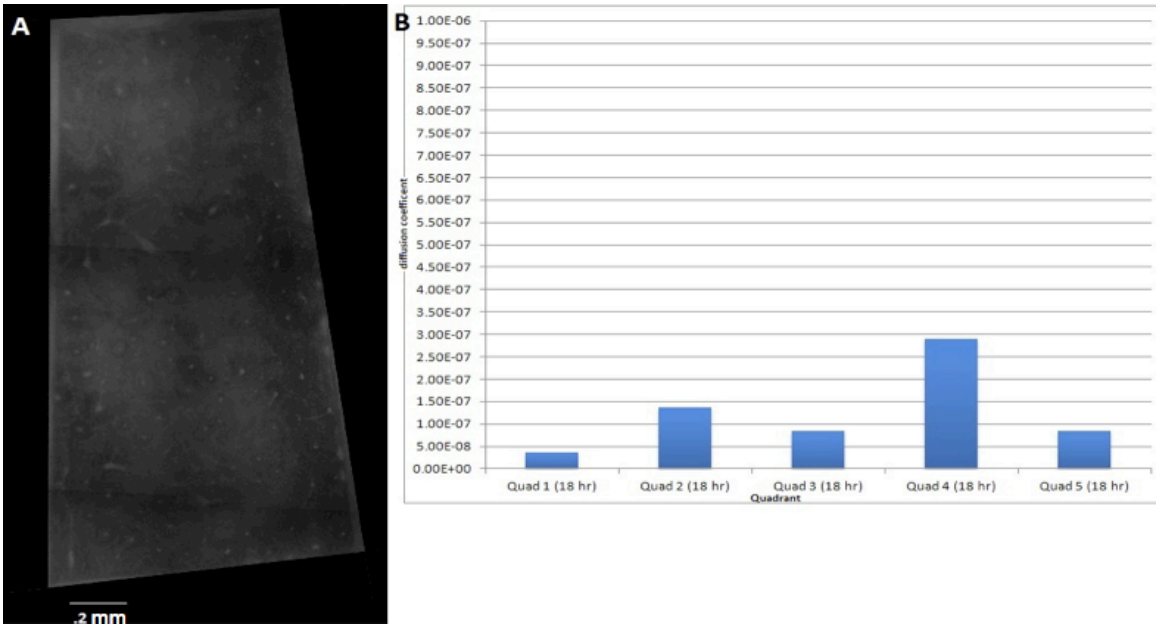

Sample 2	Diffusion coefficient cm^2/s	Sum of squares
Quad 1 (18 hr)	3.73E-08	3,693
Quad 2 (18 hr)	1.36E-07	2,824
Quad 3 (18 hr)	8.45E-08	1,961
Quad 4 (18 hr)	2.91E-07	1,813
Quad 5 (18 hr)	8.45E-08	767
Average	1.27E-07	
StDev	9.82E-08	
St error	4.39E-08	

Figure 4.5 (A) Image of the bone slice. (B) Comparison of the diffusion coefficient for each quadrant. Values of the diffusion coefficient reported in cm^2/s. Results in table correspond to this sample.

This trial produced positive results due to almost seamless montaging. Within the image one can clearly see the canal system with the bone. Visually one can notice the radial canals appear to be connected, and the dye did not pool in any of the larger Haversian canals, as each Haversian canal appears as a bright dot, surrounded by darkness, not a large pool of faded light (higher resolution image included in appendix D). As one looks across the tissue, one can notice particular areas into which no dye diffused, and other areas that are well lit up, which is the expected pattern, as some areas are connected, and others are isolated. This particular trial produced some of the best possible data, as evidenced by the low SSE values, and the concentration curve shown in figure 4.2 for quadrant five of this sample.

Section 2, Sample 3, 18 hours diffused

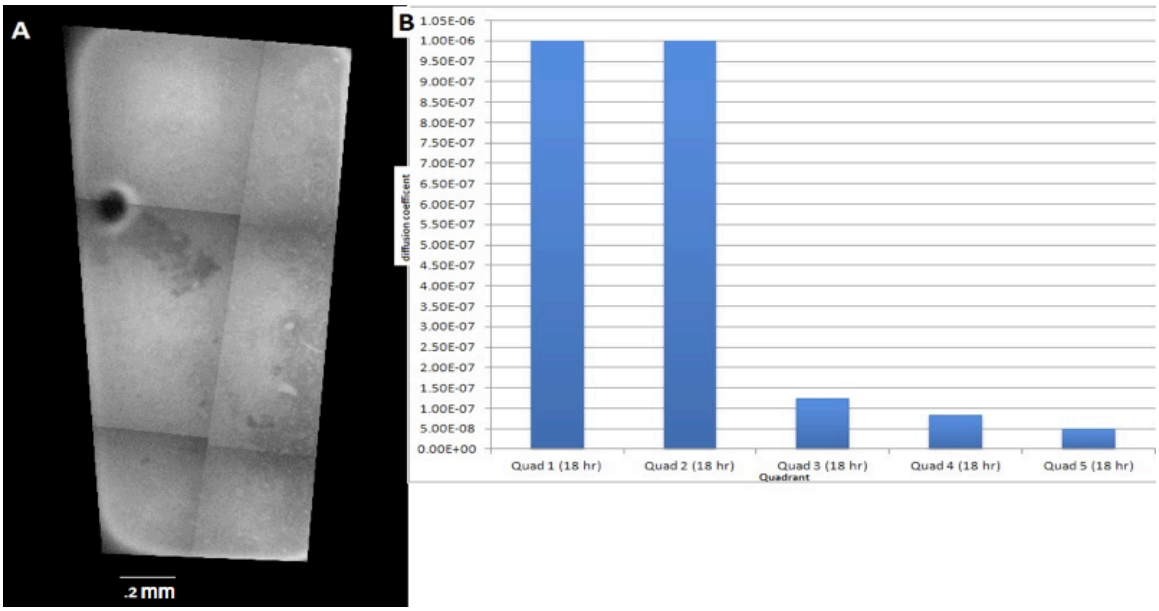

Sample 3	Diffusion coefficient cm^2/s	Sum of squares
Quad 1 (18 hr)	NM	55489
Quad 2 (18 hr)	NM	35,084
Quad 3 (18 hr)	1.25E-07	73,688
Quad 4 (18 hr)	8.47E-08	94,648
Quad 5 (18 hr)	4.96E-08	101,272
Average	8.64E-08	
StDev	3.76E-08	
St error	2.17E-08	

Figure 4.6 (A) Image of the bone slice. (B) Comparison of the diffusion coefficient for each quadrant. Values of the diffusion coefficient reported in cm^2/s. Results in table correspond to this sample. NM represents a non-measurable region.

For this trial, we see the image was washed out, meaning that the fluorescence was near the upper limit of 255, and the viewer is unable to distinguish features within the sample. Additionally there is a large air bubble within the data that skewed the results. To further complicate matters the flatness of the field of image montaging was done poorly, which again creates sharp peaks at the points where the photos are placed together. That being said, the upper quadrants produced results that were non-measurable, and thus are

not included in the summary data. However, the lower quadrants did produce values in the expected range, and the data from this trial is still valid.

Section 2, Sample 4, 18 hours diffused

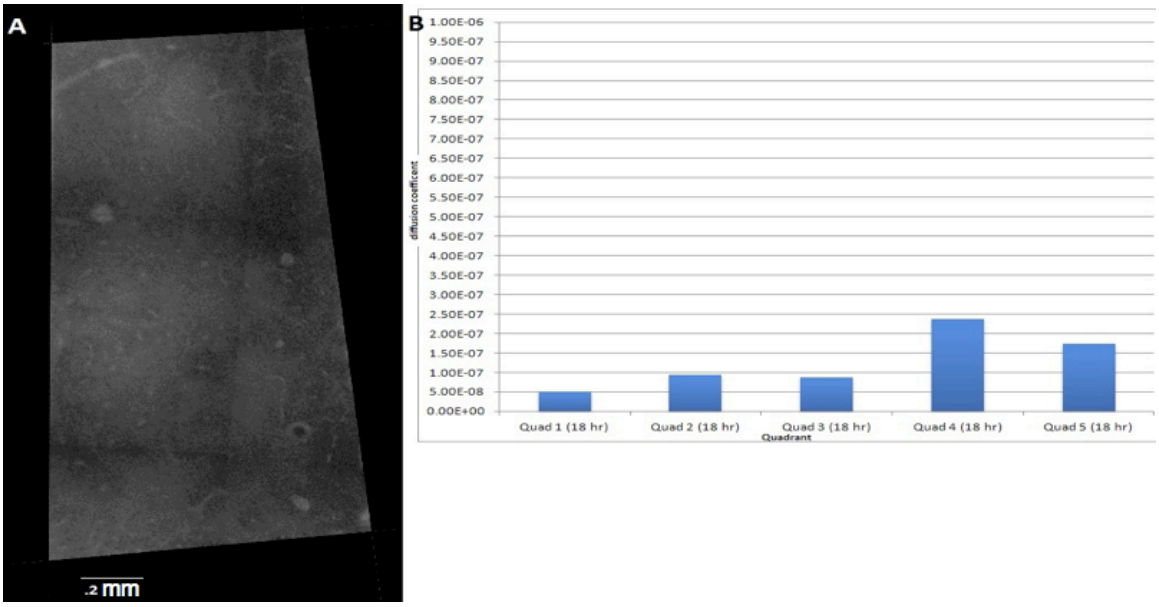

Sample 4	Diffusion coefficient cm^2/s	Sum of squares
Quad 1 (18 hr)	5.09E-08	13,607
Quad 2 (18 hr)	9.45E-08	3,437
Quad 3 (18 hr)	8.64E-08	5,428
Quad 4 (18 hr)	2.36E-07	4,196
Quad 5 (18 hr)	1.73E-07	4,483
Average	1.28E-07	
StDev	7.51E-08	
St. error	3.36E-08	

Figure 4.7 (A) Image of the bone slice. (B) Comparison of the diffusion coefficient for each quadrant. Values of the diffusion coefficient reported in cm^2/s. Results in table correspond to this sample.

As we have seen from most of the data from Section 2 of the bone, this set of data produces values within the expected range to due image clarity and the dye not pooling in a particular area. We again are able to see the radial canals as well as a few Haversian canals (see appendix D). The sum of the squares value

isn't as low as we have seen in Sample 2, but with the exception of quadrant 1, they are not as high as some of the values we observed in Sample 1 (75,000). Overall, this sample produced consistent results with diffusion coefficients falling within similar ranges.

Section 2, Sample 5, 18 hours diffused

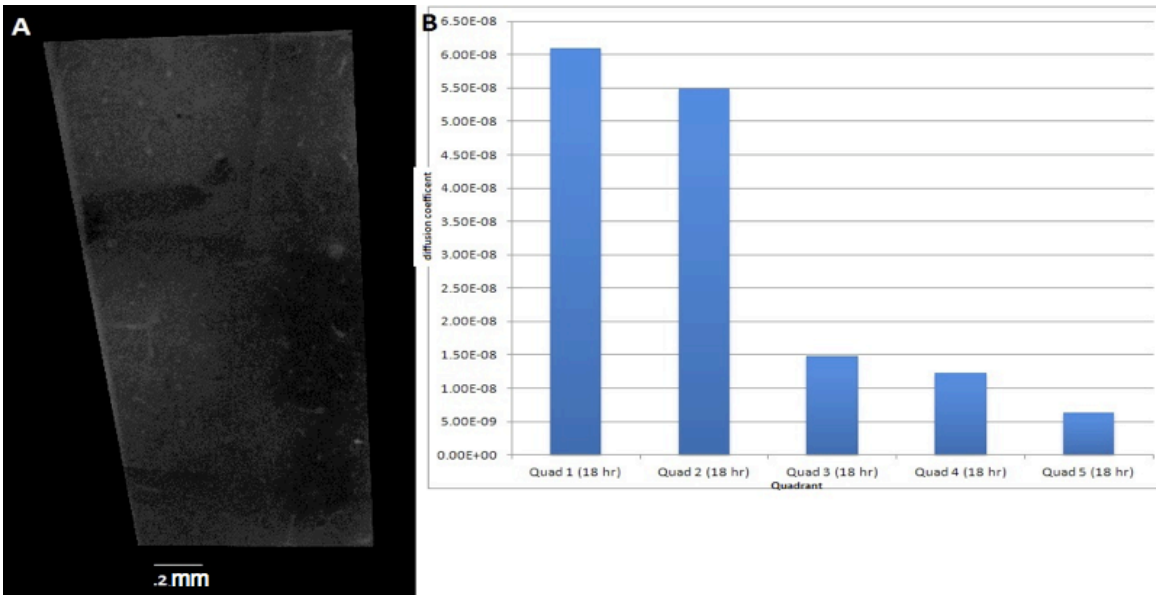

Sample 5	Diffusion coefficient cm^2/s	Sum of squares
Quad 1 (18 hr)	6.10E-08	1,870
Quad 2 (18 hr)	5.48E-08	1,500
Quad 3 (18 hr)	1.48E-08	1,206
Quad 4 (18 hr)	1.23E-08	1,378
Quad 5 (18 hr)	6.29E-09	304
Average	2.98E-08	
StDev	2.59E-08	
St. error	1.16E-08	

Figure 4.8 (A) Image of the bone slice. (B) Comparison of the diffusion coefficient for each quadrant. Values of the diffusion coefficient reported in cm^2/s.. Note the change in the scale on graph B. Results in table correspond to this sample

This trial produced positive results in all quadrants, with values so low that to display the values the spacing on the x-axis was lowered compared to the previous four graphs. To support the statement that his section produced some

of the best values, the sum of the squares values is the absolute lowest of any trial. The rear portion of the sample appears to have almost no influx of dye, with the exception of a slight glow of some Haversion canals, it is for the most part completely black. This sample produced, consistently across all five quadrants, the lowest diffusion coefficients.

In general, the 18 hour data from section 2 consistently produced viable data, with only 2 quadrants deemed as non-measurable. This particular data set had the highest number of successful data points, and the lowest SSE values.

Section 2 30 hours diffused

Section 2, Sample 1, 30 hours diffused

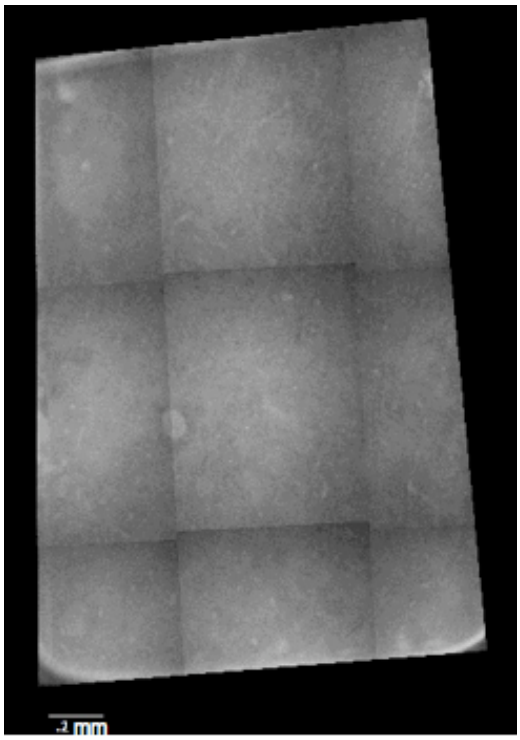

Figure 4.9 The "Skewed" image taken from Section 2, Trial 1, 30 hours diffused

The image taken for the 30 hour diffused counterpart of Trial 1 section 2 was improperly montaged by the computer program and produced unusable

data. Each quadrant produced “peaking” at the lines created when the image was not properly montaged. This could be due to uneven field of lighting. Image montaging is dependent on an algorithm that picks out distinguishing features on the edges that allow for the individual photos to seamlessly overlap. In this photo that did not occur, and this was due to the surface of the bone, which was not completely flat, thus putting the photo out of focus. The lack of focus made each image blurry, and not easily montaged. Additionally the corners of this image show a slight white band which is a referred to as an edge effect, meaning a brighter band appears on the edges of a photos. Although this may seem to be a minor detail, data collection on the edge of each sample is crucial (see transport model chapter 3) and changing that initial value would add a lot of error the calculated diffusion coefficient. No usable data was obtained from this sample.

Data from Section 2, Sample 2, 30 hours diffused

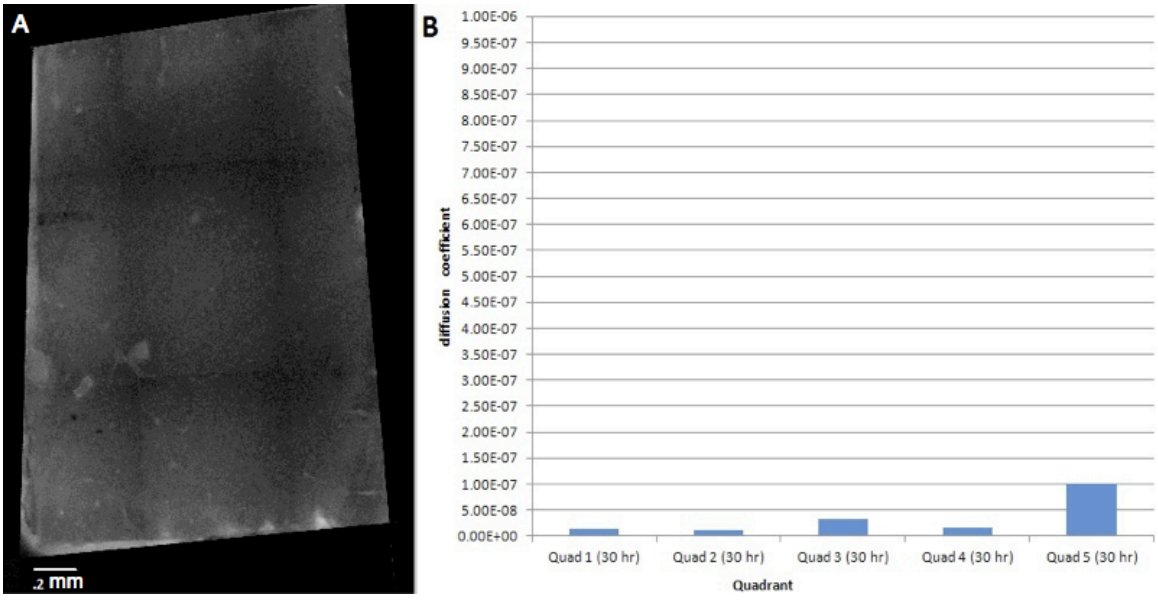

Sample 2	Diffusion coefficient cm^2/s	Sum of the squares
Quad 1 (30 hr)	1.36E-08	24,283
Quad 2 (30 hr)	1.09E-08	9,880
Quad 3 (30 hr)	3.36E-08	10,449
Quad 4 (30 hr)	1.55E-08	6,245
Quad 5 (30 hr)	1.00E-07	7,489
Average	3.47E-08	
StDev	3.75E-08	
St. Error	1.68E-08	

Figure 4.10 (A) Image of the bone slice. (B) Comparison of the diffusion coefficient for each quadrant. Values of the diffusion coefficient reported in cm^2/s. Results in table correspond to this sample.

This trial produced excellent results due to almost seamless montaging and imaging. The SSE values, although not extremely low are acceptable when compared to the values produced from the other trials. Within the image one can clearly see the canal system with the bone and we were able to obtain results within the expected range. The tortuosity of the bone appears to be high, and the dye did not pool in any of the larger Haversian canals.

Data from Section 2, Sample 3, 30 hours diffused

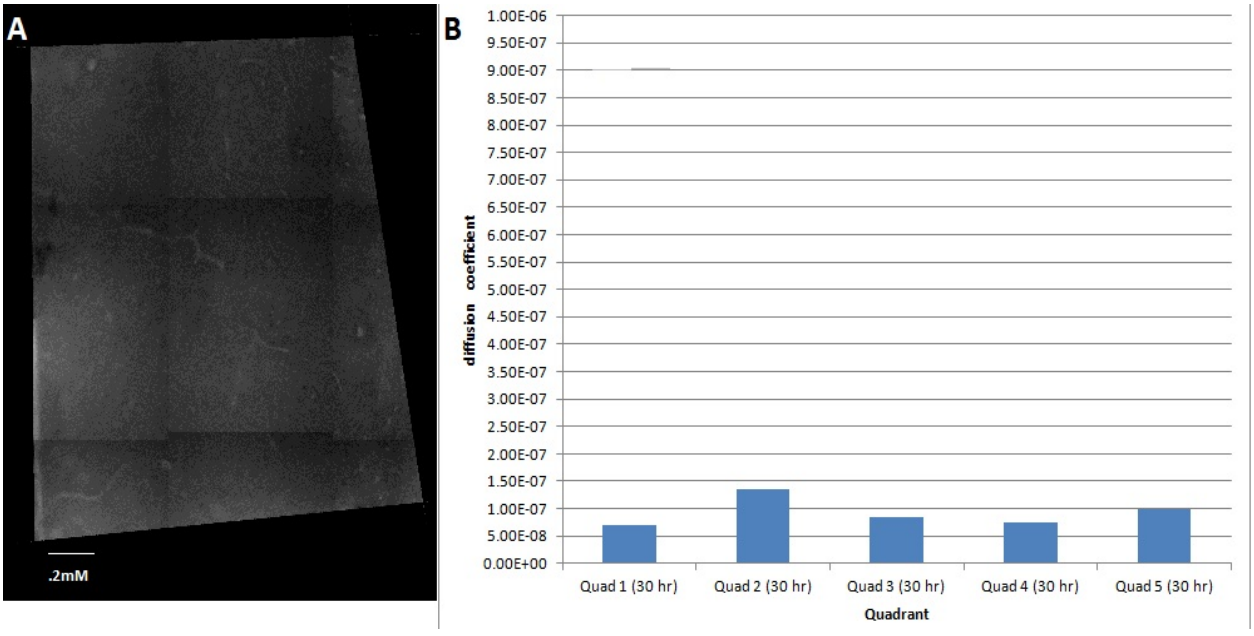

Sample 3	Diffusion coefficient cm^2/s	Sum of squares
Quad 1 (30 hr)	7.00E-08	6,737
Quad 2 (30 hr)	1.36E-07	1,388
Quad 3 (30 hr)	8.36E-08	4,122
Quad 4 (30 hr)	7.36E-08	10,052
Quad 5 (30 hr)	1.00E-07	4,436
Average	9.27E-08	
StDev	2.70E-08	
St Error	1.20E-08	

Figure 4.11 (A) Image of the bone slice. (B) Comparison of the diffusion coefficient for each quadrant. Values of the diffusion coefficient reported in cm^2/s. Results in table correspond to this sample.

Similar to the previous 30 hour sample this sample produced excellent results. There are some noticeable seams in the montaging, but not enough to skew the MATLAB curve fit. The SSE values are for the most part low, with the exception of quadrant 4. Within this image one can clearly see the radial canal system, (Volksmann canals) as opposed to just the Haversian canals. There is a slight edge effect across the left edge of the pore where the dye was allowed to diffuse in, which may cause errors within the data, as well as irregular features on the right edge. The pores look almost like veins running across the tissue (see appendix D for more enlarged photos). This is one of the few images with this feature, but it proves to the validity of the experiment, it particular the high tortuosity of the tissue sample.

Data from section 2, Sample 4, 30 hours diffused

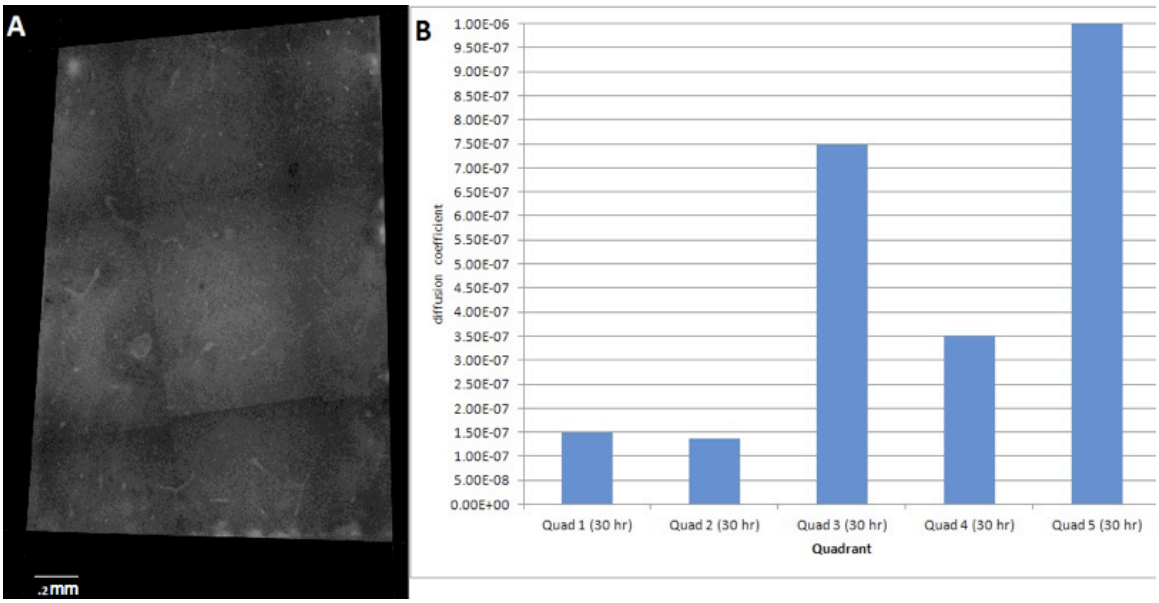

Sample 4	Diffusion coefficient cm^2/s	Sum of squares
Quad 1 (30 hr)	1.50E-07	9,595
Quad 2 (30 hr)	1.3609E-07	13,714
Quad 3 (30 hr)	7.47368E-07	11,530
Quad 4 (30 hr)	3.50376E-07	10,173
Quad 5 (30 hr)	NM	19,440
Average	3.46E-07	
StDev	2.85E-07	
St Error	1.43E-07	

Figure 4.12 (A) Image of the bone slice. (B) Comparison of the diffusion coefficient for each quadrant. Values of the diffusion coefficient reported in cm^2/s. Results in table correspond to this sample. NM represents a non-measurable region.

Within this particular image, we see positive results in the central region of bone, but there appears to be pooling around the lower edge, possibly due to improper sealing, which is skewing the data in quadrant 5. However quadrant 1,2,3 and 4 were measurable and thus will be in the calculated overall average diffusion coefficient. The canal system is again pronounced in some regions of this particular tissue, although there was a difficulty in creating a successful montage as demonstrated by the pronounced lines throughout the sample. Also

it should be noted the SSE values are higher in this particular sample. The SSE value for the non-measurable quadrant was twice greater than the other SSE values.

Data from Section 2, Sample 5, 30 hours diffused

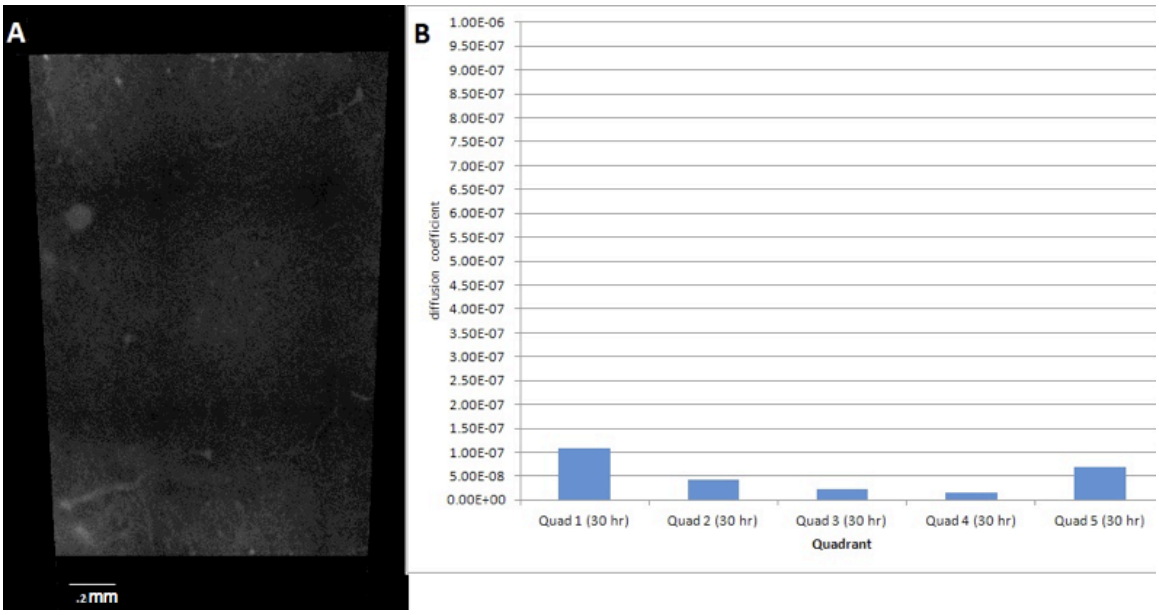

Trial 5	Diffusion coefficient cm^2/s	Sum of the squares
Quad 1 (30 hr)	1.09E-07	1,976
Quad 2 (30 hr)	4.27E-08	2,587
Quad 3 (30 hr)	2.36E-08	1,345
Quad 4 (30 hr)	1.55E-08	424
Quad 5 (30 hr)	6.91E-08	1837
Average	5.20E-08	
StDev	3.80E-08	
st error	1.70E-08	

Figure 4.13 (A) Image of the bone slice. (B) Comparison of the diffusion coefficient for each quadrant. Values of the diffusion coefficient reported in cm^2/s. Results in table correspond to this sample.

In the last 30-hour sample, we again see similar diffusion coefficients across the sample. This is must likely due to an uneven illumination of the sample, which is not a perfectly flat field. The montaging in this sample is not ideal, as it seems to fade out in between the various images in the central region of the sample. In the lower edge of the sample we see a pronounced gradient indicating that it is highly connected. There are also pronounced Haversian canals throughout the sample. The sum of the squares value is also low for this particular trial.

Data from section 3

In section 2, we saw only one sample that needed to be completely discarded, in section 3, we see 6 full samples as well as a few quadrants that were unusable due to either montage error, or the "washing out" due to ineffective camera settings on the microscope. Besides operator error, it is also possible that these tissues were just not connected radially, and there was no influx of dye, and no signal registered.

18 hours diffused

Data from Section 3, Sample 1, 18 hours diffused

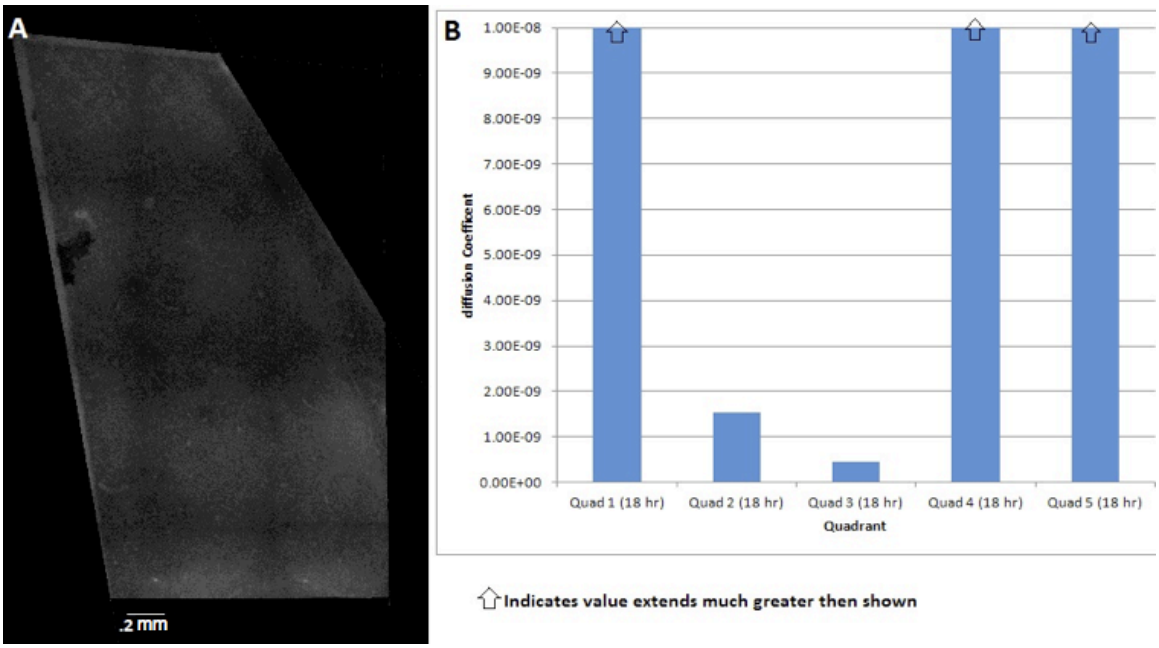

Sample 1	Diffusion Coefficient cm^2/s	Sum of squares
Quad 1 (18 hr)	NM	2,098
Quad 2 (18 hr)	1.54E-09	3,698
Quad 3 (18 hr)	4.43E-10	1,706
Quad 4 (18 hr)	1.00E-07	7,249
Quad 5 (18 hr)	NM	11,519
Average	3.40E-08	
StDev	5.72E-08	
St error	3.30E-08	

Figure 4.14 (A) Image of the bone slice (B) Comparison of the diffusion coefficient for each quadrant. Values of the diffusion coefficient reported in cm^2/s. Table results corresponding to this sample . Note the arrow indicating the values extend higher then graph (1.0×10^{-6}). And the graph is not to scale compared to the other graphs. Table corresponding to the Image A and Chart B

As a whole, the data obtained from this sample was not as acceptable as the previous trials from section 2. We see the results we expected from quadrant 2 and 3, but quadrant 1 and 5 matched the levels of fluorescein sodium salt diffusing in water. This is most likely because of pooling effect in the Haversian

canals, and poor montaging. Additionally, the shape of this particular sample is skewed, and although this was somewhat corrected for in the data manipulation, it still has an apparent effect on the data.

Data from Section 3, Sample 4, 18 hours diffused

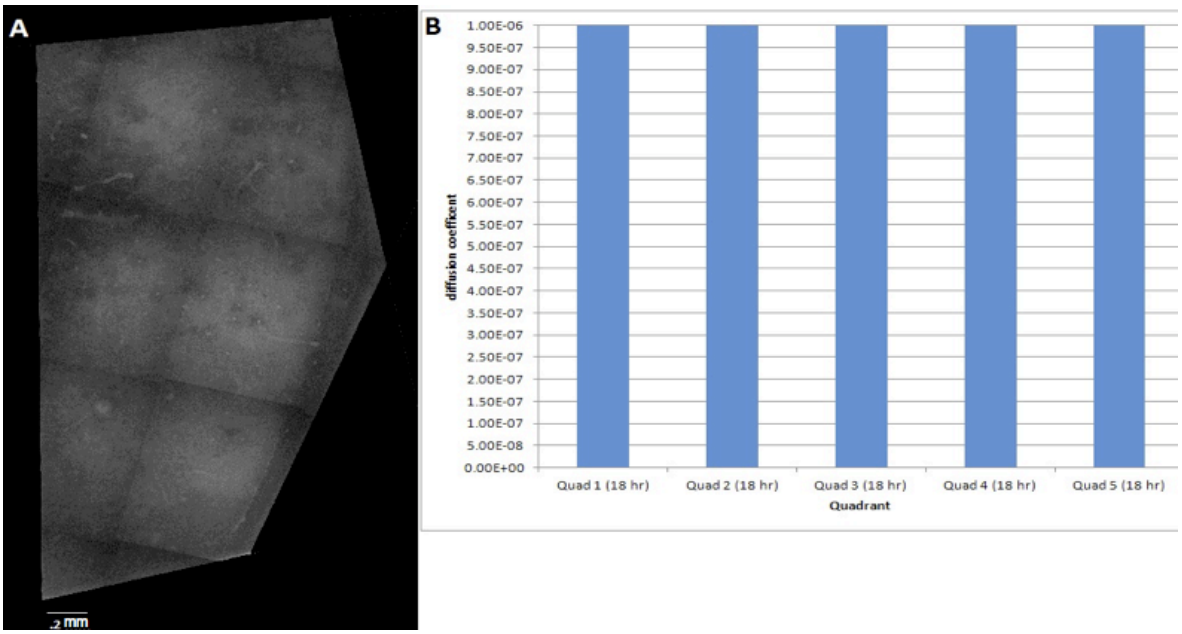

Sample 4	Diffusion coefficient cm^2/s	Sum of squares
Quad 1 (18 hr)	NM	44,888
Quad 2 (18 hr)	NM	60,912
Quad 3 (18 hr)	NM	217,406
Quad 4 (18 hr)	NM	40,379
Quad 5 (18 hr)	NM	38,039

Figure 4.15 (A) Image of the bone slice. (B) Comparison of the diffusion coefficient for each quadrant. Values of the diffusion coefficient reported in cm^2/s. Results in table correspond to this sample. NM represents a non-measurable region.

In this trial, the data did not produce measurable diffusion coefficients. We see in this sample the characteristic "grid" pattern within the montaging, as well as an irregular sample shape. Additionally, there are large illuminated pools in the sample surrounded by dark regions, which are most likely due to

"Haversian canal pooling" (discussed in section 2.6). This entire sample was non-measurable, however we opted to display it as an example of a sample with high SSE values and that resulted in only non-measurable values. The CT data discussed in the literature review section found the total porosity of the canine's left tibia to be only 2.95 ± 0.91%, and radial porosity was 0.60 ± 0.17% [22]. Additionally radial connectivity was 175 ± 87 mm^3 [23]. Although it is possible that lipid content within the canals caused the dye to pool, it is more likely, based on the porosity and connectivity values, that we see an unequal distribution of the diffusive flow, which creates a data set that does not fit the transport model, and thus cannot result in an accurate determination of a diffusion coefficient. To conclude, this sample demonstrates that the inability to calculate more diffusive coefficients for this section of bone is probably related to porosity of the tissue, and montaging errors.

Section 3, Sample 5, 18 hours diffused

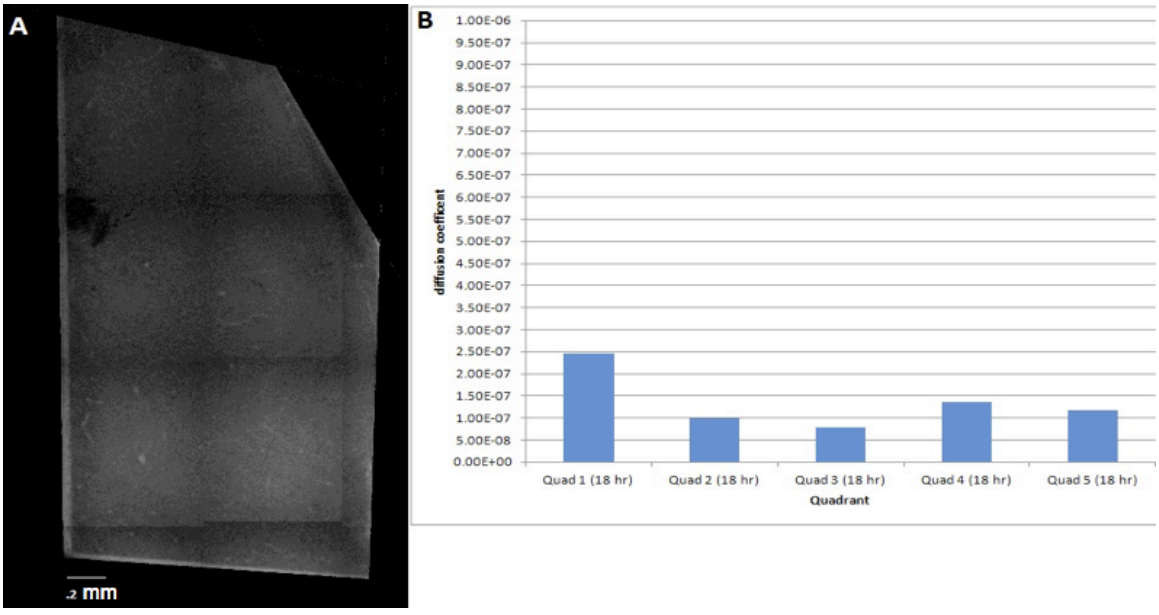

Sample 5	Diffusion coefficient cm^2/s	Sum of squares
Quad 1 (18 hr)	2.45E-07	10,658
Quad 2 (18 hr)	1.00E-07	6,212
Quad 3 (18 hr)	7.82E-08	25,587
Quad 4 (18 hr)	1.36E-07	1,813
Quad 5 (18 hr)	1.18E-07	48,837
Average	1.36E-07	
StDev	6.51E-08	
St error	2.91E-08	

Figure 4.16 (A) Image of the bone slice. (B) Comparison of the diffusion coefficient for each quadrant. Values of the diffusion coefficient reported in cm^2/s. Results in table correspond to this sample.

In this sample we see numbers similar samples from section 2. Although the tissue sample is irregularly shaped, and not perfectly montaged, all sections produced measurable values with reasonable SSE's. Ultimately this section is proof that even with less than perfect montaging, viable data is obtainable if pooling does not occur, which is the phenomenon seen in the previous sample.

Remainder of samples from section 3

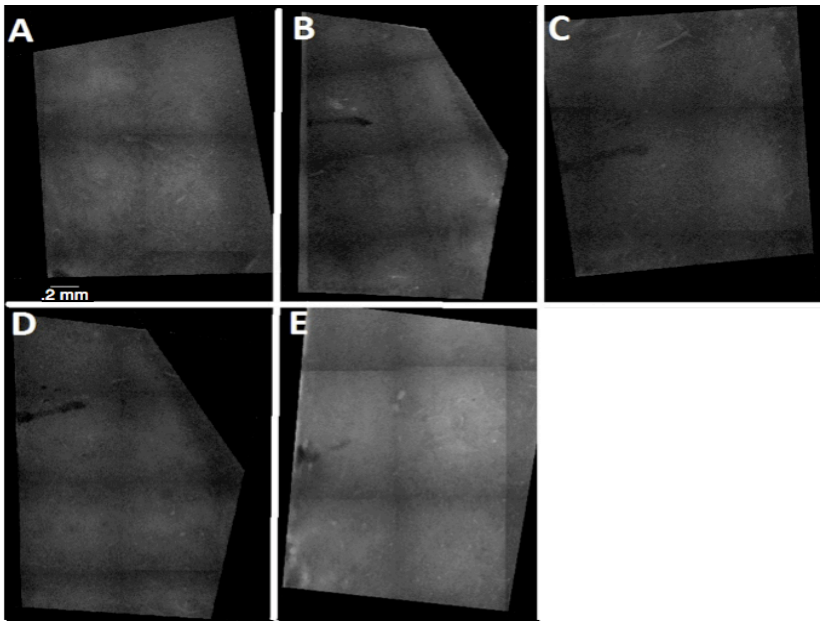

Figure 4.17 (A) Section 3, Sample 1, 30 hours diffused (B) Section 3, Sample 3, 30 hours diffused,(C) Section 3, Sample 3, 18 hours diffused, (D) Section 3, Sample 2, 30 hours diffused, (E) Section 3, Sample 2, 18 hours diffused

These samples did produce useful data and this is due to multiple reasons. Images A, C, and E appear to be fully diffused. This is most likely due to high connectivity of the radial canals, in conjunction with pooling within the larger Haversian canals. However it is difficult to make this assessment as all of the images were montaged unsuccessfully, and we can see a pronounced grid pattern in each sample. Images B and D are not symmetrically shaped, meaning that the sealing of the rear edge most likely failed, and dye leeched in through the back. Image E is washed out, and was unable to produce data, because it gives the illusion that the dye had fully saturated the sample. As discussed previously, it is probable, due to the result, that the sample's surface was not uniformly cut, and the microscope was unable to focus properly. In images B,C,D, and E we see centrally located on the diffused end a pronounced black line extending into the sample. This was also discussed previously and indicated experimental error in marking the exposed surface for diffusion. Within all the images, it is difficult to pick out the characteristic canal systems we have seen in previous samples, which also indicates problems in focusing. For these reasons, the best-fit curve program was unable to fit the data to the model, and thus data was not used.

Data from Section 3, Sample 4, 30 hours diffused

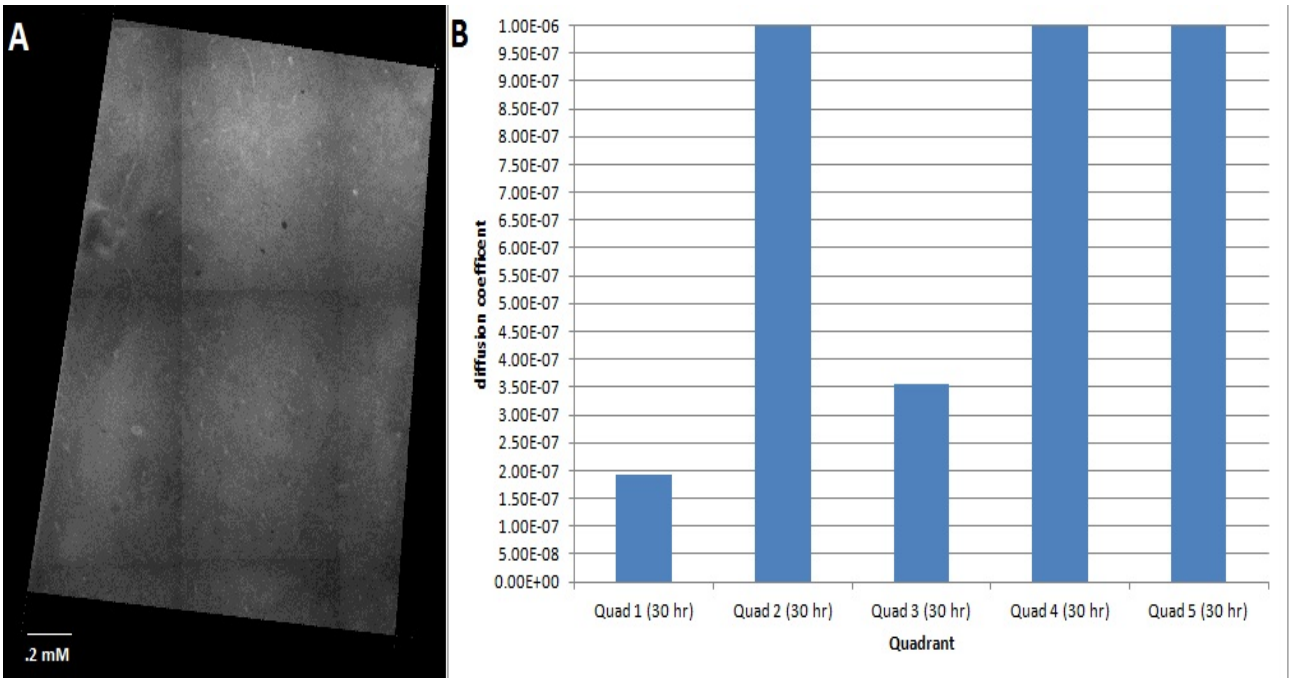

Trial 4	Diffusion coefficient cm^2/s	Sum of squares
Quad 1 (30 hr)	1.91E-07	220782.755
Quad 2 (30 hr)	NM	132522.8149
Quad 3 (30 hr)	3.55E-07	28298.3278
Quad 4 (30 hr)	NM	19621.90064
Quad 5 (30 hr)	NM	8363.265759
Average	2.73E-07	
StDev	1.15708E-07	
St. Error	8.18182E-08	

Figure 4.18 (A) Image of the bone slice. (B) Comparison of the diffusion coefficient for each quadrant. Values of the diffusion coefficient reported in cm^2/s. Results in table correspond to this sample. NM represents a non-measurable region.

In this sample, two sections, quadrant 1 and 3 produced viable data, and quadrants 2,4, and 5 produced non-measurable result. We hypothesize that this was due to the pooling effect created by the high lipid content within the bone samples. If you examine the circular bright field located in the central region of the tissue, quadrant 2, you can see that a lot of the dye had built up in this area,

and failed to travel through the entire tissue. Because bone is not homogenous in structure and contains carbohydrates and lipids, one may encounter this type of phenomena throughout the tissue depending on what portion of the bone was selected for examination.

Data from Section 3, Sample 5, 30 hours diffused

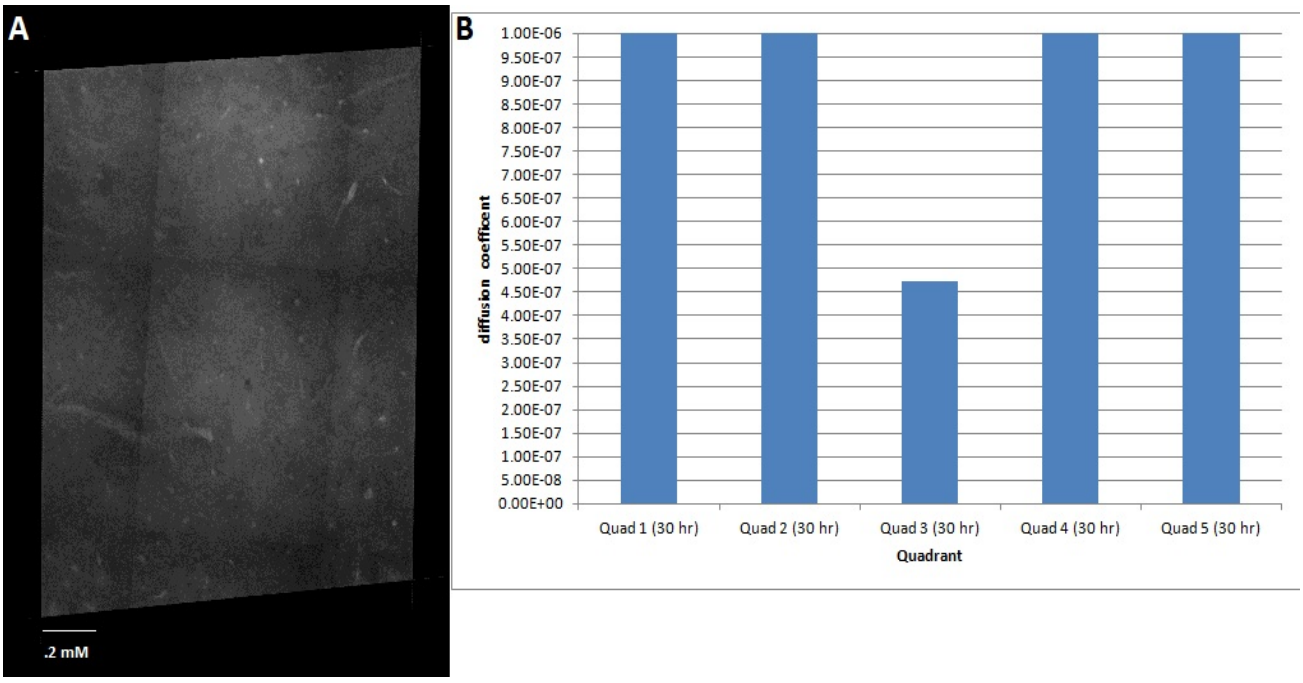

Trial 5	Diffusion coefficient cm^2/s	Sum of squares
Quad 1 (30 hr)	NM	47,805
Quad 2 (30 hr)	NM	36,353
Quad 3 (30 hr)	4.74436E-07	15,767
Quad 4 (30 hr)	NM	20,944
Quad 5 (30 hr)	NM	4,283

Figure 4.19 (A) Image of the bone slice. (B) Comparison of the diffusion coefficient for each quadrant. Values of the diffusion coefficient reported in cm^2/s. Results in table correspond to this sample. NM represents a non-measurable region.

The central region of the sample, quadrant 3, results in an expected diffusion value, however it is surrounded by non-measurable quadrants. The sample is in focus, and we can observe various canals in the sample, and the

montaging is, although not perfect, fairly seamless. It almost appears that the dye stopped roughly 1 mm into the bone and pooled there.

4.4 Discussion

Figure 4.20 displays all of the measureable diffusion coefficients.

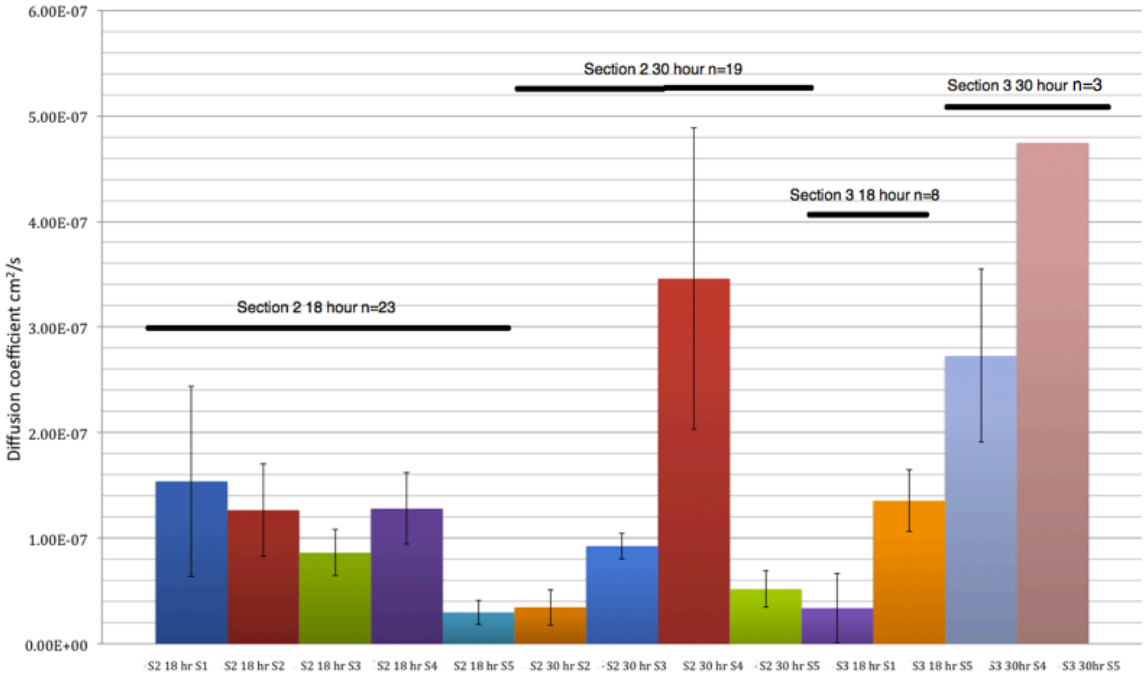

Figure 4.20 All previously discussed diffusion coefficients labeled by section #, time of diffusion, and sample #. Note there is no standard error on section 3, 30 hour sample 5 because it only had one measurable quadrant. Table for graph, including standard error, can be found in appendix G.

Statistical analysis consisted of 2-tailed t-test, unpaired data, unequal variances, using an α=.05 (95% confidence limit). No difference was obtained between the section 2, 18 hour data and the section 3, 18 hour data, indicating that the two populations could be grouped together.

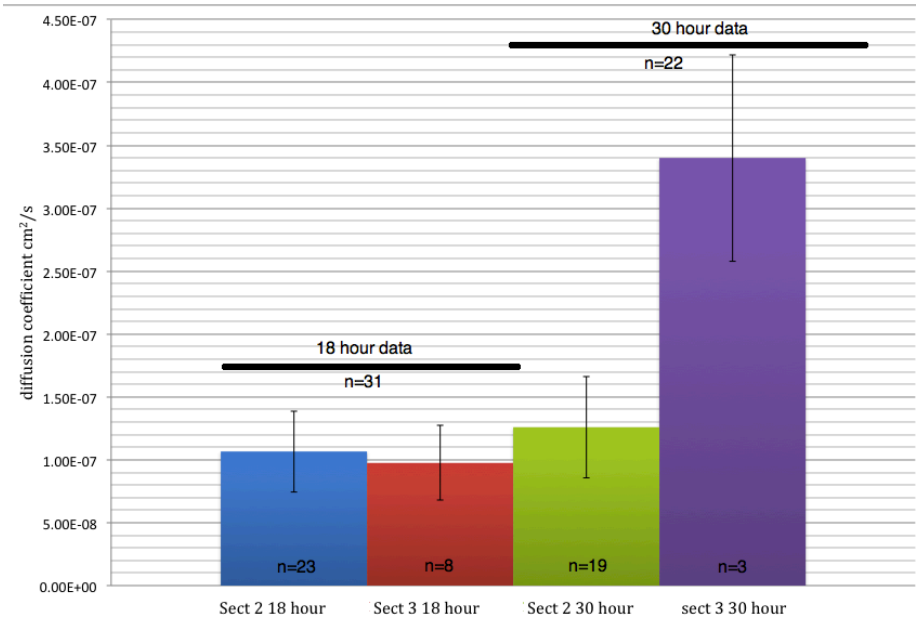

Figure 4.21 Comparison of two different data sets (18 hour and 30 hour). P-value for 18 hour comparison is .80 and for the 30 hour comparison was .09.

The same type of T-test was repeated, this time comparing all of the 18 hour data to the 30 hour data regardless of location in the bone sample. No difference was obtained, allowing us to average all the data.

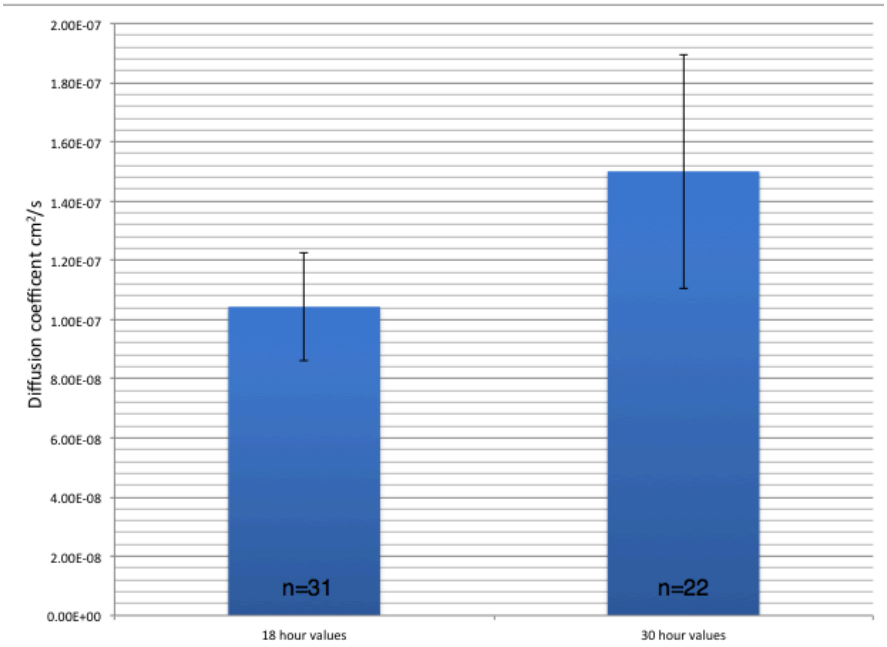

Figure 4.22 Comparison of all 18 hour data to all 30 hour data. A P-value of .31 was obtained when comparing the 18 hour values to the 30 hour values

Given that we can group all the different test parameters as one from the t-test calculations, the value of the diffusion coefficient in bone was found to be $1.27 \times 10^{-7} \pm 1.96 \times 10^{-8}$ cm^2/s.

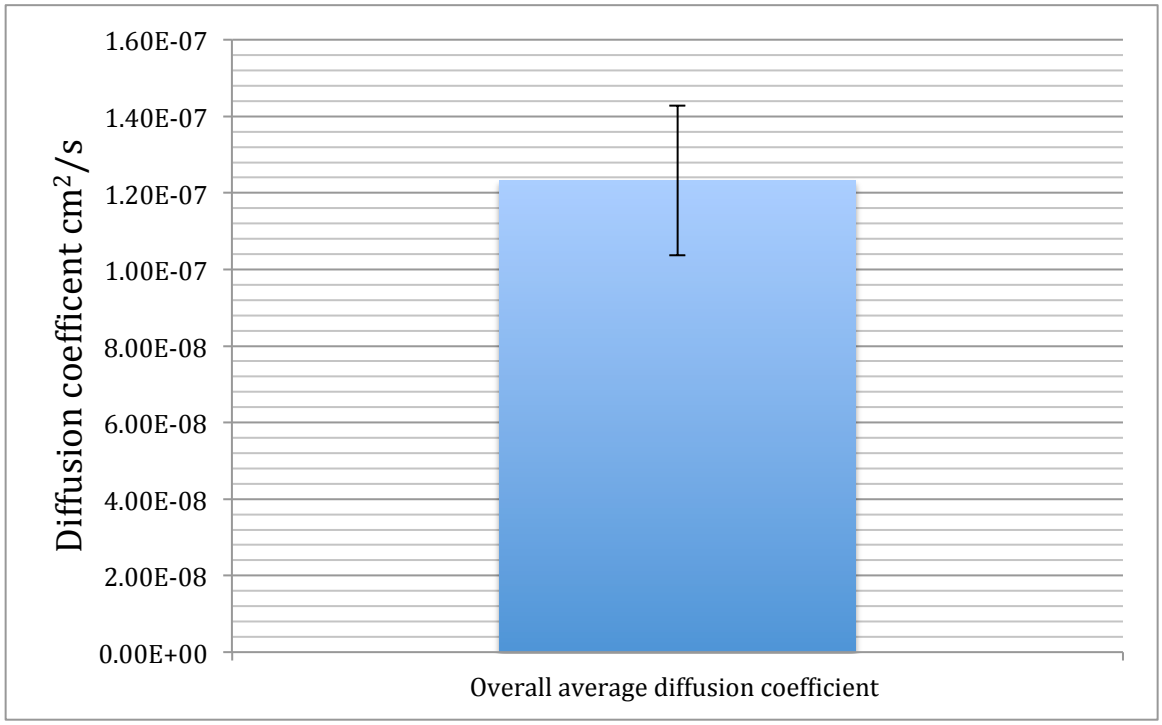

Figure 4.23 Overall average calculated diffusion coefficient with standard error bar in cm^2/s

Significance of this value

Before discussing the physiological significance of this value, it is first necessary to discuss the error associated with it. One of our goals was to develop a methodology that measures diffusion precisely. Our experiment averaged 51 values across 2 sections of bone and the error associated with our final value is 15.4%. Given the range of previously reported values, (table 2.5) this small error is acceptable for this type of experiment.

As discussed in chapter 2, there are extreme discrepancies among various researchers of the true values of diffusion within bone tissue (Table 2.5). This is for a number of reasons, the first being the animal model used to measure diffusion, as some researchers used a rat model however this animal lacks osteons and does not have a bone microstructure that is similar to humans. The second being the molecule used to test diffusion, as an amphipathic molecule would be most suitable as it is most similar to the signaling factors naturally produced and diffusing through bone, and because they will interact with the lipid environment within bone, giving us more accurate measurements. And last, one should account for diffusion across the entire heterogeneous structure, and not just a single canaliculi or Haversion canal. It is clear that our value lies in between the range of previously discovered (table 2.5). Given that we used an animal model that contained osteons, a amphipathic molecule, and a measured diffusion across an entire bone sample, it makes sense that our value is slower then *Wang et al* value which focused on diffusion within a canaliculi, but not as slow as the *Knothe-Tate* value which focused on only the dense region of bone contained between 2 canaliculi and used a larger test molecule. To provide a timeframe for diffusion, we can use Einstein's approximation equation to quantify the time it takes a given molecule to diffuse an average distance in two dimensions[44] .

$$t \approx \frac{x^2}{4\,D_{ij}} \tag{20}$$

Where x is the distance traveled, t is the time required, and D_{ij} is the diffusion coefficient. On average, the distance between a Haversion canal and an osteocyte is 250 μm. Recalling Table 2.5 and the diffusion coefficients listed within it, one can now determine times required for their test molecule to diffuse this average distance, the lower bound being less then one minute, (Wang *et al.* [28]) and the highest being 200 hours (Patel and Knothe-Tate [26]). Our value, which used the identical marker as the Wang study, concludes it would take 20 minutes for diffusion to occur within an osteon without loading. Our marker is relatively small at only 376 Da, whereas some of the major proteins and growth factors diffusing into bone, such as insulin, are on the magnitude of 6000 Da. Thus, it can be inferred that larger molecules would take longer to diffuse, however, our study provides a baseline for small nutrients, vitamin D (calciol), which is about 384 Da.

Knowing the diffusion coefficient now allows one to calculate the flux given the following equation[44]:

$$J = -D\frac{\partial C}{\partial x} \tag{21}$$

Where J is the Flux expressed either in number of atoms per unit area and per unit time (atoms/m^2-s) or in terms of mass flux (kg/m^2-s), D is the diffusion coefficient, and the derivative is the concentration distribution of the diffusing molecules. Thus, given a timeframe and a distance, one could now calculate flux, which would prove useful given the different distances molecules must travel

within bone tissue and also the various concentrations of nutrients and signaling molecules within an organism.

Discussion on measurements from bone section 4

We had also run tests on the endosteal region of section 4 of the bone sample, using identical protocols as used on bone section 2 and 3. However, due to the high auto-florescent values of this section, we were unable to obtain a fluorescein sodium salt signal above that given threshold. These values can be seen in the table included in appendix E and F. Of the 25 total trials run, only two produced a viable signal above the auto-florescent threshold. Even of the two that produced a signal, the data was not measurable. We hypothesize this was due to a lack of radial connectivity within the samples selected from this section, which limited the dye's ability to diffuse within the bone. This pattern trended down the bone, as the samples proximal to the kneecap produced the largest set of data, 42 measured values were found in section 2, 13 values in section 3, and 0 in section 4. It is likely that the region 2, which was closest to the epiphyseal (growth plate) maybe be more porous to allow an influx of nutrients to promote elongation and growth, whereas, sections 3 and 4 were more centrally located in the diaphysis, and thus not remodeling and growing as rapidly. This being said, it would be probable the radially connectivity is extremely low in this section, which would mean a less influx of nutrients, or in our case, the dye, hindering ones ability to measure diffusion. We hypothesize that applying a mechanical force may increase the number of measured values through the tissue, in

particularly in the lower sections which must be more dense due to their need to withstand greater normal stress. Discussion of future recommendations will be made in chapter 5 relating to this topic.

CHAPTER V

CONCLUSIONS AND RECOMMENDATIONS

The diffusivity of fluorescein sodium salt (376 Da) in canine tibia was measured in vitro in PBS at 37°C. To model our results we used a finite diffusion transport equation in rectangular coordinates, 1-D, focusing on radial diffusion into bone tissue. Lastly no mechanical loading or external stimuli was applied to the bone, and there was no production or consumption of materials/nutrients by the bone sample. However there was pooling observed because of the lipid content of the environment diffused through and the amphipathic properties of the diffused molecule.

5.1 Conclusions

The following "exciting" conclusions were made:

- Diffusion becomes more limited as one moves to a region located in the central diaphysis of the bone.

- The sample of bone being tested has to have some degree of radially connectivity in order for diffusion to be measured given the conditions and transport model listed above.
- The experimental design can be repeated with the addition of other experimental variables such as mechanical loading, mentioned in Chapter 1
- In locations where diffusion could be measured and quantified with the transport model, the diffusivity was found to be $1.27 \times 10^{-7} \pm 1.96 \times 10^{-8}$ cm^2/s given the conditions listed above.

5.2 Limitations

The following limitations were observed:

- Sample radial connectivity and porosity was not uniform throughout, and was difficult to assess before testing. Additionally we have no CT evidence of our own samples connectivity, only the samples taken from the test subjects left tibia.
- Measurements were done with a 3×10^{-7} (FITC) molarity. Average physiological molarities of small nutrients are lower then this, for example glucose is 3×10^{-9} M. However the use of solutions with concentrations lower then 3×10^{-7} M FITC solution resulted in a very low signal that was undetectable after 48 hours.
- The time required to cut, mount, and image an adequate number of samples could cause an error in the time element of the diffusion calculation. Our max time was 4 hours.
- Deciding the exposure time and intensity of each image proved difficult, as the higher the intensity selected, the better the image, however this also

increased the level of auto florescence of the control samples. Additionally the montaging of images was never completely seamless.

- The transport model was only in 1 direction, and it is possible for the solute to diffuse in more than just that direction, despite it only being ≈250 microns thick. This is pronounced in the Harvision canals which appear to be lit up in most images.
- The test molecule is much smaller then some of the important signaling molecules that are known to diffuse through bone tissue, such as insulin and other large proteins (> 1000 Da). One would need to synthesize one of these molecules bonded to a fluorescent marker if they wanted to test the diffusivity of larger molecules.
- All tests were conducted in vitro, and thus other variables that play an important role in transport, including pressure gradients, mechanical loading, electrical gradients and other concentration gradients were absent.
- The MATLAB code would default to a diffusion coefficient of 1.0×10^{-6} if it was unable to find a valid relationship between the experimental curve and theoretical curve, and thus this sample was deemed non-measurable.
- Imaging needs to be performed quickly, on the same microscope, as the intensity of light is directly related to the concentration in the material. Different microscopes have different levels of intensity of fluorescent light depending on the length of time the mercury bulb has been used.

5.3 Recommendations

The following are the recommendations for further studies in order to better understand the diffusivity in bone.

1) One must be thoroughly trained to operate the robotic microscope in order to produce successful images. Understanding of software, fluorescence microscopy, and camera adjustments are crucial in successfully and quickly (study is time dependent) analyzing the images.

2) Surface topography of the samples is important, a well polished bone piece produces a much clearer image than one that was improperly cut. One should take caution in cutting the samples. Precise cutting is easier and less time consuming then polishing the samples. The thinner the slice of bone that can be cut to image, the better the images appear.

3) A traditional two-chambered diffusion cell should be used to confirm all data produced from this experiment.

4) Other florescent molecules and tracers exist of different sizes and structures and should be used to further the data found in this paper.

5) Mechanical loading and other external variables should be applied to this setup, and compared to this baseline transport rate data.

REFERENCES

1. Somayajula,D.A., Biocompatiblity of osteoblast cells on titanium implants. Masters Thesis, Cleveland State University. (2008) pg. 5.

2. Wang X., Nyman J.S., Dong X., Reyes M., Fundamental Biomechanics in Bone Tissue Engineering. Morgan & Claypool publishing. (2010) pg. 15- 25.

3. Martin, R.B., Burr, D.B., Sharkey, N.A., Skeletal tissue mechanics. Springer. (1998) pg. 221,-222.

4. Bilezikian, J. P., Lawrence G. R ., Martin J.T., Principles of Bone Biology. Academic Press. (2011) pg. 1-30.

5. Bilezikian, J.P, Raisz, L.G., Rodan, G.A. Principles of Bone Biology. Academic Press. (1996). pg. 1-10.

6. Schlaffler, M.B., Burr, D.B., Stiffness of compact bone: effects of porosity and density. Journal of Biomechanics. (1988) Volume 21-1. pg. 6-13.

7. Beno T., Yoon Y., Cowin S.C., Fritton S.P. Estimation of bone permeability using accurate microstructural measurements. Jouranl of Biomechanics. (2006) Volume 39. pg. 2378- 2387.

8. Dirksen T.R., Marinetti G.V. Lipids of bovine enamel and dentin and human bone. Calc Tissue Res. (1970) Volume 6 pg. 1-10.

9. Pietrazk W.S., Woodell-May J. The composition of human cortical allograft bone derived from FDA/AATB-screened donor. Journal of Craniofacial Surgery. (2005) Volume 4 pg. 579-85.

10. Black J., Mattson R., Korostoff E. Haversian osteons: size distribution, internal structure, and orientation. Journal of Biomedical Material. (1974) Volume 8 pg. 299-319.

11. Cooper D., Turinsky A., Sensen C., Hallgrimsson B. Effect of voxel size on 3D micro-CT analysis of cortical bone porosity. Calcified Tissue International. (2007) Volume 80 pg. 211-219.

12. Weinger J.M., Holtrop M.E. An ultrastructural study of bone cells: the occurrence of microtubules, microfilaments and tight junctions. Calc. Tissue Res. (1974) Volume 14 pg. 15-29.

13. Dillaman R.M., Roe R.D., Gay D.M., Fluid movement in bone: theoretical and empirical. Journal of biomechanics. (1991) Volume 24 pg. 163-177.

14. Mishra S. Knothe-Tate M.L. Effect of lacunocanalicular architecture on hydraulic conductance in bone tissue: implications for bone health and evolution. The Anatomical Record. (2003) Volume 273A pg. 752-762.

15. Truskey G,A., Yuan F., Katz, D.F. Transport Phenomena in Biological Systems. Pearson Prentice Hall Bioengineering. (2009) Chapter 1,7.

16. Burg, Karen J.L, Porter, Scott, Kellam, James F. Biomaterial developments for bone tissue engineering. Biomaterials. (2000) Volume 21 pg. 2347- 2359.

17. Hulbert S. F., Young F. A., Mathews R. S., Klawitter J. J., Talbert C. D., Stelling F. H. Potential of ceramic materials as permanently implantable skeletal prostheses. Journal of Biomaterials Research. (1970) Volume 4 pg. 433-456.

18. Lanza, P.L., Vacanti R. Principles of Tissue Engineering. Academic press. (2007) pg. 360-365.

19. Saltzman, M.W., Tissue Engineering: Engineering Principles for the Design of Replacement Organs and Tissues. Oxford Press (2004) pg. 256-265.

20. Demirel Y., Nonequilibrium Thermodynamics: Transport and Rate Processes in Physical, Chemical and Biological Systems. Elsevier. (2007) pg. 357-360

21. Meinel L., Karageorgiou V., Fajardo-Snyder R.B., Shinde-Patil V., Zichner L., Caplan D., Langer R., Vunjak-Novakovic G. Bone tissue engineering using human mesenchymal stem cells: effect of scaffold material and medium flow. Annuals of Biomedical Engineering, (2004) Volume 32 pg. 112-122.

22. Wen, D. Cortical Bone Tissue Engineering: Scaffold design and cell selection. Doctoral Dissertation, Cleveland State University. May 2009

23. Pallua, N., Suscheck, C.V. Tissue engineering from lab to clinic. Springer. (2011) pg. 140-143

24. Hollinger J.O., Einhorn T.A., Doll, B.A., Sfeir, C. Bone Tissue Engineering. CRC Press. (2000) pg 231-245.

25. Knothe-Tate M.L., Knothe, U. An ex vivo model to study transport processes and fluid flow in loaded bone. Journal of Biomechanics. (1999) Volume 33 pg. 247-254

26. Patel R.B., O'leary J.M., Bhatt S.J., Knothe-Tate M.L., Determining the permeability of cortical bone at multiple length scales using fluorescence reco after photobleaching technique. 51st Annual Meeting of the Orthopedics Research Society. (2007) Paper No. 14.

27. Mishera S., Knothe-Tate M.L. Effect of Lacunocanalicular architecture on Hydraulic Conductance in Bone Tissue: Implications for Bone Health and Evolution. The Anatomical Record. (2003) Volume 273 pg. 752-762.

28. Wang L., Wang Y., Han Y., Henderson S.C., Majeska R.J., Weinbaum S., Schaffler M.B. *In situ* measurement of solute transport in the bone lacunar-canalicular system. PNAS. (2005) Volume 102 pg. 23

29. Banks-Sillsa, L.B., Ståhlec P., Svenssonb I., Eliaza N. Strain driven transport for bone modeling at the periosteal surface. Mathematical Biosciences. (2011) Volume 230 pg. 37-44.

30. Keanini R.G., Roer R.D., Dillaman R.M. A theoretical model of circulatory interstitial fluid flow and species transport within porous cortical bone. Journal of Biomechanics (1995) Volume 28 pg. 901-914.

31. Knothe-Tate, M.L., Steck R., Forwood M.R., Niederer. P., In Vivo demonstration of load-induced fluid flow in the Rat Tibia and its potential implications for processes associated with functional adaptation. The Journal of Experimental Biology. (2000) Volume 203 pg. 2737-2745

32. Knothe-Tate M.L., Niederer P., Knothe U. In vivo tracer transport thru the lacunocanalicular system of rate bone in an environment devoid of mechanical loading. Bone. (1998) Volume 22 pg 107-117.

33. Knothe-Tate M.L., Knothe U., Nieder P. Experimental Elucidation of Mechanical Loading induced fluid flow and its potential role in bone metabolism and functional adaptation. American Journal of the Medical Sciences. (1998) Volume 316 pg. 189-195.

34. Lang S.B., Stipanich N.B., Soremi E.A. Diffusion of glucose in stressed and unstressed canine femur in vitro. Annuals New York Academy of Science. (1974) Volume 238 pg. 139-48.

35. Fernández-Seara M.A., Wehrli S.L., Wehrli F.W. diffusion of exchangeable water in cortical bone studied by nuclear magnetic resonance. Biophysical Journal. (2002) Volume 82 pg. 522-529.

36. Periasamy N., Verkma A.S., analysis of fluorophore diffusion by continuous distributions of diffusion coefficients: application to photobleaching Measurements of Multicomponent and Anomalous Diffusion. Biophysical Journal. (1998) Volume 75 pg. 557–56.

37. Landolt-Börnstein. Zahlenwerte und functionen, 6. Auflage, II. Springer-Verlag, (1969) Volume 5 pg. 645.

38. Wang, Y.L., Taylor, D.L. Fluorescent microscopy of living cells in culture. Academic press. (1989) pg. 13-135.

39. Diaspro A. Optical Fluorescence Microscopy: From the Spectral to the Nano Dimension. Springer. (2010)

40. Li G.P., Bronk J.T., An K.N., Kelly P.J. Permeability of cortical bone of canine tibiae. Microvascular Res. (1987) Volume 34 pg. 302-10

41. Wen D., Androjna C., Amitt V., Belovich J., Midura R. Lipids and Collagen Matrix Restrict the Hydraulic Permeability Within the Porous Compartment of Adult Cortical Bone. Annals of Biomedical Engineering. (2010). Vol. 38 pg. 558–56

42. An H.Y., Friedman R. J., Animal models in orthopedic research. CRC Press. (1999) pg. 284

43. Pluen, A. Paolo, A.N., Jain, R.K., Berk D.A., Diffusion of Macromolecules in Agarose Gels: Comparison of Linear and Globular Configurations. Biophysical Journal (1999) Volume 77 pg. 542–55

44. Haberlandt, R., Molecules interaction with surfaces and interfaces. Springer (2004). pg 130.

APPENDICES

Appendix A

Explanation of MATLAB Code

Data was imported to MATLAB via the "xlsread" function and named "data." This matrix is what all subsequent calculations will be done on. The number of columns in each matrix differs, from 200 to 260. Each column represents a distance of 10 pixels into the sample tissue that the dye had diffused into. To convert the pixels into mm, an image of a 1 mm marker was taken under the same microscope that all the bone images were taken under. This image was then processed to decide the distance that one pixel corresponds to, which was exactly 0.000812 mm. The length of the matrix was extracted from the "data" matrix and named "dlength." Dlength created a matrix of linearly spaced whole numbers spaced from 1 to the number of columns in the matrix "data" (ex 1, 2, 3, ……260). Element by element multiplication was performed on dlength, meaning each element was multiplied by 10, the number of samples, and then .00082--the length of a pixel to a mm. The matrix dlength now had a range of 200-260 elements (depending on the length of the given sample), and each element corresponding to a mm distance into the tissue. This matrix will be used as the set of data contained on the y-axis of e graph.

Next the auto-fluorescent values were subtracted from the entire matrix by using element-by-element operations. The previously described "autoflur" variable was subtracted from the "data" matrix. This created a new matrix, still titled "data," that now had values that correlated only to the fluorescein sodium

salt signal diffused through the tissue. If values were negative or 0, they would be regarded as part of the background (no fluorescein sodium salt signal) and the next series of functions would not treat those numbers the same as positive integer values.

Each bone sample matrix was then broken into five quadrants, resulting in five separate diffusion coefficients per sample. This was accomplished by dividing the total number of rows in the sample by five, giving us one dummy variable we named "z." The average value for "z" was between 40-75, and multiplying z by five equals the total number of columns in the image matrix.

The average intensity value was calculated, excluding 0-values. Again, zero values were excluded because they are not representative of any type of diffusion, rather the black background. This never presented an issue in the first 200 averaged columns, but in some cases the last 100 columns didn't conclude in identical rows. This was because the bones were not perfect squares, meaning they did not produce perfect square matrices. However, because the code was written to exclude any 0 values the code only averaged non-zero values, and thus this was never any issue. In summary, some diffusion paths ended more abruptly than others, and as we are averaging across a range of 50-75 rows (≈.5 mm) it would skew the diffusion coefficient value if the zero values were included in the average.

In summary, diffusion occurred from column 1 to the final column of the matrix (≈column 250). The matrix consists of 300-500 rows, which were

divided into five sections, thus producing five equal matrices with the same number of columns as previously described (≈250) and 1/5 of the total number of rows (≈70). These matricies were averaged, excluding zero values, to produce five single row matrices, with the same number of columns (≈250). These five matrices were named "section1," "section2," "section3," "section4," and "section5," with the numerical value of 1 representative of the upper most region of the image, and 5 representing the lowest region of the image.

Graphical output. The "dlength" matrix, which was the total distance of the tissue converted from pixels to mm, was graphed on the x-axis against the "section#" matrix graphed on the y-axis. All five were placed on one graph, each having a separate marker to distinguish between each section. The highest possible fluorescence or y-value was 255, and the greatest possible x-value was just under 3 mm; however each graph varied, again because of the variation in size of the bone slices. Graphs were labeled according to the section of bone they were taken from, the amount of time diffused, a number (1-5) signifying the trial (each bone beam had five portions or "trials" sliced from it), and the type of dye used (fluorescein sodium salt in all cases) e.g. Sect2-18hr-5-FITC Files were exported out of MATLAB and saved as TIFF images using the same naming pattern as the graph title. In conclusion, 30 graphs were produced, each displaying five data sets of decreasing fluorescent values vs distance.

Transport model and curve fit. To find a best fit curve, we looked at each "section#" vector individually. As stated previously, the "section#" vector was

an average of a small portion of the bone tissue. We sought to find the diffusion coefficient by modeling our experimental data to a theoretical model. Our theoretical model leads to an analytical solution for the diffusion coefficient, given all the other variables are accounted for. This equation accounts for one-dimensional unsteady diffusion in a finite medium using rectangular coordinates. The following is the fully derived equation; the next section of this text will describe the derivation and validation of the equation, but it is necessary for this section to display the full equations to demonstrate how MATLAB fit a curve to it.

$$\theta = 1 - \theta' = 1 - 2\sum_{n=0}^{\infty} \frac{(-1)^n}{(n+1/2)\pi} \cos\left[\left(n + 1/2\right)\pi\,\eta\right] \exp\left[-\left(n + 1/2\right)^2 \pi^2\,\tau\right] \quad (21)$$

Where θ is dimensionless concentration is $\frac{C_i - C_0}{C_1 - C_0}$ where C_i is the concentration found in tissue at a given position (all points of matrix "section#"), C_1 is initial concentration at boundary condition in tissue (value at element 1,1 of "section#" matrix), C_0 is initial concentration in tissue and η, dimensionless distance is $\frac{y}{L}$ where y is the current distance and L is total length of sample. Lastly τ, characteristic time, is $\frac{t\,D_{ij}}{L^2}$ where t is time, D_{ij} is the diffusion coefficient and L is the total length of sample.

Comparison of the theoretical model to the experimental data. For our analysis, we used fluorescent intensity as concentration, thus all values for C_i corresponded to the "section#" matrix. The C_1 variable corresponded to the fifth element of the "section#" matrix. We opted not to start it at the first value in the

matrix because it did not accurately represent the start value as it was distorted by an edge effect in nearly all images. C_0 was 0 in all cases because we subtracted the auto-fluorescent values from all matrices, thus eliminating any reason that the tissue should have any fluorescent value before any dye was diffused through it.

The distance variable, y, corresponded to the "dlength" matrix described previously. The L variable was the last element of the "dlength" matrix because that was the maximum/total distance of the sample. Lastly t, time, was entered in manually, either 64,800 seconds (18 hours) or 108,000 seconds (30 hours).

The MATLAB code we wrote varies values for D_{ij} and compares them to our experimental results. To describe the process broadly, MATLAB first assigns the specific values we discussed previously to algebraic variables described in the 1-D finite diffusion equation. Then it assigns various guess values to the unknown variable, D_{ij} , and compares them to our experimental values for θ against it. Thus, the program was coded to make an initial guess for D_{ij} , produce theoretical θ values, convert those to theoretical fluorescent intensity, and compare those theoretical fluorescent values to the experimental fluorescent values.

This process work hinges on creating a program that loops to solve the infinite series model. Looping allows the equation to converge on a particular value, the solution. The loop is a repeating function that increases the value of n and plugs new calculated values back into the equation (n is a whole number

integer that increases by 1 e time the infinite series repeats itself, starting at 0). We then needed to determine how many iterations we would need to run, or more simply put, the maximum n-value. Running the loop indefinitely wastes time, and under-running the loop would gives us inaccurate values. Using ideal values for all of the variables discussed above, it was determined that running the loop 200 times produced a sufficiently converged value for θ in a minimal amount of time. Each time the loop was run, it plugs in all of the variables on the right side of the one-dimensional unsteady diffusion equation (y, L, a guess for D_{ij}, and t). E time it runs it produces a variable it stores as "thetaterm." "Thetaterm" is added each time to the variable name "thetaprime" ("thetaprime" was initially is given a value of 0). In the next run of the loop the value for the n variable increases by 1, until it reaches 200. Ultimately, "theatprime" gradually converges around the 120th run of the loop, but to increase our confidence we extend the loop to a value of 200. "Thetaprime" is then subtracted from 1 to produce the variable "theta." "Theta" is then multiplied by C_1 to produce C_i, which is the theoretical fluorescent value in that tissue. This is repeated for all values y, the distance in the tissue, and stored in the "dlength" matrix. All values are stored in a matrix titled "conc." Lastly, the "conc" matrix is reversed, meaning the final value becomes the first value, via the function "filpr." This is done for simplicity when viewing graphically, as the theoretical model creates a profile from diffusing right to left, whereas our images diffused left to right. When the program completes, there is a perfect diffusion curve, with equal points compared to those of the experimental diffusion curve.

As mentioned earlier, to find the best matching theoretical experimental curve, we varied the variable of interest, D_{ij}, then applied the "least sum of the squares" methodology to decide what D_{ij} produced the best fitting curve. A matrix was created of 5600 different diffusion coefficients, ranging from 1×10^{-4} to 1×10^{-11} and was created under the variable name "difftable." "Difftable" was specified to make linearly spaced guesses around the D_{ij} ranges that previous research publications hypothesized as D_{ij} in bone tissue. The following table shows the number of iterations it made between each range. (table 3.8)

Table A1 number of guess given a range of diffusion coefficients

D_{ij} Coefficient Range	Number of iterations
1×10^{-4} to 1×10^{-5}	400
1×10^{-5} to 1×10^{-6}	800
1×10^{-6} to 1×10^{-7}	1000
1×10^{-7} to 1×10^{-8}	1000
1×10^{-8} to 1×10^{-9}	800
1×10^{-9} to 1×10^{-10}	800
1×10^{-10} to 1×10^{-11}	800

Using one D_{ij} iteration at a time, MATLAB created, using the looping code described previously, a diffusion profile, compared each individual theoretical

value to our experimental value, and summed the square of the difference between those two values. It then entered that final summation in the "difftable" matrix in the column next to the D_{ij} value it corresponded to. This process then repeated, with a new D_{ij}, for a total of 5,600 times (the number D_{ij} guesses). Fundamentally the program is a loop within a loop, meaning it plugs in a D_{ij} value, runs it through the θ loop to solve the infinite series equation, compares all of its theoretical values to experimental values, and repeats the entire process using a new D_{ij} value. After this is carried out 5,600 times a preloaded MATLAB function named "min" finds the minimum value of all the of sum of the square values (column 2 in the "difftable"). This minimum lies in the same row as the best possible diffusion coefficient. The loop was instructed to run one final time with that best possible value and plot it against the experimental data. A graph is then produced and visually checked to ensure the program function properly. The graph is then saved in TIFF format, under the file name "section of bone/trial/quadrant of bone/particular time diffused.TIFF. The D_{ij} is then saved and named under the file name "section of bone_trial that particular_time_diffused" in an Excel workbook.

Appendix B

MATLAB Code to calculate D_{ij}

```
% updated data analysis

clc;

clear;


%-------------******Preliminary Functions*****----------------------
--

[data]=xlsread('E:\Rendered Excel Files\Sect2-18hr-4-FITC.xls');


%optimize the y axis to not be in pixels but in mm

l=length(data(1,:));

dlength=linspace(1,l,l);

l=l*.000812*10;

dlength=dlength.*.000812*10;


%variable l is the total length of the tissue

fprintf('length of given tissue is %f mm \n',l)


%divide the number of rows by 5, to get the number of rows you will
average

z=length(data(:,1))/5;

z=fix(z);


%subtract off your autoflur value from the entire matrix that is
predetermined and written down

%in the lab notebook

autoflur=33.28;

data=data-autoflur;

fprintf('your calculated autoflur is %f \n',autoflur')
```

```
%-- ****Averaging function without including 0 and neg values***----

%%Loops for averaging each section, dummy variable are i,j,
indicating

%%matrix dimesions, and q,s,u,w,y which are the unaveraged sections.

%%section1,section2 etc etc are the final averaged values

q=data(1:z,:);

lengthq = size(q);


section1 = zeros(1,lengthq(2));

for i = 1:(lengthq(2))

   sum = 0;

   count = 0;

   for j = 1:(lengthq(1))

       if (q(j,i) > 1)

            sum = sum + q(j,i);

            count = count + 1;

       end

   end

   if (count ~= 0)

          section1(i) = sum/count;

   end

end


% repeat for second section

y=data(z:(2*z),:);

lengthy = size(y);

section2 = zeros(1,lengthy(1))

for i = 1:(lengthy(2))

   sum = 0;

   count = 0;
```

```
   for j = 1:(lengthy(1))
       if (y(j,i) > 1 )
            sum = sum + y(j,i);
            count = count + 1;
       end
   end
    if (count ~= 0)
          section2(i) = sum/count;
    end
end

% repeat for third section
s=data(2*z:(3*z),:);
lengths = size(s);
section3 = zeros(1,lengths(1));
for i = 1:(lengths(2))
   sum = 0;
   count = 0;
   for j = 1:(lengths(1))
       if (s(j,i) > 1)
            sum = sum + s(j,i);
            count = count + 1;
       end
   end
if (count ~= 0)
   section3(i) = sum/count;
    end
end

 % repeat for fourth section
```

```
u=data(3*z:(4*z),:);
lengthu = size(u);
section4 = zeros(1,lengthu(1));
for i = 1:(lengthu(2))
   sum = 0;
   count = 0;
   for j = 1:(lengthu(1))
       if (u(j,i) > 1)
            sum = sum + u(j,i);
            count = count + 1;
       end
   end
   if (count ~= 0)
   section4(i) = sum/count;
   end
end

% final section
 w=data(4*z:5*z,:);
lengthw = size(w);
section5 = zeros(1,lengthw(1));
for i = 1:(lengthw(2))
   sum = 0;
   count = 0
   for j = 1:(lengthw(1))
       if (w(j,i) > 1)
            sum = sum + w(j,i);
            count = count + 1;
       end
   end
```

```
   if (count ~= 0)
   section5(i) = sum/count;
   end
end


%-----------------****curve fitting*****------------------
%using a hand coded sum of squares method
%known values
 length=l;  %mm
 time=86400; %s
 neu=dlength./l;


%  We are mesuring diff
%create a table of various diffusions (1000) from 1e-4 to 1E-10
ranging
%with equal expeditial increasing values between each decimal
element1=linspace(1E-4, 1E-5, 100);
element2=linspace(1E-5, 1E-6, 100);
element3=linspace(1E-6, 1E-7, 200);
element4=linspace(1E-7, 1E-8, 400);
element5=linspace(1E-8, 1E-9, 600);
element6=linspace(1E-9, 1E-10,600);
element7=linspace(1E-10, 1E-11,600);


diff1=[element1 element2 element3 element4 element5 element6
element7];
 difftable = zeros(2600,2);
for k = 1:1:2600
    diff=diff1(k);
    difftable(k,1) = diff1(k);
    %actual function we are fitting to
```

```
 thetaprime = 0;

      for n=[0:1:200]

      thetaterm=((((2*(-
1)^n))/((n+1/2)*pi))*(cos((n+1/2)*pi*(neu)))*(exp(-
(n+(1/2))^2*(pi*pi).*((time.*diff)./length^2))));

      thetaprime=thetaterm+thetaprime;

      end

 theta=1-thetaprime;

 conc=section1(5).*theta;

 %change to up and down

 conc=fliplr(conc);

 %compare the sum of all the squares and place in a table

 %---NOTE IT IS HERE YOU MUST CHANGE THE SPECIFIC SECTION------

 sumsq = 0;

 for m = 1:1:max(size(section1))

     sumsq = sumsq + ( (conc(m) - section1(m))^2 );

 end

 difftable(k,2) = sumsq;

end

% Find Minimum R^2 Value Index

[MinR2 MinDifIndex] = min(difftable(:,2)


% Rerun data for best fit

diff = difftable(MinDifIndex, 1);

 thetaprime = 0;

 for n=[0:1:200]

 thetaterm=((((2*(-
1)^n))/((n+1/2)*pi))*(cos((n+1/2)*pi*(neu)))*(exp(-
(n+(1/2))^2*(pi*pi).*((time.*diff)./length^2))));

 thetaprime=thetaterm+thetaprime;

 end

 theta=1-thetaprime;
```

```
 conc=section1(5).*theta;

 %change to up and down

conc=fliplr(conc);

%Conc is the important variable of intrest that is plotted vs.
distance

fprintf('The best fit diff coeff. is %E \n', diff);

fprintf('The best fit sum of square value is %f \n', MinR2);



%-------------*****discussion of variables******--------------------
-

%this is a brief overview of all the variables highlighted in
textbooks

%theta is theta, which is (ci-c0)/(c1-c0)

%KNOWN

%c0 should be 0, as we already subtracted off autoflu

%ci IS THE VALUE OBTAINED IN THE TISSUE

%c1 IS YOUR INTIAL TISSUE READING.

% neu is is neu, or y/L, meaning your (current distance)/(total
distance)

% KNOWN

% the y value will change with the c1 value

%tau, this is the variable of interst

%tau is (time*Diff coefficent)/total length^2

%in our code we have NOT hidden this variable, instead it is
explicity

%written.

% time value which in my case would be 18 or 30 hours

% t=86400;

%total length is known

%********variable of interest is diffusion

% theta=1-thetaprime;

% conc=d(1,1).*theta;

% conc=fliplr(conc);
```

```
%------------------****Plot functions***-------------------------

%this is for the section by section vs theoritical


%----MAKE SURE YOU GRAPH THE CORRECT SECTION--------------------

plot(dlength(1:max(size(section1))),section1,'b:+',dlength(1:max(siz
e(section1))),conc(1:max(size(section1))),'g:o' )

axis([0,1.65,0,100])

grid on

xlabel('distance in mm')

ylabel('Greyscale pixelation')

legend('actual experimental value','theoretical best fit value', 0)

title('Section2-18hr-Trial4-quandrant 1')


%-------Use this plot function to show all of the experiment data---
---

%%This is the updated plot function keeping axis steady, of the
averaged

%%values

%plot(dlength,section1,'g:d',dlength,section2,'c:s',dlength,section3
,'r:o',dlength,section4,'m:x',dlength,section5,'b:+')

% xlabel('distance in mm')

% ylabel('Greyscale pixelation')% legend('average of upper
section','average of mid section 1','average of mid section
2','average of mid section 3', 'average of final section',0)

% axis([0,1.65,0,125])

% grid on

% title('Sect2-30hr-5-FITC')

%SIDE NOTE et time you test a different section you must replace the

%section number 8 times.
```

Appendix C

MATLAB Code to find auto fluorescent values

```
clc;
clear;
[data]=xlsread('E:\Rendered Excel Files\Control-Sect2-1-FITC.xls');
lengthq = size(data);
d = zeros(1,lengthq(2));
for i = 1:(lengthq(2))
   sum = 0;
   count = 0;
   for j = 1:(lengthq(1))
       if (data(j,i) ~= 0
            sum = sum + data(j,i);
            count = count + 1;
       end
   end
   d(i) = sum/count;
end
z=mean(d)
fprintf('the average of this control sample is %f',z);
```

Appendix D

Examples of higher resolution bone sample images

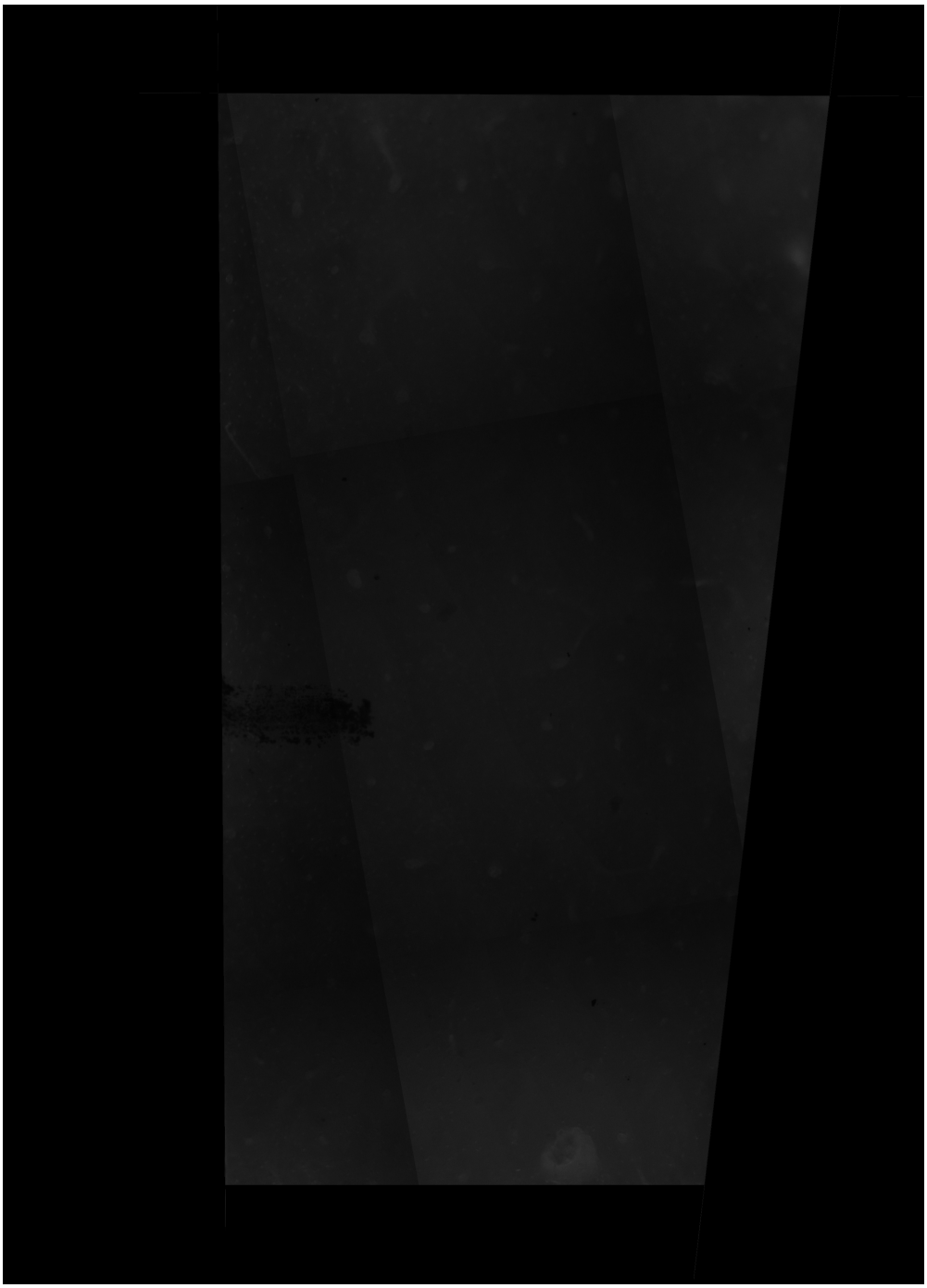

Figure D1. control, section 3, trial 1

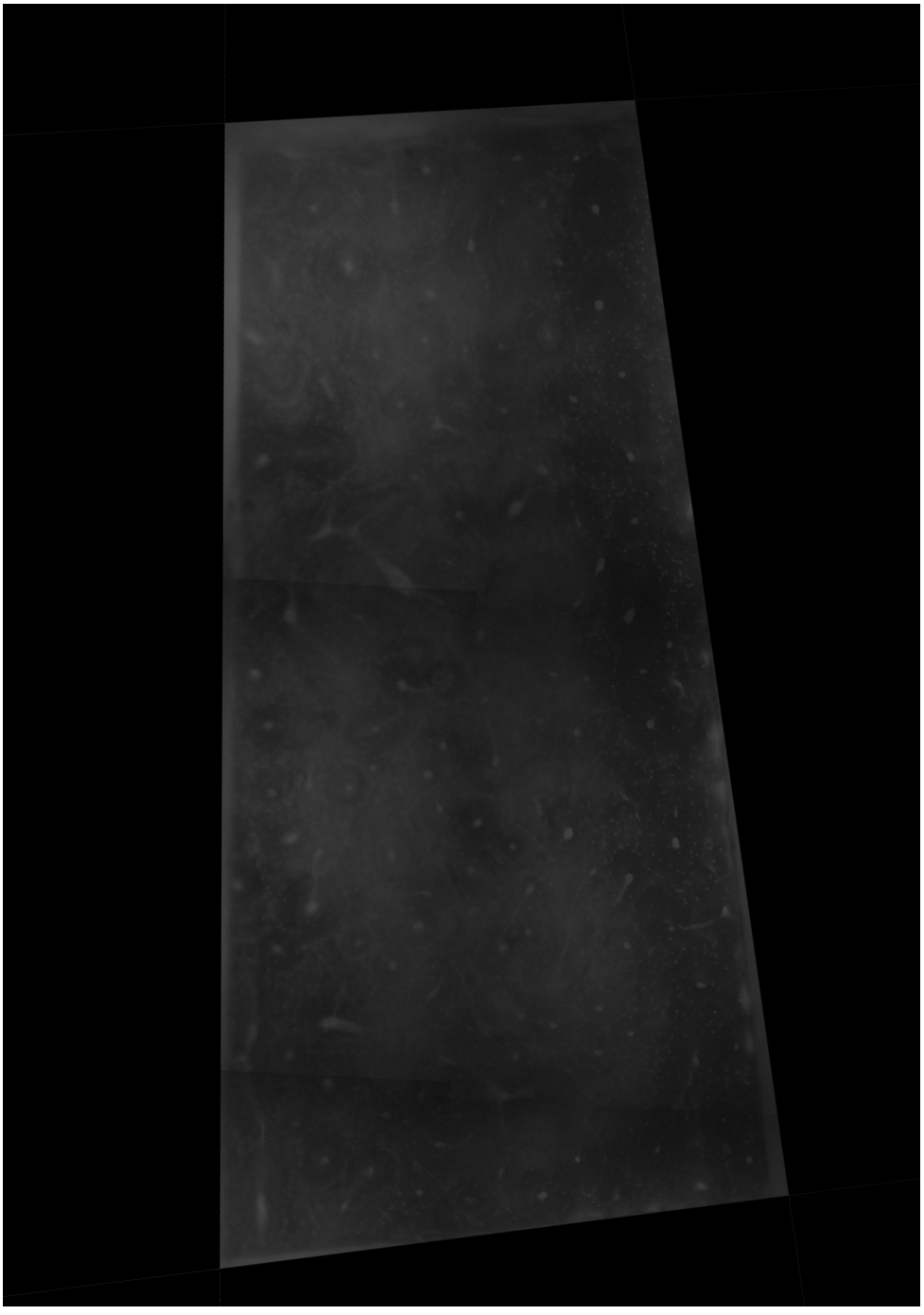

Figure D2. section 2, 18 hour diffused, trial 2

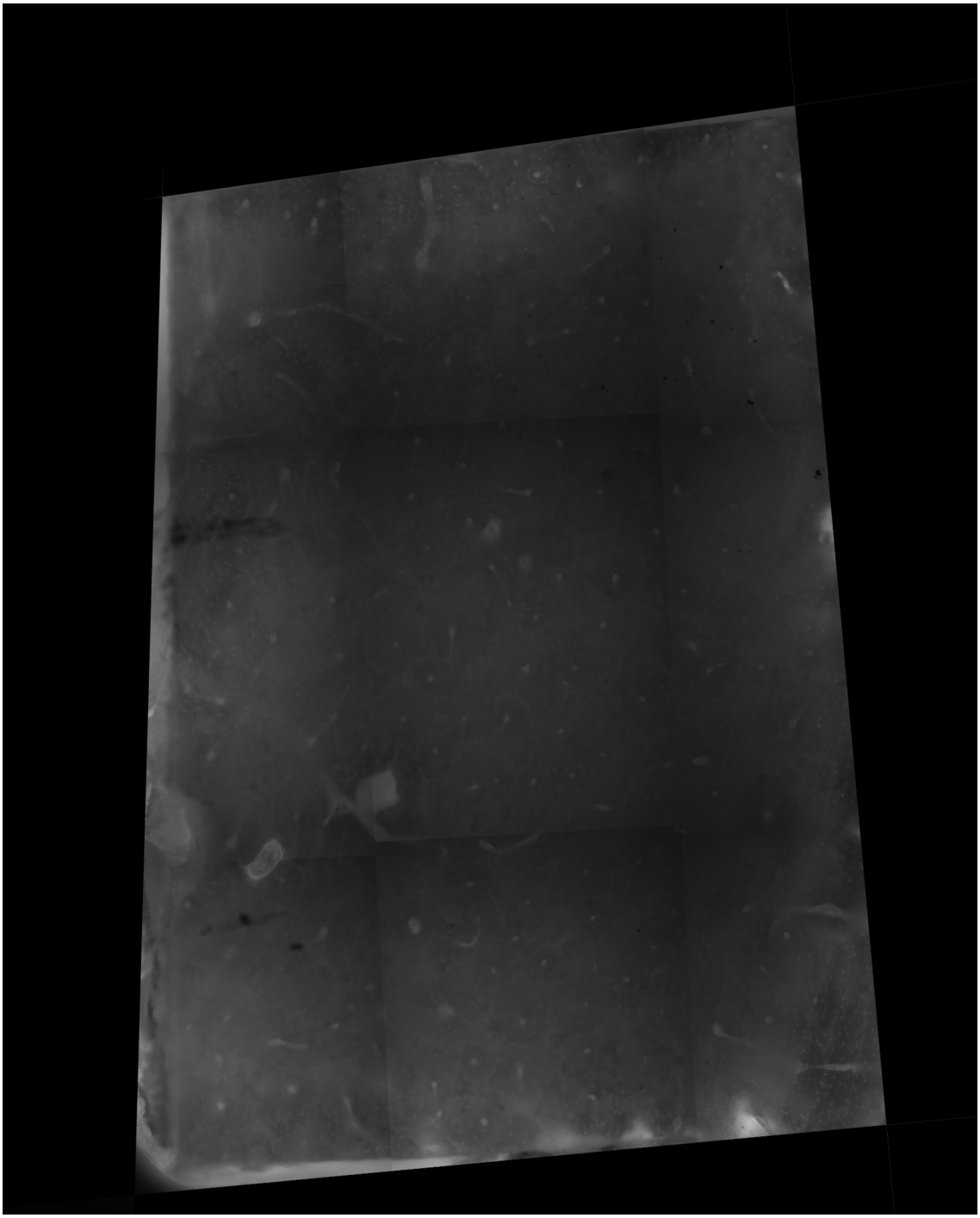

Figure D3. section 2, 30 hours diffused trial 2,

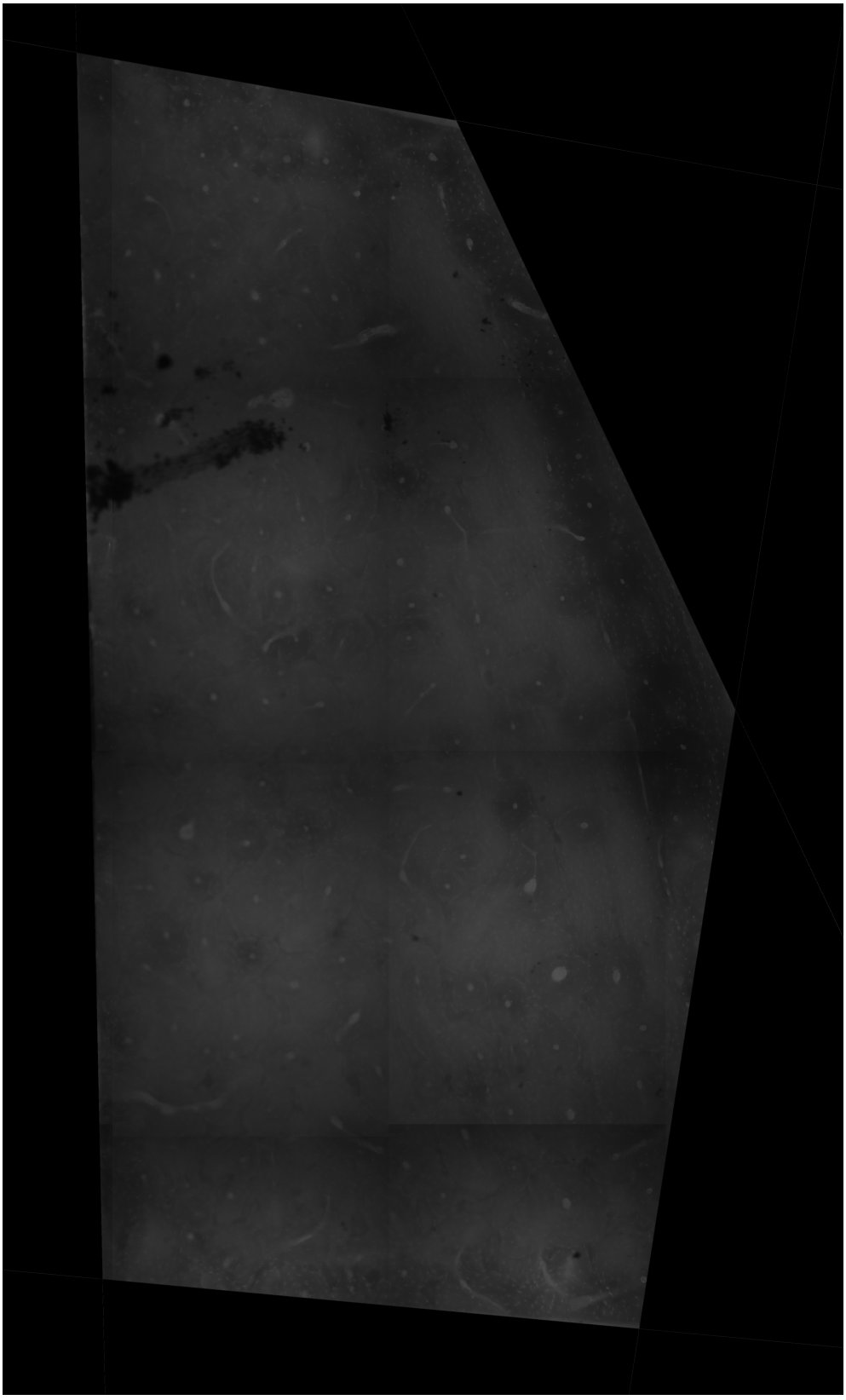

Figure D4. section 3, 18 hour diffused, trial 3

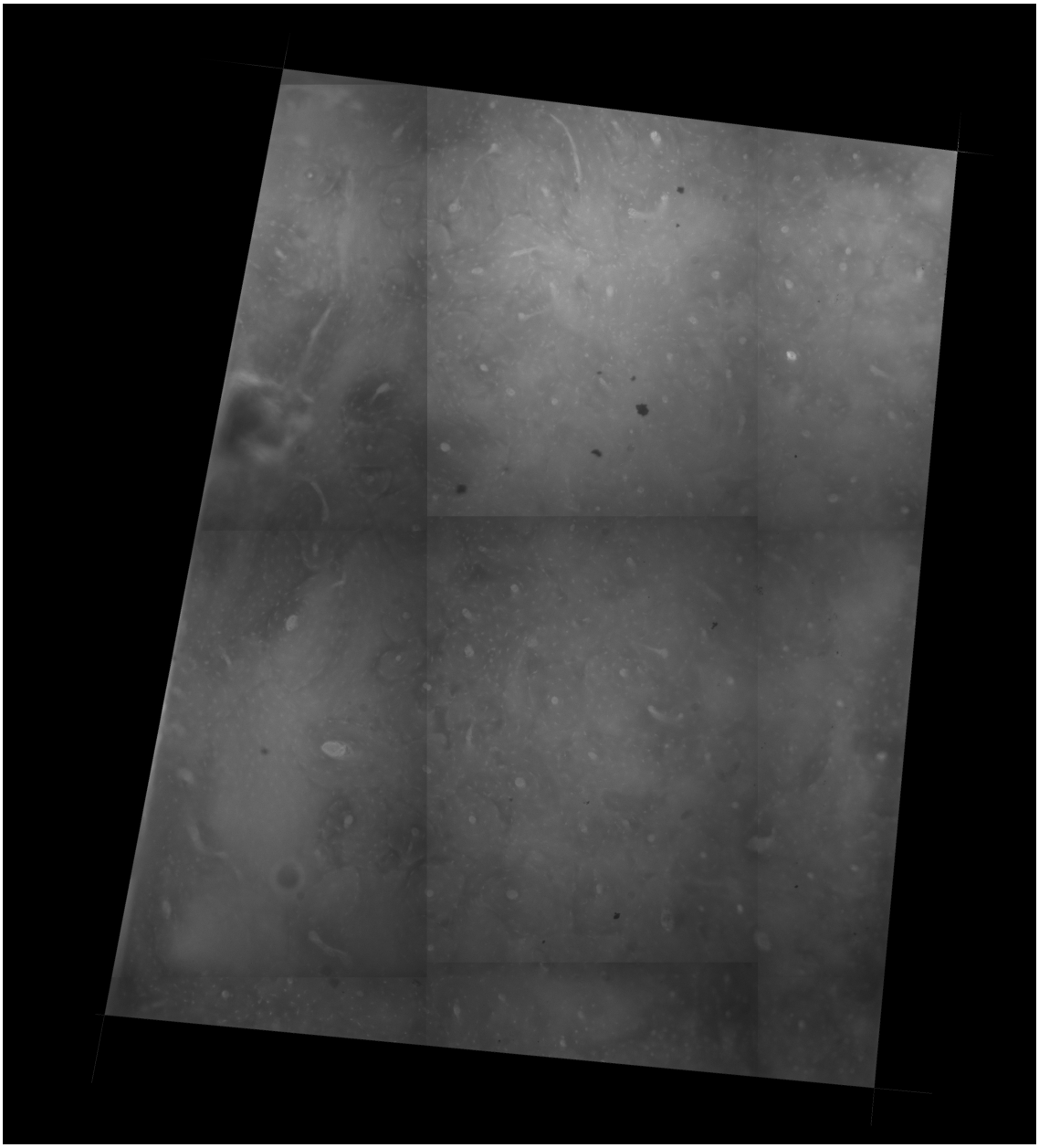

Figure D5. section 3, 30 hour diffused, trial 4

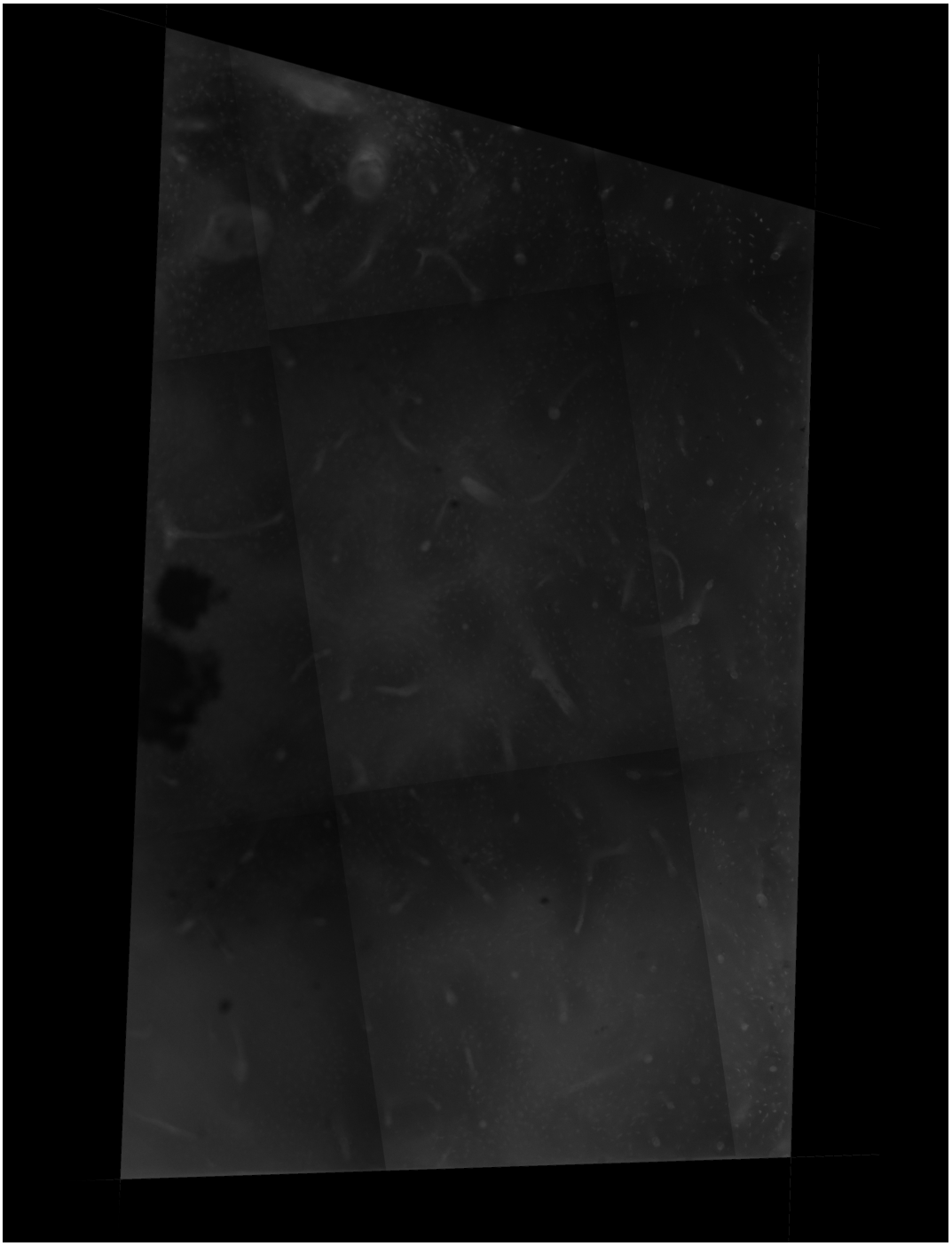

Figure D6. section 4, 18 hours diffused, trial 4

Figure D7. section 4, 30 hours diffused, trial 4

Appendix E

Data from section 4

Table E1, analysis of the number of time a signal was observed over the auto fluoresce value. Note when a signal was observed the best fit diffusion coefficient was always 1 x 10^{-6} cm^2/s

Sect. 4	FITC Signal		FITC
18 hour		30 hour	
Sample 1		Sample 1	
Quad 1	No	Quad 1	No
Quad 2	Yes	Quad 2	No
Quad 3	Yes	Quad 3	No
Quad 4	Yes	Quad 4	No
Quad 5	Yes	Quad 5	No
Sample 2		Sample 2	
Quad 1	No	Quad 1	No
Quad 2	Yes	Quad 2	No
Quad 3	Yes	Quad 3	No
Quad 4	Yes	Quad 4	No
Quad 5	No	Sample 5	No
Sample 3		Trial 3	
Quad 1	Yes	Quad 1	No
Quad 2	Yes	Quad 2	No
Quad 3	Yes	Quad 3	No
Quad 4	Yes	Quad 4	No
Quad 5	Yes	Quad 5	No
Sample 4		Sample 4	
Quad 1	No	Quad 1	No
Quad 2	No	Quad 2	No
Quad 3	No	Quad 3	No
Quad 4	No	Quad 4	No
Quad 5	No	Quad 5	No
Sample 5		Sample 5	
Quad 1	No	Quad 1	No
Quad 2	No	Quad 2	No
Quad 3	No	Quad 3	No
Quad 4	No	Quad 4	No
Quad 5	No	Quad 5	No
Total times signal is observed	12	Total times signal is observed	0

Appendix F

Sample MATLAB output from Section 4

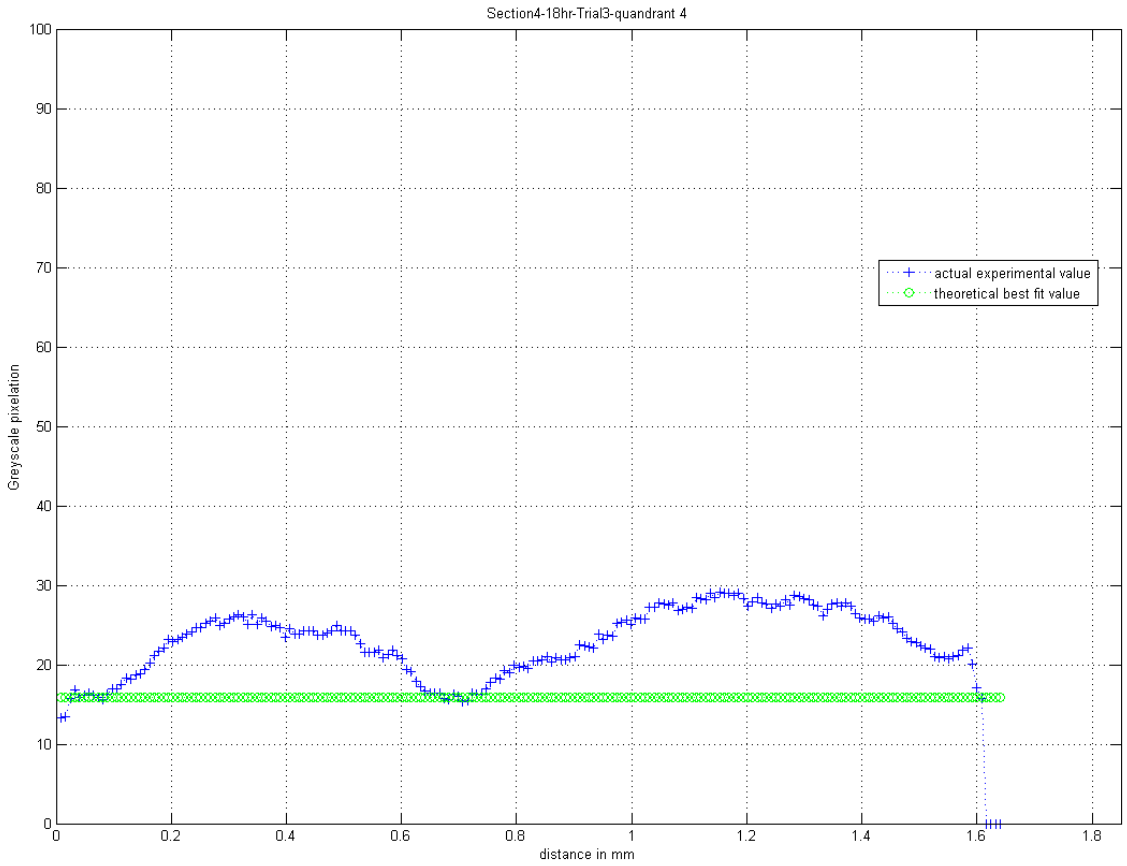

Figure F1. Example of the produced MATLAB plot applied to a quadrant in section 4 that produced a signal above the auto florescence level. Note the low values of the plot, and the line converges on a value of 1 x 10^{-6} cm^2/s

Appendix G

Procedure

Experimental procedure 2.0

Goal: To use a 1-D mathematical model derived from unsteady state heat conduction to develop a diffusivity model of various small molecules into bone.

A) The sample

1) A sample was obtained from CCF, it is the taken from a older canine sample, and preserved in 1X PBS. The bone sizes will need to be roughly 3 mm by 5mm by 30mm.

2) The entire bone sample will be placed in a mold of of biocompatible orthodontic resin.

3) The molds are carved from pink rubber easers and can be reused roughly 10 times before a new mold must be made

4) After the sample hardens (24 hr) one side, the periosteum l, is exposed by cutting this outer edge using the diamond saw thus allowing uni-directional transport or the given macromolecule.

5) The sample is then placed in PBS for 24 hrs at room temperature

6) The sample is now ready to be diffused in a given FITC solution

B) The setup

1) We have obtained our diffusion apparatus, from Ron Midura at the Cleveland Clinic, which has been custom manufactured for this exact experimental setup when applying a load to the sample. The device is capable of applying a force as it has a piezoelectric transducer which exerts a force on the bone, but for this initial set-up, we will not be exerting a force.

2) A majority of the work will be conducted in the Tissue Culture lab (Part of the Biochemical lab in SH 418), as most of the necessary analytical equipment is contained within that lab.

3) For unloaded diffusion, samples are placed in 1 well of a 6 well plate.

4) The six well plate should be cleaned, normally with ethanol and allowed to dry 24 hrs before the start of the experiment, and then rinsed with DI water.

5) The max dimensions of a tested bone for diffusion are dependent on whether it will be loaded or not and are stated in part A of this section.

6) The given solution will then be placed in the well, no exact amount is necessary as long as it fully submerges the sample.

C) The conjugate (given test solution)

1) For trial runs, we will be adding fluorescein sodium salt (Sigma-Aldrich 46960) based on its low cost and the probability that it should diffuse fairly quickly due to its low MW (376 Kda).

2) The molarity of the solution was based on a calculation of the average molarity of insulin in the body, which is 1 nanogram per 1 mL of a given solution found in the body

3) Solutions were made from 0.3 M, 0.03 M, 0.003 M respectively until we reached 3.0E-7 molar, which is close to physiological molarity of insulin.

4) Anything less then 3.0E-7 is an acceptable level to collect data at.

5) Final trials will add an either an insulin-fluorophore conjugate (yet to be determined the exact solution) or a Parathyroid hormone to the previously described setup.

D) The Incubator

1) The incubator is located in the tissue culture lab

2) The six well plate, containing the sample and the fluorescent solution, will be placed in the incubator at some given time (time zero).

3) The Incubator should be set at 37*C and have a Carbon Dioxide Concentration of 5%

4) Carbon dioxide levels must be carefully monitored an alarm will go off if it falls below 5% in humidified air

E) Preparation, after diffusion, to analyze the bone

1) After the Incubation period has expired, the bone sample will be promptly taken to the Bone saw machine in SH 470,

2) The previously described bone saw will cut the samples, laterally, on the order of at least less then 100 microns.

3) Approximately 20 samples can be obtained from one sample, although the extrema (tail ends) of the sample should be discarded.

3) These sample will be placed on a slide, glued down and mounted using Vectashield Hard Set and a coverslip.

4) The samples should be labeled with a date, length of diffusion, and Molarity of diffused solution and placed in a slide folder and transported to the robotic scope at the Cleveland Clinic Imaging lab (2^{nd} floor, west wing)

F) Robotic Microscope Imaging

1) Load all the given samples into the Robotic fluorescent scope

2) Turn on the scope, camera, and mercury power source

3) Take extreme caution whenever touching the camera, even the slightest movement will distort your montage

4) Open Image-Pro

5) Use the X, Y, Z dial to move the robotic stage, never move it manually

5) Click on the Macro Tab and scroll down to Large_FOV_Acquire

6) Answer the given instructions, understand that it is easier to image one sample at a time, as you shouldn't ever need to image more then 8

7) Choose a given acquisition mode (Fluero), filter, objective gain and exposure time (in ms)

8) Make sure you have the correct Fluero filter loaded in the machine

9) Define your scan dimensions, the program will ask you to locate the left right up and down edge of your sample, when done you must click the Define button.

10) Enable predictive focus, you will be prompted to create several predictive points, first you must delete all the stored points, using the Oasis Turboscan box, auto move to different points, adjust the Z, and add the point, then click update

11) you shouldn't need more then 10 points

12) Start the scan, shade correct, and keep the gain and exposure constant.

13) Batch process your scanned image, it is under the macro Tab

14) Save the Image to your jump drive and take back to CSU for analysis

G) Image analysis

1) Use Image pro to extract a 2-D gre yscale array of the level of fluorescence of each pixel

2) Process this image in MATLAB, looking for a Conc. Curve

Appendix H

Table of all averaged diffusion coefficients including their standard error.

Table H1 All found data.

Section 2			
18 hour data			
Trial 1	Found Diff	Sum of squares	Signal to noise ratio
Quad 1 (18 hr)	4.91E-08	12435.49025	1.32
Quad 2 (18 hr)	5.36E-08	10666.8339	1.87
Quad 3 (18 hr)	4.00E-08	8178.109573	2.3
Quad 4 (18 hr)	1.18E-07	21553.91705	2.49
Quad 5 (18 hr)	5.09E-07	75793.8193	3.01
Average	1.54E-07		2.19
StDev	2.01E-07		
St error	8.98E-08		
Trial 2			
Quad 1 (18 hr)	3.73E-08	3693.257536	1.08
Quad 2 (18 hr)	1.36E-07	2823.955904	0.97
Quad 3 (18 hr)	8.45E-08	1961.256122	0.96
Quad 4 (18 hr)	2.91E-07	1812.925309	1.13
Quad 5 (18 hr)	8.45E-08	767.522362	0.87
Average	1.27E-07		1
StDev	9.82E-08		
St error	4.39E-08		
Trial 3			
Quad 1 (18 hr)	NM	55489.03294	4.55
Quad 2 (18 hr)	NM	35084.24183	3.32
Quad 3 (18 hr)	1.25E-07	73688.1956	4.09
Quad 4 (18 hr)	8.47E-08	94648.02686	3.22
Quad 5 (18 hr)	4.96E-08	101272.3758	2.95
Average	8.64E-08		3.62
StDev	3.76E-08		
St error	2.17E-08		
Trial 4			
Quad 1 (18 hr)	5.09E-08	13607.46689	1.56
Quad 2 (18 hr)	9.45E-08	3436.608684	1.21
Quad 3 (18 hr)	8.64E-08	5427.581427	1.55
Quad 4 (18 hr)	2.36E-07	4195.950846	1.47
Quad 5 (18 hr)	1.73E-07	4482.966796	1.36
Average	1.28E-07		1.43
StDev	7.51E-08		
St. error	3.36E-08		
Trial 5			

Quad 1 (18 hr)	6.10E-08	1870.017889	1.23
Quad 2 (18 hr)	5.48E-08	1500.311146	0.91
Quad 3 (18 hr)	1.48E-08	1206.034256	0.75
Quad 4 (18 hr)	1.23E-08	1378.351579	0.71
Quad 5 (18 hr)	6.29E-09	304.936162	0.52
Average	2.98E-08		0.82
StDev	2.59E-08		
St. error	1.16E-08		
30 hour data			
Trial 2			
Quad 1 (30 hr)	1.36E-08	24283.29822	1.37
Quad 2 (30 hr)	1.09E-08	9879.972754	1.13
Quad 3 (30 hr)	3.36E-08	10449.13766	1.45
Quad 4 (30 hr)	1.55E-08	6245.654517	1.26
Quad 5 (30 hr)	1.00E-07	7488.940673	1.77
Average	3.47E-08		1.41
StDev	3.75676E-08		
St. Error	1.68007E-08		
Trial 3			
Quad 1 (30 hr)	7.00E-08	6737.087167	1.33
Quad 2 (30 hr)	1.36E-07	1387.676449	1.1
Quad 3 (30 hr)	8.36E-08	4122.415311	1.47
Quad 4 (30 hr)	7.36E-08	10052.27105	1.84
Quad 5 (30 hr)	1.00E-07	4435.512972	1.62
Average	9.27E-08		1.47
StDev	2.70216E-08		
St Error	1.20844E-08		
Trial 4			
Quad 1 (30 hr)	1.50E-07	9595.382641	1.4
Quad 2 (30 hr)	1.3609E-07	13714.18722	1.38
Quad 3 (30 hr)	7.47368E-07	11530.34355	1.94
Quad 4 (30 hr)	3.50376E-07	10173.30874	1.65
Quad 5 (30 hr)	NM	19439.96596	1.47
Average	3.46E-07		1.57
StDev	2.85E-07		
St Error	1.43E-07		
Trial 5			
Quad 1 (30 hr)	1.09E-07	1975.647851	1.01
Quad 2 (30 hr)	4.27E-08	2586.797377	0.71
Quad 3 (30 hr)	2.36E-08	1344.514182	0.85
Quad 4 (30 hr)	1.55E-08	423.944666	0.66
Quad 5 (30 hr)	6.91E-08	1837.295756	1.02

Average	5.20E-08		0.85
StDev	3.8005E-08		
st error	1.69964E-08		
Section 3			
18 hour data			
Trial 1			
Quad 1 (18 hr)	NM	2097.875325	0.68
Quad 2 (18 hr)	1.54E-09	3698.212901	0.82
Quad 3 (18 hr)	4.43E-10	1706.109414	0.75
Quad 4 (18 hr)	1.00E-07	7249.128019	0.98
Quad 5 (18 hr)	NM	11518.83893	0.88
Average	3.40E-08		0.83
StDev	5.72E-08		
St error	3.30E-08		
Trial 4			
Quad 1 (18 hr)	NM	44888.19025	1.57
Quad 2 (18 hr)	NM	60912.58636	1.43
Quad 3 (18 hr)	NM	217406.2154	1.81
Quad 4 (18 hr)	NM	40379.57277	1.41
Quad 5 (18 hr)	NM	38039.29015	0.97
Average			1.43
StDev			
St error			
Trial 5			
Quad 1 (18 hr)	2.45E-07	10657.84228	0.64
Quad 2 (18 hr)	1.00E-07	6211.699866	0.83
Quad 3 (18 hr)	7.82E-08	25587.17692	1.26
Quad 4 (18 hr)	1.36E-07	1812.925309	1.46
Quad 5 (18 hr)	1.18E-07	48837.25633	1.62
Average	1.36E-07		1.16
StDev	6.51E-08		
St error	2.91E-08		
30 hour data			
Trial 4			
Quad 1 (30 hr)	1.91E-07	220782.755	2.2
Quad 2 (30 hr)	NM	132522.8149	2.31
Quad 3 (30 hr)	3.55E-07	28298.3278	1.88
Quad 4 (30 hr)	NM	19621.90064	2.33
Quad 5 (30 hr)	NM	8363.265759	1.65
Average	2.73E-07		2.08

StDev	1.15708E-07		
St. Error	8.18182E-08		
Trial 5			
Quad 1 (30 hr)	NM	47805.49473	2.07
Quad 2 (30 hr)	NM	36353.29394	1.61
Quad 3 (30 hr)	4.74436E-07	15767.76156	1.68
Quad 4 (30 hr)	NM	20944.70608	1.64
Quad 5 (30 hr)	NM	4283.04952	1.16
Average	4.74E-07		1.62
StDev			
St. Error			
Overall 18hr avg	1.04E-07		
Std error	1.63E-08		
Overall 30hr avg	1.50E-07		
Std error	3.31E-08		

Appendix I

P-value comparison of inner quadrants to edge quadrants to ensure proper sealing.

Table I1 edge to center P values

Section 2	P-Value when comparing the average of the 2 outer edges to the 3 inner
18 hour data	
Sample 1	0.31
Sample 2	0.27
Sample 3	0.83
Sample 4	0.74
Sample 5	0.82
30 hour data	
Sample 2	0.35
Sample 3	0.67
Sample 4	0.70
Sample 5	0.04
Section 3	
18 hour data	
Trial 1	0.0
Trial 4	1
Trial 5	0.23
30 hour data	
Trial 4	0.67
Trial 5	0.49